SYNTHETIC AND SPECTROSCOPIC STUDIES OF DIRHODIUM COMPLEXES RELEVANT TO C−H FUNCTIONALIZATION CATALYSIS

by

Katherine P. Kornecki

A dissertation submitted in partial fulfillment of

the requirements for the degree of

Doctor of Philosophy

(Chemistry)

at the

UNIVERSITY OF WISCONSIN – MADISON

2013

Date of final oral examination: 06/24/2013

The dissertation is approved by the following members of the Final Oral Committee:

John F. Berry, Associate Professor, Inorganic Chemistry
Shannon S. Stahl, Professor, Inorganic Chemistry
Clark R. Landis, Professor, Inorganic Chemistry
Jennifer M. Schomaker, Assistant Professor, Organic Chemistry
Thomas Brunold, Professor, Inorganic Chemistry

Synthetic and Spectroscopic Studies of Dirhodium Complexes Relevant to C–H Functionalization Catalysis

Katherine P. Kornecki

Under the supervision of Associate Professor John F. Berry

University of Wisconsin – Madison

Abstract

Dirhodium complexes have a long-standing importance in C–H functionalization chemistry, but little is known about the reactive intermediates on which this chemistry relies. The first part of this dissertation focuses on intermediates in catalytic C–H amination chemistry: In Chapter 3, the catalyst $Rh_2(esp)_2$ (esp = α,α,α',α'-tetramethyl-1,3-benzenedipropanoate) is studied spectroscopically and electrochemically to gain insight into its robust nature. These studies implicate the stability of a one-electron oxidized $Rh_2^{II,III}$ state in the high level of activity reported for this catalyst. In Chapter 4, two complexes that are structurally analogous to $Rh_2(esp)_2$ with chelating dicarboxylate ligands based on a resorcinol backbone are synthesized. These new complexes are electronically dissimilar to $Rh_2(esp)_2$, since the ligands are more readily oxidized than the Rh_2 core, as observed by cyclic voltammetry. In catalytic studies, it is shown that these new catalysts perform equally well in intramolecular amination as parent catalyst $Rh_2(esp)_2$, but fail to achieve the same level of efficiency in intermolecular amination.

The results of this study further implicate the importance of mixed-valency in intermolecular amination. In Chapter 5, the synthesis and catalytic activity of a new purposefully mixed-valent Rh_2-amidate catalyst is reported. The new catalyst, $Rh_2(espn)_2Cl$ (espn = α,α,α',α'-tetramethyl-1,3-benzenedipropanamidate), achieves higher turnover numbers in intramolecular amination than parent catalyst $Rh_2(esp)_2$. Chapter 6 is focused on the exploration of intermediates in Rh_2-mediated carbenoid chemistry. Methods for preparing a metastable solution of a donor/acceptor carbene complex of $Rh_2(TPA)_4$ (TPA = triphenylacetate) are described; the carbenoid intermediate is characterized by NMR, resonance Raman and X-ray absorption spectroscopies, all corroborated by DFT analysis.

In summary, the work presented in this dissertation establishes the importance of mixed-valency for increased turnover in C–H amination catalysts. Isolation of the first Rh_2-carbenoid provides experimental support for the previously theoretically-based catalytic reactivity of Rh_2-carbenoids.

DEDICATION

This work is dedicated to my parents, Lucyna and Andrzej Kornecki, who have always supported my curiosity and encouraged me to pursue anything that I want to do, even when it takes me far away from home. This work is also dedicated to all adventurous spirits, for there will always be unexplored places, and places worth exploring again.

ACKNOWLEDGMENTS

I would like to thank my advisor, Professor John Berry, for his encouragement and mentorship throughout my time at Madison, and for taking the gamble of hiring me, even after seeing my performance on my first couple of cumes. John gave me a great deal of freedom throughout my graduate career to work on whatever was most interesting to me at the moment, and I appreciate him a great deal for that. Because of this approach, I've come to realize that research is really just about having your own drive and determination, and about making your own mistakes. Thank you, John, for guiding me during these formative years.

I'd like to thank my fellow Berry Group members: Amanda, Ryan, Brian, Wes, Travis, Tristan and Tim. Somehow everything keeps working, and it's surely a group effort! I wish them all the best. I would also like to extend a special thanks to previous group members: Dr. Michael Nippe has been an inspiration to me, and I am very grateful for his kindness and support. Dr. Eugenia Turov has taught me so much about chemistry as well as life, and I am so lucky to have such an amazing friend and confidante.

I would like to thank Professors Clark Landis and Shannon Stahl for sitting on my committee over the years and challenging me to become a more thoughtful scientist. Their input and guidance has helped me to focus on areas that needed work, and though I am still not perfect, I have grown very much with their help. I would also like to thank Professors Thomas Brunold and Jennifer Schomaker for agreeing to read my thesis and sit on my final committee. The opportunity to interact with so many caring and knowledgeable professors has been a great privilege during my time at UW.

None of this work would have been possible without the world-class facilities that I had at my disposal every day. I would like to thank Dr. Ilia Guzei for teaching me the basics of crystallography, and for his unending patience whenever I made him explain the same exact thing to me over and over again. I would like to thank Dr. Charlie Fry, Dr. Monica Ivanovic and Dr. Bob Shanks for their amazing upkeep of the NMR/EPR facility, and Dr. Martha Vestling for her meticulous care of the MS facility.

Over the past year, I have had the good fortune of participating in a collaborative NSF center for the study of C-H functionalization, and I am infinitely grateful for all of the connections and productive discussions that were fostered by the center. I would especially like to thank Professor Huw Davies and his students Fred, Felicia, Slava and Katie for being excellent collaborators: Chapter 6 would not have come to fruition without their help. In that regard, I would also like to extend thanks to Prof. Kyle Lancaster for XAS measurements, as well as Prof. Jochen Autschbach for computational work.

On a less science-y note, I want to thank my climbing friends for always reminding me that life exists outside the confines of the chemistry building – living in Madison would not have been as much fun without them. And BW <3.

Finally, and most significantly, thank you Mom, Dad and Adam, for your unconditional love.

TABLE OF CONTENTS

Chapter 2

Introduction to Dirhodium Catalyzed C-H Functionalization

Chapter 3

Evidence for a One-Electron Mechanistic Regime in Dirhodium Catalyzed Intermolecular C–H Amination

Chapter 4

Dirhodium Complexes that Bear Redox-Noninnocent Ligands and their Performance in Intra- and Intermolecular C–H Amination

Chapter 5

Introducing a Mixed-Valent Dirhodium(II,III) Catalyst with Increased Longevity in C–H Amination

Chapter 6

Spectroscopic Characterization of a Donor/Acceptor-Stabilized Dirhodium Carbenoid Intermediate

Appendix 1

CCHF Collaboration:
Synthesis of a Mixed-Valent Rh_2-carboxamidate with Chiral Ligands

LIST OF TABLES

LIST OF FIGURES

LIST OF SCHEMES

Chapter 1

Wisconsin Initiative for Science Literacy: Introduction for a General Audience

1.1 Inorganic Chemistry

Chemistry is a vast science with thousands upon thousands of highly specialized subcategories. Perhaps you've heard of organic chemistry – if not, you have probably interacted with organic matter in the forms of food, fuel and medicine. Perhaps you've also heard of nuclear chemistry, theoretical chemistry, biochemistry, nanotechnology – the list could go on. But rarely is inorganic chemistry mentioned. Why is that? I think it is because inorganic chemistry is actually the broadest of the chemical sciences. All these other fields are merely subsets of inorganic chemistry. Inorganic chemistry is the study of all the elements that are not hydrocarbons (but including hydrogen and carbon separately). And truth be told, many elements interact with hydrocarbons pretty regularly, so inorganic chemistry is really an umbrella term.

Inorganic materials are ubiquitous (and essential) in nature, but we don't often give it much thought. Air and water are composed of inorganic molecules. Salt, sand, rocks, gems, minerals – all inorganic. Alloys like steel, or precious metals like silver and gold are inorganic materials as well, but what is often overlooked is that some of the most interesting inorganic chemistry occurs in solution when metal ions have formed bonds with other molecules to make metal complexes. Metal complexes are amenable to study because they often have properties that allow them to interact with various types of light (this is called "spectroscopy", see section 1.4.2). In a sense, we can "shine light" on a question and get some answers about what it is exactly that metal complexes do.

1.2 Catalysis and Energy

Our economy is heavily driven by chemistry: plastics, fuels, batteries, pharmaceuticals – you name it! Unfortunately, many chemical processes require a lot of energy (e.g. heating, cooling, light) and create a lot of waste (e.g. greenhouse gases, toxic chemicals). From an environmental perspective, energy usage and waste are heavily interconnected, especially since "energy" typically comes from the combustion of fossil sources. One of the goals of modern chemistry is to find ways to minimize the amount of energy used and harmful waste generated by chemical reactions.

Catalysts are molecules that can help achieve the goals of energy and waste reduction in multiple ways. For instance, a catalyst can allow a reaction that typically requires high temperature to be accessible at room temperature. A catalyst can make a reaction happen faster, thus saving energy by limiting the time necessary for completion. A catalyst can also cause a reaction to be more selective for a particular end product, thus preventing waste due to separations, purifications and unwanted materials.

The study of catalysis is multifaceted, spanning catalyst design and methodology all the way to reactor optimization. Understanding exactly how a catalytic process works is incredibly important for the purpose of making improvements to existing systems, as well as designing new systems with a specific purpose in mind. In this dissertation, an important class of catalysts that contain two rhodium (Rh) atoms is investigated.

1.3 C−H Functionalization

One of the most common chemical bonds in nature and in commercial feedstocks (derived from oil refining) is the hydrocarbon (C−H) bond. In order to give molecules new properties, molecules must be modified by something called *functionalization*. Being able to do this in a selective manner is highly important to the pharmaceutical and commodity chemical industries. A functional group is an atom or group of atoms that are covalently bonded to part of a molecule (Figure 1.1). In traditional synthetic chemistry, functional groups are exchanged for new functional groups. Unfortunately, there are two major pitfalls associated with this strategy. One issue is that not all functional groups can be immediately exchanged for the new functional group of your choice: it may require multiple exchanges to get to your desired product (and copious chemical and energetic waste). Another problem is that you cannot exchange functional groups where there are none: any part of a molecule that doesn't have pre-existing functionality (i.e. C−H bonds) is thus effectively off-limits.

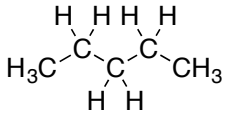

a) An *unfunctionalized* hydrocarbon

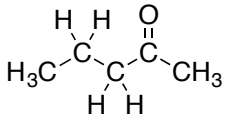

b) A hydrocarbon with an oxygen-containing *functional group*

Figure 1.1 Understanding functional groups.

The whole idea behind C−H functionalization is to find ways to use C−H bonds as latent functional groups. The difficulty in this approach is that, as I've already mentioned, most molecules contain *many* C−H bonds! To selectively pick one from hundreds requires special help from a catalyst.

1.4 Studying Dirhodium Complexes

1.4.1 Oxidation States

Rhodium is a rare and precious transition metal; it is one of the "Platinum Group Metals" along with platinum, palladium, iridium, ruthenium and osmium, so called because these metals often occur together in various mineral deposits in nature.[1] All of the metals in the platinum group are well known for their catalytic properties, and since they do not tarnish, they are often used in jewelry. It is quite likely that you have a mixture of some of these metals in the catalytic converter above the exhaust pipe of your car, and possibly plating a fancy ring or bracelet as well.

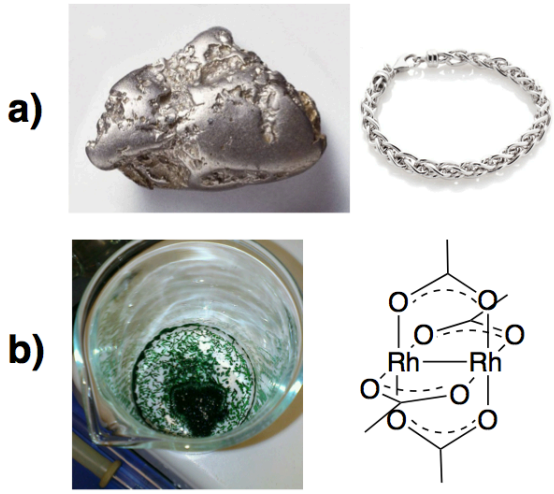

Figure 1.2 a) Elemental rhodium (oxidation state Rh^0). b) (left) Molecular Rh_2 (oxidation state Rh^{+2}) in a beaker; (right) a generalized structure for Rh_2 carboxylate complexes.

Dirhodium complexes, unlike elemental, metallic rhodium, are *molecular* metal complexes. Molecular metal complexes typically have fewer valence electrons around the metal atom nucleus than they would in their metallic form – that is to say, the metal atom is in a non-zero oxidation state. I've included a picture of what Rh_2 complexes look like in real life (Figure 1.2b). Rh_2 complexes are typically green-colored solids, but their color can change depending on their chemical environment and varying oxidation state. We can learn a lot about how these catalysts work by observing color changes during reactions and thus gain insight into their catalytic properties. Dirhodium complexes are well known for their ability to act as catalysts in C–H functionalization reactions,[2] but little is known about the factors that govern their reactivity: this is why these species merit study.

1.4.2 Spectroscopy

Light and matter have a close relationship. Similar to how you can't see anything when you're standing in a dark room, you often can't learn much about molecules without light. Certain wavelengths of light excite molecules in specific ways; this is the basis of different types of spectroscopy. These so-called "excitations" are observable by various instruments and give you information about what molecules look like, and potentially how they behave.

Chemical bonds are held together by electrons, so it makes sense that when electrons are either added or removed from molecules, this will change molecular properties. The addition or removal of electrons is called reduction and oxidation, respectively. In the case of dirhodium compounds, it is easiest to add or remove electrons from the Rh–Rh bond. Oxidizing one of the Rh_2 catalysts that is studied extensively in this dissertation ($Rh_2(esp)_2$) causes a change in this catalyst's interaction with visible wavelengths of light. Upon oxidation, it changes from green to red (Figure 1.3). This is a particularly nice example since we can visually see the change, but we can also use a technique called UV-Vis spectroscopy to give us more details about these color changes; UV-Vis spectroscopy measures the amount of visible or UV light that is absorbed by a sample of your compound. Using UV-Vis spectroscopy to study $Rh_2(esp)_2$ was significant: we ultimately learned that when the catalyst is in its oxidized (red) state, it is active in C–H functionalization reactions, contrary to what was previously proposed in the literature. This study led us to develop a new catalyst in Chapter 5 that is more stable in its oxidized state than $Rh_2(esp)_2$.

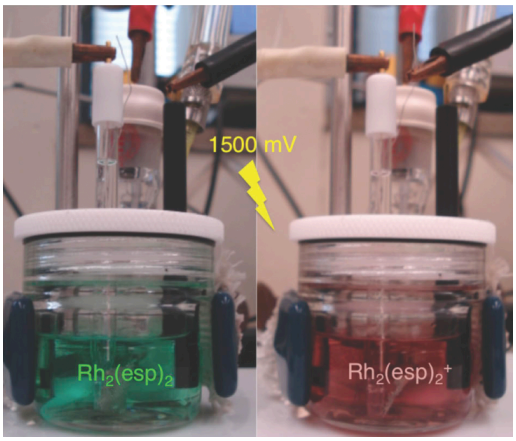

Figure 1.3 Using electrodes to oxidize $Rh_2(esp)_2$ causes a visible color change.

When we isolate a carbon-containing catalytic intermediate in Chapter 6, this new isolated species is readily distinguished from its light green starting material by its deep ocean blue color, which we can also monitor by UV-Vis spectroscopy (Figure 1.4).

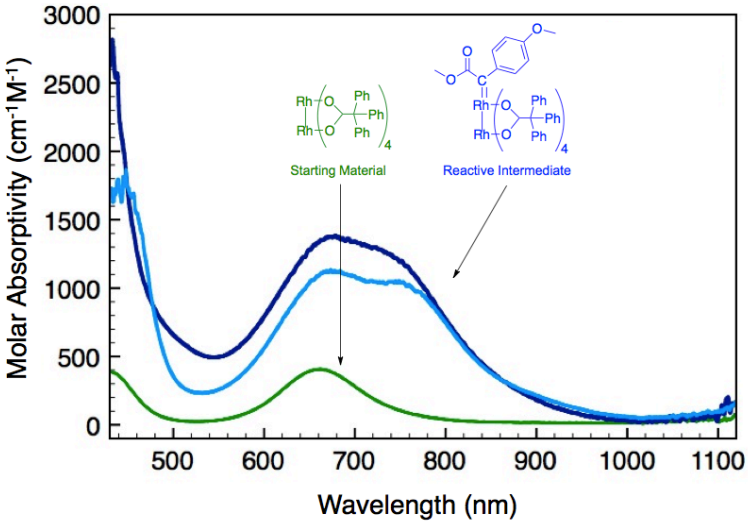

Figure 1.4 A UV-Vis spectrum of a Rh_2 complex (starting material), overlayed with spectra of a trapped reactive Rh–Rh=C intermediate used in C–H functionalization.

This change in color is an indication of a weak interaction with a reactive carbon fragment. We learned more about the bonding between the reactive carbon fragment and the Rh–Rh unit by other spectroscopies well: Nuclear Magnetic Resonance (NMR) spectroscopy gave us information about the connectivity of atoms in our intermediate by exciting specific types of nuclei in a magnetic field using electromagnetic radiation (radio frequencies). Resonance Raman spectroscopy is a type of vibrational spectroscopy; it also gave us information about connectivity by exciting bond vibrations, for example, the vibrational frequency of the weak Rh=C bond. X-Ray Absorption spectroscopy gave us information about the specific bond distances in our intermediate by providing enough energy to our sample to eject an electron from each Rh atom; the interference caused by that electron with other neighboring electrons on its way out of the molecule can be measured and provide structural information. Additionally, we can theoretically predict all of these spectroscopic results, and depending on how well our prediction matches experimental data, we can develop a highly accurate picture of the electronics of our intermediate.

1.5 Understanding Catalytic Species

Developing accurate models of catalysts is important for multiple reasons. Since catalysis is a science that is centered around the idea of efficiency, small improvements in activity and selectivity are meaningful. Understanding the molecular underpinnings that impart various reactivity traits is one way to start methodically modifying catalysts to perform exactly in the way you desire. Furthermore, being able to substantiate a

theoretical model with experimental data makes predictive chemistry more plausible. Theory does not carry as much clout without experimental support.

Although synthetic methodology has advanced rapidly in the field of Rh_2-catalyzed C–H functionalization, the mechanistic understanding of these reactions is limited due to the lack of information about the electronic structure of the intermediates involved in these transformations. This dissertation presents an advance in the understanding of Rh_2-mediated chemistry by providing insight into the structure and activity of important intermediate species in various Rh_2-catalyzed C–H functionalization reactions.

I hope that through this chapter I've managed to convince you that the work presented in this dissertation is both exciting and important! Thank you for reading!

References

1) Greenwood, N. N.; Earnshaw, A. *Chemistry of the Elements, 2nd Ed.* Butterworth-Heinemann, New York: 1997.
2) Davies, H. M. L.; Manning, J. R. *Nature* **2008**, *451*, 417.

Chapter 2

Introduction to Dirhodium C–H Functionalization Chemistry

This chapter is adapted from sections of "Metal-Metal Bond Containing Complexes as Catalysts for C–H Functionalization", a submitted manuscript for *Progress in Inorganic Chemistry*. Authors: Kornecki, K. P.; Powers, D. C.; Ritter, T.; Berry, J. F.

2.1 Metal-Metal Bond Containing Complexes

Metal–metal (M–M) multiple bonds in coordination compounds were first described in anionic Re halide clusters such as $[Re_3Cl_{12}]^{3-}$ and $[Re_2Cl_8]^{2-}$ 50 years ago.[1,2] Since then, M–M bonds based on virtually every transition element have been prepared (Table 2.1).[3]

Table 2.1 Number of compounds containing M_2^{n+} cores in 2005.

V 11	Cr >500	Mn	Fe 3	Co 8	Ni 9
Nb 7	Mo >1100	Tc >50	Ru >500	**Rh** **>1500**	Pd 3
Ta	W >110	Re >550	Os ~70	Ir 9	Pt >100

By the 1980s M–M bonding in Mo_2,[4,5] Tc_2,[6] Ru_2,[7] Rh_2,[8] Cr_2,[8] Pt_2,[9] W_2,[10] Os_2,[11] and Ir_2 compounds,[12] mostly second- or third-row transition metals, had been described. M–M bond-containing coordination compounds of Nb(II)[13] and Pd(III)[14,15] were first synthesized in the late 1990s. Aside from quadruply bonded Cr_2 compounds, which were first reported in 1844,[16,17] M–M bonded first row transition metal compounds have historically been less well known. Co_2 compounds were first synthesized in 1987,[18]

followed by V_2 and Fe_2 compounds, first synthesized in the 1990s.[19-21] Rh_2 complexes are the most abundant M–M bond containing coordination compounds.[3]

Of all the reported M–M bond containing species, only Rh_2 complexes have a long-standing importance in catalysis. Recent synthetic and mechanistic investigations have revealed catalytic roles for both Ru_2[22] and Pd_2 [23] complexes as well, however the most effective catalysts for C–H functionalization are still Rh_2 complexes.[24] This dissertation will solely focus on Rh_2 complexes and the structural and electronic factors that contribute to their ability to act as catalysts.

2.2 M–M Bonding

The valence orbitals of the transition metals are d orbitals, and it is d-orbital overlap that must be considered when discussing M–M bonds. In a given binuclear transition metal complex in which the metal centers are within bonding distance, three types of orbital overlap can occur. The d_z^2 orbital of each metal atom can overlap to form σ bonding and antibonding combinations, the d_{xz} and d_{yz} orbitals can overlap forming π-bonding and antibonding sets, and the d_{xy} and $d_{x^2-y^2}$ orbitals can overlap to form δ bonding and antibonding orbitals. In the absence of exogenous ligands on the metal atoms, the relative energies of these orbitals would be based solely on the degree of orbital overlap; the orbitals would increase in energy as follows: $\sigma < \pi_1,\pi_2 < \delta_1,\delta_2 < \delta^*_1,\delta^*_2 < \pi^*_1,\pi^*_2 < \sigma^*$ (Figure 2.1).

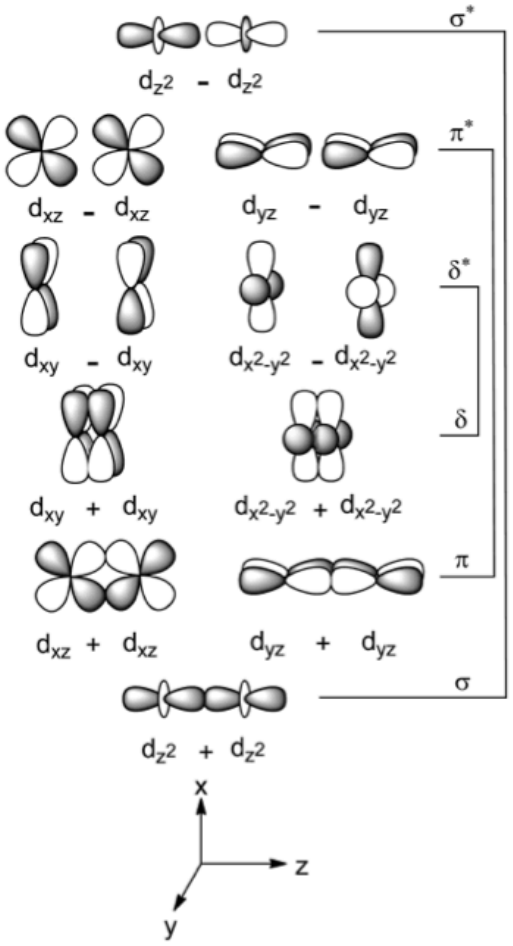

Figure 2.1 Bonding and antibonding combinations of d orbitals used to construct M–M bonds.

As ligands are added to the binuclear unit, those orbitals that engage strongly in metal–ligand (M–L) bonding will be utilized mainly for that purpose and will therefore contribute little to M–M bonding.[2] For example, the compounds reviewed here generally will have four σ-donor ligands (L) attached to each metal atom in a roughly square disposition, $L_4M–ML_4$, where L represents only the atoms coordinated to the metal centers. If we allow these M–L bonds to form along the x and y vectors (Figure 2.1), then

the lone pairs of the L atoms will be properly oriented in such a way as to interact strongly with the $d_{x^2-y^2}$ -derived orbitals. Thus, this set of δ and δ* orbitals will be used solely to make M–L bonds and will not contribute strongly to M–M bonding. In $L_4M–ML_4$ compounds that have all of the M–M bonding orbitals filled and all of the antibonding orbitals empty, we find a maximum M–M bond order of four, corresponding to a $\sigma^2\pi^4\delta^2$ electron configuration.[3] Both oxidation or reduction of complexes with the $\sigma^2\pi^4\delta^2$ configuration decreases the bond order. For example, there are two ways to make M–M triple bonds in the $L_4M–M\ L_4$ geometry: The first is to remove the two δ electrons as in Mo_2(III,III) complexes yielding an "electron poor" $\sigma^2\pi^4$ triple bond; the second is to add two electrons to the δ* antibonding orbital yielding an "electron-rich" $\sigma^2\pi^4\delta^2\delta^{*2}$ triple bond. In the case of Rh_2 compounds, we will deal with an "electron-rich" $\sigma^2\pi^4\delta^2\delta^{*2}\pi^{*4}$ single bond. In instances when heavily donating equatorial ligands are used, the energy of the $d_{x^2-y^2}$ -derived antibonding orbitals is increased, rearranging the relative orbital ordering from $\sigma^2\pi^4\delta^2\delta^{*2}\pi^{*4}$ to $\sigma^2\pi^4\delta^2\pi^{*4}\ \delta^{*2}$.

2.3 Important Physical and Spectroscopic Properties Rh_2 Complexes

Spectroscopic and electrochemical methods are useful for studying catalysts in solution, and the Rh–Rh bonds in the compounds discussed here give rise to some unique spectral features and electrochemical properties that can be used to assess the electronic structure of the catalysts. Some of the most useful spectroscopic methods are reviewed

below with examples of physical features of various Rh_2 complexes that will be discussed later in the context of catalysis.

2.3.1 Absorption Spectroscopy

One of the simplest methods for assessing the electronic structure of Rh–Rh bond-containing compounds is electronic absorption spectroscopy. This method directly probes electronic transitions, which can be readily correlated to a molecular orbital picture, giving insight into bonding. Most importantly, changes in metal oxidation states are typically accompanied by major changes in the features of the electronic spectrum. Thus, absorption spectra of catalysts *in situ* allow for an assessment of metal oxidation states by comparison with the expected signature absorption features.

Rh_2(II,II) tetracarboxylates show two distinct bands in the visible region, Band I at ~600-700 nm, and Band II at ~450 nm. Although conflicting assignments of Band I appear in the literature,[25-29] a preponderance of evidence favors assignment of this band as the Rh_2 $\pi^* \rightarrow Rh_2$ σ^* HOMO to LUMO transition. This evidence includes the observed x,y polarization of this band,[25] a 297 cm^{-1} vibronic progression observed at 15 K attributable to the Rh–Rh stretching frequency of the $\pi^{*3}\sigma^{*1}$ excited state,[27] magnetic circular dichroism intensity consistent with a σ^* excited state,[30] and variation of the energy of this band as a function of the axial ligands.[25] An Rh_2-carboxylate compound characterized having no axial ligands shows Band I at very low energy, 760 nm.[31] Band II is assigned as an Rh_2 $\pi^* \rightarrow$ Rh–O σ^* transition.

Oxidation of Rh_2(II,II) tetracarboxylates to the Rh_2(II,III) level is accompanied by drastic changes in the electronic spectrum (e.g., oxidation of **a** to **d** in Figure 2.2).[32] The most striking feature is the appearance of a new band, Band Ia, at ~800 nm. The Rh_2(II,II) Bands I and II both shift to higher energy to become Band IIa and Band IIIa in the Rh_2(II,III) species, and Band IIIa gains significant intensity. On the basis of early SCF-Xα-SW calculations on $[Rh_2(OAc)_4(H_2O)_2]^+$,[33] the ground state was assigned to the $\sigma^2\pi^4\delta^2\pi^{*4}\delta^{*1}$ configuration, although subsequent EPR studies suggest a $\sigma^2\pi^4\delta^2\delta^{*2}\pi^{*3}$ configuration.[34] Nevertheless, the SCF-Xα-SW results were used to interpret the electronic spectrum. It is suggested that Band IIIa is a Rh_2 $\pi^* \rightarrow$ Rh–O σ^* transition and that Band IIa is a Rh_2 $\pi^* \rightarrow$ Rh_2 σ^* transition, as in the Rh_2(II,II) species.[33] Band Ia has been assigned tentatively as a $\delta \rightarrow \delta^*$ transition,[33] although Band Ia is absent in Rh_2(II,III) mixed acetate/acetamidate compounds;[32] the electronic origin of Band Ia is currently unknown. Observation of such a low-energy band has, however, been useful for assigning the catalyst resting state of Rh_2-mediated intermolecular C–H amination as an Rh_2(II,III) complex (shown in Chapter 3).[35,36]

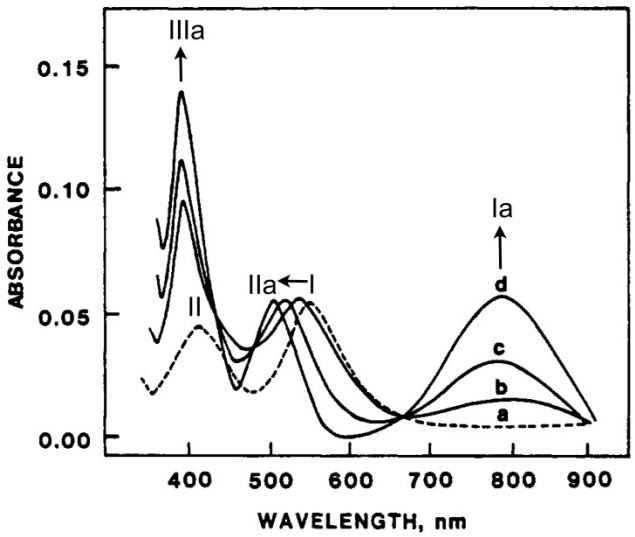

Figure 2.2 Changes in the absorption spectrum of $Rh_2(OAc)_4$ (**a**) upon electrochemical oxidation in acetonitrile. The fully oxidized species is (**d**), and (**b**) and (**c**) are spectra taken at intermediate points. Band assignments are as discussed in the text. This figure is adapted from reference [32].

The major ambiguity in the electronic structure of Rh_2(II,III) complexes is whether the compounds have a $\delta^{*2}\pi^{*3}$ or a $\pi^{*4}\delta^{*1}$ ground state. This ambiguity exists because the π^* and δ^* orbitals in Rh_2 complexes are very close in energy (*vide supra*). In UV photoelectron spectra of $Rh_2(O_2CCF_3)_4$, the π^* and δ^* bands appear overlapped in the spectrum, and a deconvolution of this feature yields an energy difference of only 0.2 eV.[37] Thus, the nature of the ligands bound to the Rh_2(II,III) core can strongly influence whether a $\delta^{*2}\pi^{*3}$ or a $\pi^{*4}\delta^{*1}$ ground state is observed.

2.3.2 Electrochemistry

Many of the catalytic processes discussed here involve chemical steps that are accompanied by M-centered redox chemistry. Thus, it is pertinent to examine the electrochemical properties of catalysts to establish the nature of any redox activity that may influence catalytic mechanisms. Cyclic voltammetry (CV) is the most common method for determining oxidation or reduction potentials of catalysts in solution, and is useful for assessing the reversibility of redox processes.

Rh_2 complexes typically display an electrochemical wave corresponding to the $Rh_2(II,II)/Rh_2(II,III)$ redox couple.[3] For carboxylate compounds, this wave typically appears at over +0.50 V vs Fc/Fc^+ (Fc = ferrocene), and the exact potential depends strongly on the nature of both the equatorial and axial ligands.[3] For example, the $Rh_2(II,II)/Rh_2(II,III)$ redox couple for $Rh_2(OAc)_4(CH_3CN)_2$ appears at +0.77 V in acetonitrile solution,[38] and substitution of the equatorial OAc^- ligands for the more electron withdrawing trifluoroacetate (TFA^-) ligands, i.e. in $Rh_2(TFA)_4(CH_3CN)_2$, leads to a potential of +1.40 V,[39] a change of nearly 0.7 V. The effects of different axial ligands are less pronounced. The redox potential of $Rh_2(OAc)_4$ in a broad range of solvents varies from +0.77 V (in acetonitrile) to +0.58 V (in methanol) versus Fc/Fc^+.[38] Dirhodium complexes with *N,O* donor ligands or *N,N* donor ligands have been observed to display further oxidation waves to $Rh_2(III,III)$ and $Rh_2(III,IV)$ species[40,41] as well as reduction waves to $Rh_2(I,II)$ species,[3] though potential roles for this reduced state in catalysis are not yet known.

2.4 Catalyst Design and Synthesis

Based on the perceived importance of ligand structure on selectivity of group transfer reactions (vide infra), a variety of ligands have been developed for Rh_2 complexes; several common catalysts have been compiled in Figure 2.3 and will be referred to throughout this chapter. The effect of ligands on chemo- and enantioselectivity has been reviewed elsewhere,[42-45] here we will focus on the impact of ligand variation on the redox behavior of Rh_2 complexes and the resulting effect on reactivity. Below is a brief discussion of some of the ligand classes that have been used in dirhodium catalyzed reactions; the ligand classes will be introduced, and subsequently, a brief discussion of reactions catalyzed by these complexes will be presented.

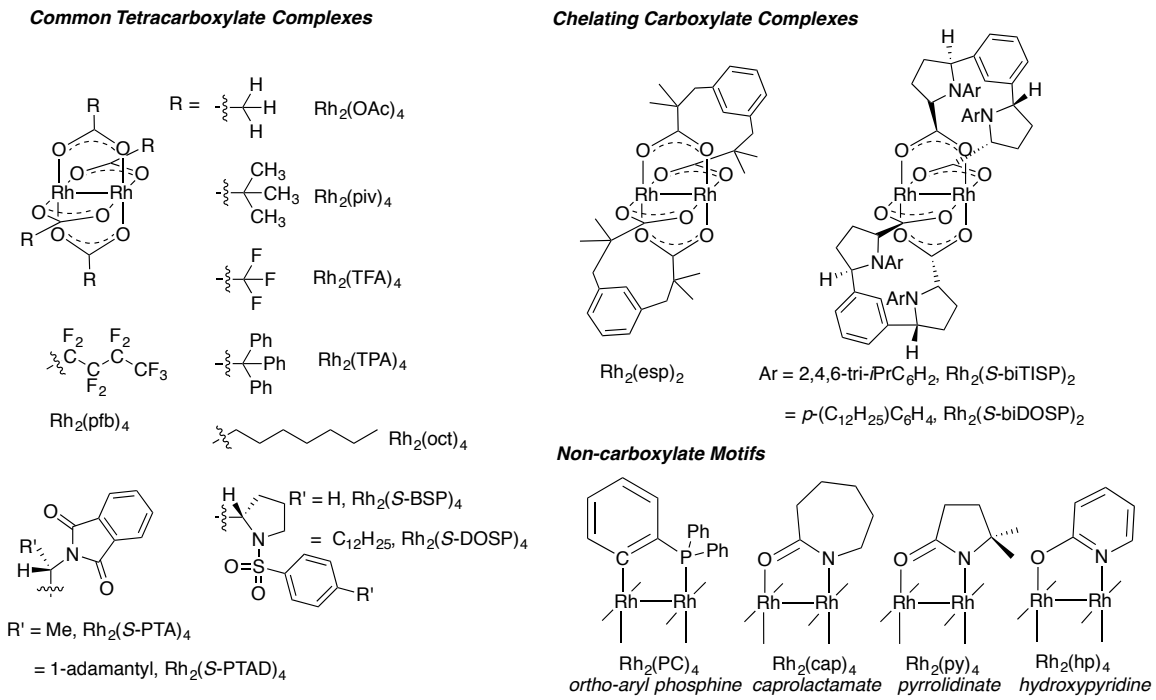

Figure 2.3 Common ligands and Rh_2 complexes used in C–H functionalization.

2.4.1 Rh_2-Carboxylates

The archetypical Rh_2 tetracarboxylate, $Rh_2(OAc)_4$, is easily prepared by treatment of $RhCl_3 \cdot 3H_2O$ with sodium acetate in a mixture of ethanol and acetic acid (Scheme 2.1a).[46,47] Carboxylate exchange is another useful synthetic method for accessing Rh_2-carboxylate species, whereby compounds such as $Rh_2(OAc)_4$ or $Rh_2(TFA)_4$ react with an excess of carboxylic acid to achieve ligand exchange (Scheme 2.1b).[48,49] Rh_2-tetracarboxylates can also be prepared from $K_4Rh_2(CO_3)_4$,[50] which reacts irreversibly with carboxylic acids to yield the Rh_2-tetracarboxylate product and expel bicarbonate which is converted to CO_2 under the reaction conditions (Scheme 2.1c).[51] Chiral Rh_2-tetracarboxylates may also be prepared through the use of optically pure carboxylic acids, such as naturally occurring amino acids, as ligands.[52-55]

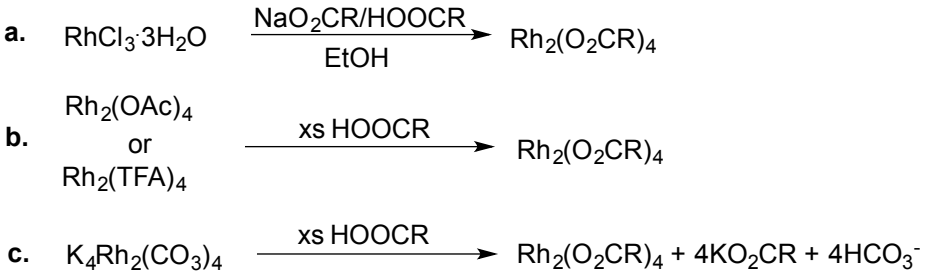

Scheme 2.1 General synthesis of dirhodium compounds a) Starting from mononuclear Rh(III) b) Ligand metathesis starting from dimeric Rh_2(II,II) c) Starting from Rh_2(II,II) carbonate

The most common preparative method for making $Rh_2(OAc)_4$ yields the deep blue/green bis-methanol adduct from a recrystallization of the crude reaction (Scheme 2.2a).[46] Methanol can be removed from the axial positions by heating under vacuum, and

two resulting compounds have been described. Prolonged heating at 100 °C will convert $Rh_2(OAc)_4$•2MeOH into a bright green insoluble form that is proposed to be a coordination polymer of $Rh_2(OAc)_4$ in which carboxylate oxygen atoms from one molecule can bridge to coordinate to the axial sites of the next molecule in the chain (Scheme 2.2b).[46] Heating $Rh_2(OAc)_4$•2MeOH under vacuum for less than 24 hours at 40–50°C reportedly leads to an olive green axial ligand free form of $Rh_2(OAc)_4$, which is considerably more reactive than the polymeric form.[56] Additionally, the axial ligands are labile and ligand exchange will typically take place when the Rh_2 complex is dissolved or recrystallized from the desired axial ligand as solvent.

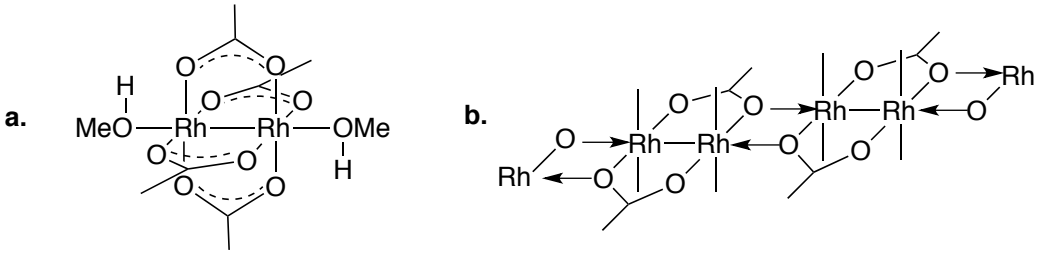

Scheme 2.2 a) $Rh_2(OAc)_4$ with two MeOH molecules axially ligated; b) General scheme for a coordination polymer of an Rh_2-carboxylate complex similar to $Rh_2(OAc)_4$.

A number of Rh_2 complexes with chelating dicarboxylate ligands have been prepared and used as catalysts for C–H functionalization.[57-60] These compounds are also prepared by carboxylate exchange. There are two important effects of using these chelating dicarboxylate ligands in catalysis. One is that these chelating dicarboxylate ligands enhance catalyst stability via the chelate effect.[59,61] Secondly, chelating ligands can lower the effective symmetry of the Rh_2 complexes, breaking the four-fold axis along

the Rh–Rh vector. With chiral, C_2-symmetric chelating dicarboxylate ligands, the resulting Rh_2 complexes will have D_2 symmetry.[57,58] This represents one strategy for influencing how chirality is conferred in asymmetric C–H functionalization.

2.4.2 Rh_2-Carboxamidates

An important class of Rh_2 catalysts are complexes of ligands that are more basic than carboxylates. These include *N,O*-donors such as hydroxypyridinates or carboxamidates. Changing from *O,O*-donor equatorial ligands to *N,O*-donors has three major effects on Rh_2(II,II) complexes. First, unlike an Rh_2-tetracarboxylate complex, an Rh_2-tetracarboxamidate compound can potentially have four isomers as shown in Scheme 2.3. The most common isomer is the *cis*-(2,2) isomer, in which each Rh atom is ligated by two N atoms and two O atoms in a *cis* orientation.[62] Second, carboxamidate ligands are more kinetically inert than carboxylates, and, to our knowledge, there is no evidence that these isomers may interconvert in solution. Third, Rh_2-tetracarboxamidate compounds have considerably lower oxidation potentials to reach the Rh_2(II,III) state as compared with that of carboxylate compounds.[62] While Doyle notes that this effect can be detrimental to carbene reactions, which fail if the catalyst becomes oxidized to the Rh_2(II,III) state, it has been possible to capitalize on this feature to use Rh_2-tetracarboxamides to catalyze oxidation reactions.[62,63] Recently, the use of discrete Rh_2(II,III) dimers has been expanded to C–H amination chemistry (as in Chapter 5).[64] Unlike Rh_2 carboxamidates, Rh_2 amidinate complexes, bearing highly electron donating

N,N-bridging ligands, are relatively rare and are infrequently used as group transfer catalysts, and are thus not discussed here.

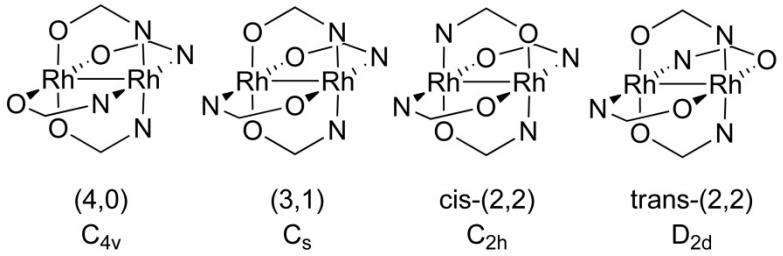

Scheme 2.3 Isomers of Rh_2-carboxamidates.

Although Rh_2-carboxamidates are less efficient at diazo compound decomposition due to their attenuated electrophilicity, [62] they find general utility in protocols for oxidation chemistry,[65,66] as well as aziridination chemistry.[67] The difference in reaction scope for Rh_2-carboxamidate complexes compared with carboxylate complexes is likely due to the fact that the former readily undergo one-electron redox processes due to lowered oxidation potential, yielding mixed-valent Rh_2(II,III) species that may be amenable to radical chemistry. Aziridination chemistry is favored by Rh_2-carboxamidate catalysts, likely due to the lower oxidation potentials observed for these species.[67] Du Bois and co-workers first made this observation in 2002 using $Rh_2(tfacam)_4$ (tfacam = F_3CCONH) for olefin aziridination,[68] followed by studies by Doyle and co-workers using $Rh_2(cap)_4$ (cap = caprolactamate) in 2005.[67]

2.5 Dirhodium Catalyzed C–H Functionalization Chemistry

C–H functionalization is a field of current interest, and many methodologies for achieving selective C–H functionalization continue to appear in the literature.[23,69-81] These can generally be classified into one of two mechanism regimes, as shown in Scheme 2.4.[24] First, in the atom-transfer mechanism (ATM), which is reminiscent of C–H functionalization reactions that take place in Cytochrome P450s,[82] a reactive metal complex having a metal-ligand multiple bond, denoted M=E, reacts to insert E directly into the substrate C–H bond to form product. In Cytochrome P450, the reactive metal complex is the thiolate-ligated heme iron cofactor and E is an oxygen atom. Conceptually, the ATM may be thought to occur either in a two step sequence, beginning with H-atom abstraction to form an iron hydroxo complex and an organic radical, followed by radical recombination to form the hydroxlyated product (Scheme 2.4a), or by a single-step, concerted insertion of E into the C–H bond (Scheme 2.4b). Evidence for the stepwise mechanism has been found in Cytochrome P450s.[82]. Importantly, E does not have to be an oxygen atom – it can be other fragments that can form a metal–ligand multiple bond.

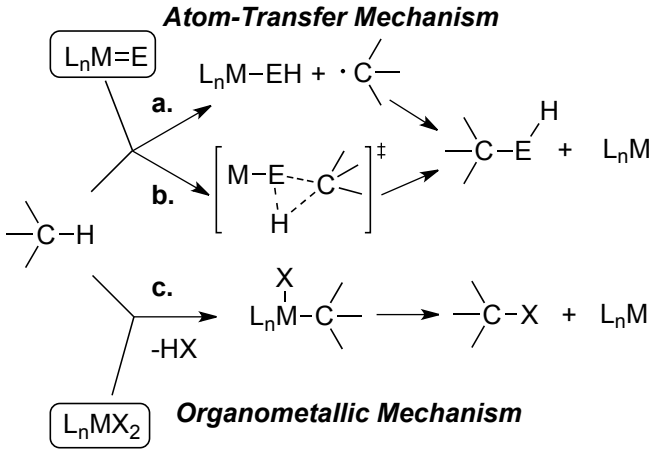

Scheme 2.4 The two general mechanistic pathways involved in C–H functionalization: a) Radical abstraction/recombination (ATM); b) Concerted insertion (ATM); c) Inner-sphere C–H insertion (OM).

The second mechanistic paradigm for C–H functionalization involves the intermediacy of species with M–C bonds, and we therefore call it the organometallic mechanism (OM) (Figure 2.4c). C–H metallation to generate the requisite M–C bonds can proceed via various pathways: oxidative addition of a C–H bond to a coordinatively unsaturated transition metal fragment,[83] electrophilic substitution reactions, and concerted metallation-deprotonation (CMD) reactions are all pathways for C–H metallation.[84] The product-forming step in the OM is frequently reductive elimination of a C–X bond-containing product (Scheme 2.4c). In any given transformation proceeding by the OM pathway, it may be necessary for ligand metathesis reactions or oxidation steps to occur between metallation and reductive elimination in order to install the desired X ligand on the metal center and to facilitate C–X reductive elimination. The pitfalls associated with

the OM include translating stoichiometric to catalytic reactivity, kinetic inertness of intermediates, and the necessity of accessory reagents to properly balance reaction stoichiometry. In contrast, ATM is elegant, assuming M=E formation is favorable.

2.5.1 Carbenoid Chemistry

Carbenes are divalent-carbon-containing species that are typically highly reactive and have been studied since the early 20th century.[85] Carbenes were first proposed in 1903 in studies of the photolytic and thermolytic decomposition of ethyl diazoacetate.[86] Staudinger demonstrated the cyclopropanation of olefins proceeding from free carbenes in 1912.[87] Free carbenes can participate in a variety of reactions such as cyclopropanation, C–H insertion, and X–H insertion,[88-90] and early reports of carbene reactivity generally noted poor selectivity when more than one reaction pathway was available (Scheme 2.5).[90]

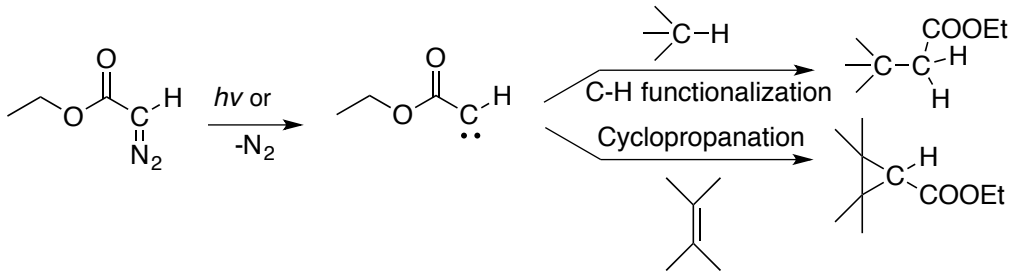

Scheme 2.5 Free carbenes participate in both C–H insertion and cyclopropanation reactions.

The first report of carbene generation from diazoalkanes by use of a transition metal was in 1952 when copper bronze and copper oxide were shown to promote insertion reactions of diazoalkanes into O−H, N−H and C−H bonds.[91] This was soon followed by reports of intramolecular ring-closing C−H insertions of diazo compounds, also catalyzed by simple copper catalysts.[92] The first intermolecular cyclopropanation from diazomethane was reported in 1963, also catalyzed by Cu.[93] Early reports of Cu-carbenoid reativity were important in that they demonstrated that selectivity in carbene reactions could be influenced by the transient stabilization of a carbene by a metal center, referred to as a metallocarbenoid. The discovery of carbenoid-type reactivity resulting from the decomposition of diazo compounds by mononuclear Cu complexes, which is still a flourishing research field,[44,94] led to broad interest in the development of metal-carbenoid chemistry.

Overview of Rh_2-Carbenoid Reactivity

Dirhodium tetracarboxylates were first used in the C–H functionalization of hydrocarbons in 1981.[95] Seminal reports by Teyssié and co-workers showed intermolecular C–C bond formation from diazo compounds with $Rh_2(TFA)_2$ (TFA = trifluoroacetate) and simple long-chain alkanes.[95] The C–H site selectivity preferences of reactions of free photolytically generated carbenes as compared to reactions using $Rh_2(TFA)_2$ were evaluated and a greater level of chemoselectivity for 2° C–H bonds over 1° C–H bonds was observed when $Rh_2(TFA)_2$ was used (Scheme 2.6). As seen in this example, Rh_2-carbenoids are typically generated by Rh_2-mediated decomposition of

diazo compounds and display electrophilic reactivity, participating in insertion reactions with electron-rich C–H bonds. This example further highlights the control of product selectivity that metal carbenoids can offer as compared to free carbenes, and Rh carbenoid intermediates have become topics of significant interest in the development of new synthetic methodologies.[90,96-100]

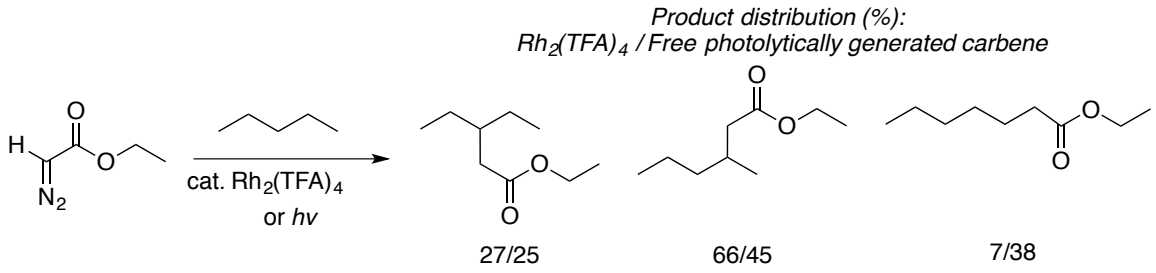

Scheme 2.6 Site selectivities using $Rh_2(TFA)_4$ as a catalyst compared with photolytically generated free carbene. Insertion into primary C–H bonds is suppressed when $Rh_2(TFA)_4$ is used as a diazo decomposition catalyst.

Current Mechanistic Understanding of Carbenoid Chemistry

A generic mechanism for carbene generation from diazo compounds and C–H insertion of the resulting carbene into a C–H bond is shown in Scheme 2.7. Diazo decomposition is generally proposed to proceed by coordination of the diazo compound to the Rh_2 core followed by N_2 expulsion to generate an Rh_2 carbenoid.[101] C–H insertion proceeds from an Rh_2-carbenoid via a proposed concerted asynchronous transition state (Scheme 2.7).[101] Rh_2-catalyzed carbene transformations can be very efficient with turnover numbers of $>10^6$ being reported for some transformations.[102] Because of the

efficiency of Rh_2 catalysts in carbenoid transformations, direct spectroscopic studies of the putative Rh_2-stabilized carbene intermediate were unavailable until the work presented in Chapter 6.

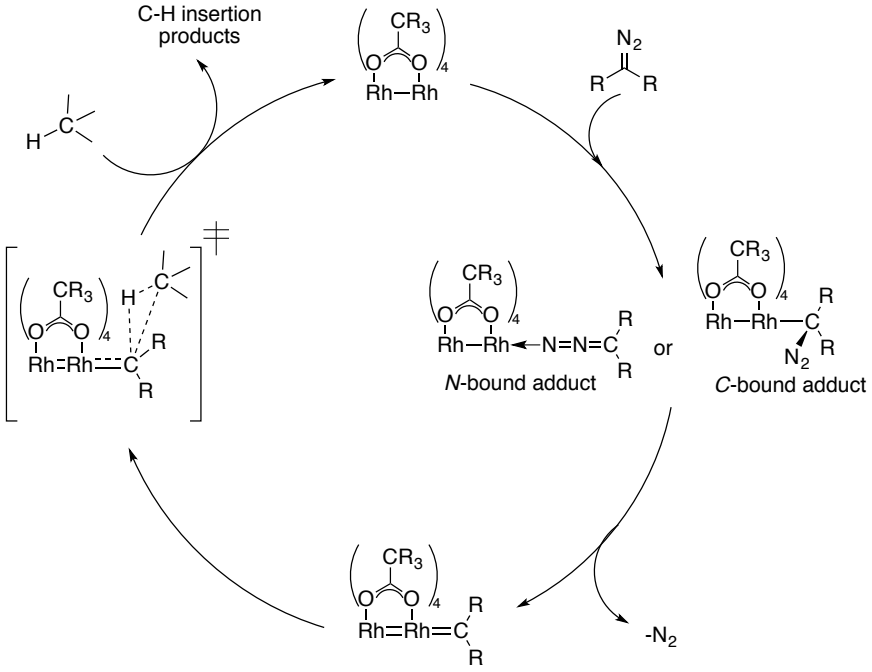

Scheme 2.7 A proposed mechanism for Rh_2-catalyzed C–H functionalization with diazo compounds

A three-center/four-electron (3c/4e) bonding manifold involving the orbitals of σ and π symmetry on both Rh atoms and the carbene/nitrene center has been proposed as important to the reactivity of dirhodium carbenes and nitrenes[103] As shown in Figure 2.4, the three σ (π) atomic orbitals combine to form three molecular orbitals: a three-center bonding orbital in which all orbitals are in phase, a non-bonding orbital having a node at

the central Rh atom, and a completely out of phase antibonding combination. In the case of Rh_2 carbene or nitrene species, the bonding and non-bonding orbitals are filled and the antibonding orbitals are empty, leading to their description as having 3c/4e bonds of both σ and π symmetry. In comparison with conventional 2c/2e bonds, the Rh–Rh–C(N) 3c/4e bonds are weaker and the antibonding combinations lie lower in energy, leading to more reactive terminal M=E (E = CR_2, NR) groups in binuclear species.[103] While we draw the Rh_2-carbenoid and nitrenoid species as having an Rh=E double bond, computed bond orders are significantly lower than 2.0 (see Chapter 6).[103]

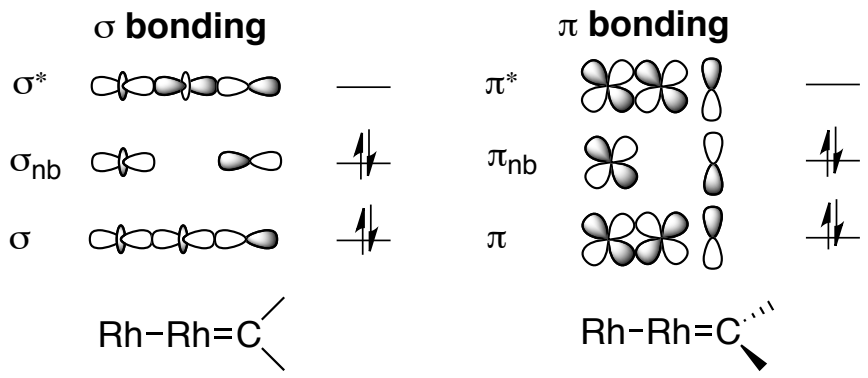

Figure 2.4 Depiction of σ and π bonding orbitals in a 3c/4e manifold for an Rh_2-carbenoid. The terminal Rh=C bond is lengthened by the 3c/4e interaction, thus enhancing reactivity.

Much of what we know about the impact of ligand perturbation on carbenoids comes from characterization of catalytic product distributions as a function of ligand

structure. An early study by Doyle and co-workers investigated the C–H functionalization of simple hydrocarbons by various $Rh_2(OAc)_4$ derivatives and indicated that site selectivity was catalyst controlled.[104-106] This study demonstrated that ligand electronic effects can effectively switch between competitive reaction pathways by influencing the relative charge on the reactive carbenoid carbon.[105] Because ligand electronic effects can so readily alter reactivity patterns, investigation of the selectivity of C–H functionalization reactions has become a prominent indirect method for understanding the nature of the Rh_2-carbene intermediate.

Since carbenoid chemistry does not rely on covalently linked directing groups in either catalyst or substrate, selectivity is a function of the delicate interplay of electronics and sterics of the putative carbene species. Electronic effects have a long-standing importance in selectivity,[106] but steric considerations are quickly becoming important predictors for this as well. Davies and coworkers have pioneered predictive steric models for understanding regio- and enantioselectivity for intermolecular reactions using donor-acceptor carbenoids;[107-110] a simplified example of such a model is depicted in Figure 2.5. When a catalyst is designed to contain bulky groups that can block substrate access, Davies and coworkers argue that the least encumbered approach of the substrate can be readily predicted, thus providing a handle for predicting selectivity. An excellent tutorial review on the subject can be found in the recent literature.[71]

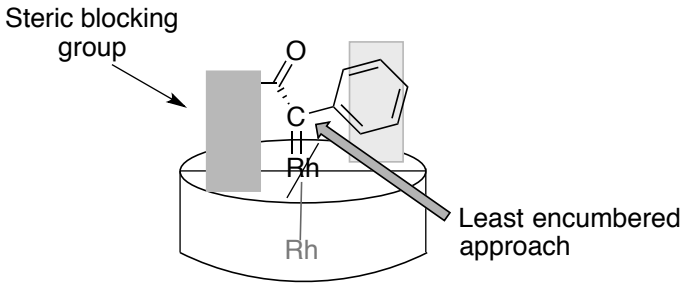

Figure 2.5 An example of a steric model for predicting catalyst selectivity.

Early mechanistic studies examined relative rates of cyclopropanation by various Rh_2 catalysts.[111] An important study by Doyle and co-workers compared cyclopropane formation from $(CO)_5W{=}CHC_6H_5$ to cyclopropane formation from $C_6H_5CHN_2/Rh_2(OAc)_4$ with alkenes.[112] Similar linear free energy relationships were observed for both the cyclopropanation of various monosubstituted alkenes by catalytic $C_6H_5CHN_2/Rh_2(OAc)_4$ as well as stoichiometric cyclopropanation reactions mediated by pre-formed carbene $(CO)_5W{=}CHC_6H_5$, suggesting that formation of an electrophilic Rh_2-carbenoid precedes cyclopropane production. Since tungsten-carbene complexes are well defined, this was the first evidence of an Rh_2 carbene complex as an intermediate in Rh_2-catalyzed cyclopropanations.[105] Subsequently, several kinetic studies have been published that outline the mechanism of N_2 extrusion from diazo compounds and propose mechanisms for both carbenoid formation and reactivity with C–H substrates.[113] Hammett analyses, KIE measurements and analysis of product distributions are generally consistent with a concerted C–H insertion mechanism, in agreement with related computational studies.[113,114]

In recent computational work, Davies and co-workers have analyzed the reaction coordinate of Rh_2 complexes with donor/acceptor and acceptor-only diazo compounds to rationalize experimentally observed differences in selectivity between these two types of carbenes (Figure 2.6).[109] It was found that donor/acceptor carbenes substantially stabilize the Rh_2-carbene intermediate, causing a late transition state with substantial charge build-up, and a high potential energy barrier to C–H functionalization (17.4 kcal/mol), making C–H functionalization with donor/acceptor carbenes rate-limiting. The barrier to C–H functionalization is lowered to only 3.5 kcal/mol when the acceptor-only diazo compound is used. This energy barrier causes selectivity to be dependent on both the electronic structure of the substrate as well as steric constraints. Thus, donor/acceptor carbenes discriminate well between small electronic differences in C–H bonds, resulting in highly chemoselective reactions.[109] These computational results are consistent with experiment; the enhanced selectivity of donor/acceptor carbenes had previously been investigated in a Hammett study of cyclopropanation of substituted styrenes. Reactions with methyl 2-diazo-2-phenylacetate (donor/acceptor compound in Figure 2.6) were shown to be strongly influenced by the electronics of the styrene ($\rho = -0.9$, on a $\rho+$ scale), whereas other diazo compounds showed no selectivity.[111]

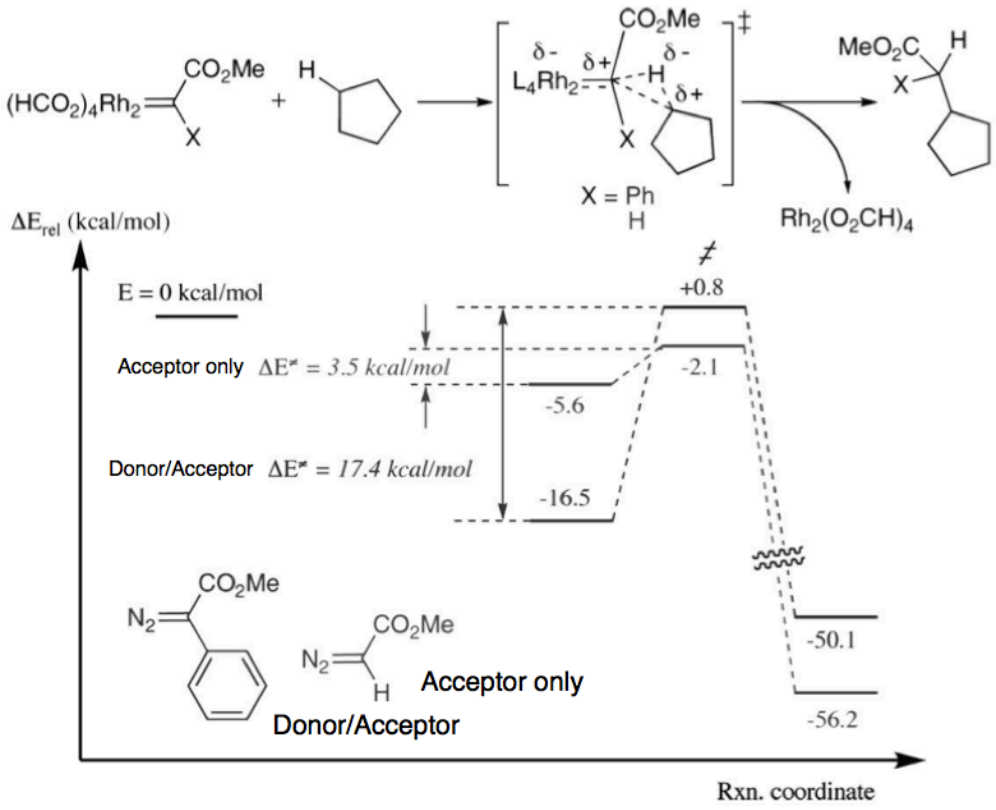

Figure 2.6 Calculated reaction coordinate for C–H insertion: donor/acceptor carbenes are more chemoselective due to enhanced stability of the Rh_2-carbenoid. Figure reprinted with permission from J. Hansen, J. Autschbach and H. M. L. Davies, *J. Org. Chem.*, *74*, 6555 (2009). Copyright 2009 American Chemical Society.

The Role of the M–M Bond in Dirhodium Carbenoid Species

Nakamura reported a computational study of the mechanism for Rh_2-carbenoid C–H functionalization in 2002 in which the role of each of the Rh centers in binuclear Rh complexes during both diazo decomposition and C–H insertion was investigated.[101] This study resulted in two important conclusions: 1) The Rh–Rh interaction is capable of

mediating significant electron delocalization, which results in both enhanced electrophilicity of the carbene carbon, as well as increased facility of Rh−C cleavage. Nakamura refers to this phenomenon as a "bifunctional electron pool", alluding to an orbital manifold that is capable of extensive electron delocalization, in this case, across three centers: the two Rh atoms and the C atom of the carbene ligand.[101] 2) The computational results substantiate the view that the mechanism of C–H functionalization is fundamentally different from organometallic C–H activations, as the Rh atoms do not ever come in contact with alkane C–H bonds. The proposed transition state is consistent with small experimentally observed KIEs and is described as concerted but asynchronous (as in Scheme 2.7). Nakamura also provided an extensive DFT comparison of monometallic Ru-carbenoid complexes [115] with Rh_2-carbenoids, focusing on the importance of the *trans*-effect to reactivity. It is worth noting that mononuclear Rh-porphyrin complexes have been reported to be active in cyclopropanation chemistry, presumably via the intermediacy of an Rh-carbenoid, as early as 1992.[116] It remains a possibility that certain ligand frameworks, such as porphyrins, can act as a bifunctional electron pool, thus facilitating group transfer reactivity.

Computational results have indicated that C–H functionalization occurs using only one of the two Rh atoms of the binuclear core, but the role of the second metal is indispensible to the high activity of these catalysts.[101] The exact role of the second metal cannot be easily investigated due to the synthetic difficulty involved in removing this second metal atom, or in making heterobimetallic analogues for comparison. The only example of a heterobimetallic complex for C–H functionalization is

$BiRh(O_2CCF_3)_3(O_2CCH_3)$.[117] This complex was first reported by Dikarev and co-workers, and later was investigated as a catalyst for diazo decomposition in collaboration with Davies and co-workers.[118] The reactivity of $BiRh(O_2CCF_3)_3(O_2CCH_3)$ was compared with isostructural $Rh_2(O_2CCF_3)_3(O_2CCH_3)$. It was found that the bismuth-containing analog performs favorably as a catalyst in metal-carbenoid transformations and is effective at low catalyst loadings (2 mol%). However, $BiRh(O_2CCF_3)_3(O_2CCH_3)$ decomposes methyl phenyldiazoacetate approximately 1600 times slower than the analogous Rh_2 complex. Computational studies are consistent with the experimental reactivity differences, and suggest that the electronic delocalization across the binuclear core lowers the energy of the C–H insertion transition state.[101] Inefficient orbital overlap between Rh and Bi precludes the binuclear core of these heterometallic dimers from participating in effective delocalization, and thus the activation barriers to group transfer are higher. The cooperativity of a heterometal with respect to C–H functionalization chemistry has been systematically investigated in a computational study describing electrophilic aromatic C–H amination.[119]

2.5.2 Nitrenoid Chemistry

C–H functionalization via nitrene intermediates, which are isoelectronic to carbenes, to generate C–N bonds is attractive for chemical synthesis due to the prevalence of nitrogen-containing molecules in biologically relevant systems.[120-122] Although the putative intermediates of Rh_2-carbene and Rh_2-nitrene chemistry have been described to be analogous in their structure and reactivity, C–H functionalization via nitrenoid

intermediates is far more mechanistically complex than C–H functionalization via carbenoid intermediates and currently is less well understood. Herein we will trace the historical origins of nitrene-type reactions, discuss the structure and reactivity of Rh_2 nitrenes, and draw comparisons between the mechanisms proposed for nitrenoid reactions with those of Rh_2-catalyzed carbenoid reactions.[122]

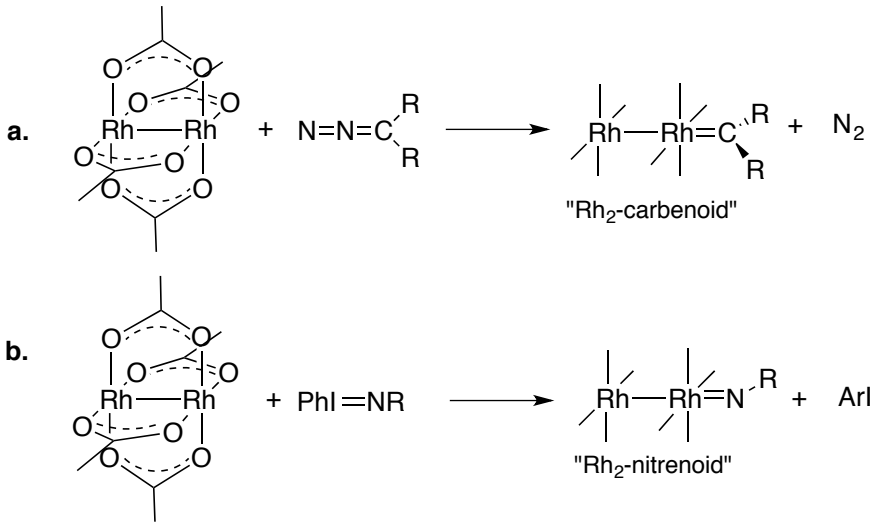

Scheme 2.8 Generation of carbenoid and nitrenoid species from Rh_2-carboxylate complexes

Development of Nitrenoid-Based Reactions

Early reports of transition-metal-mediated nitrenoid transformations utilized Cu catalysts. Kwart and Khan performed seminal work in the decomposition of organic azides and chloramine-T by mononuclear Cu complexes showing the feasibility of C−N bond forming reactions.[123] The use of iminoiodinanes has enabled significant progress to

be made in the development of synthetic methodologies based on nitrene intermediates.[124-126] The decomposition of iminoiodinanes has been observed using various mononuclear complexes (Cu, Ru, Fe, Mn, Co, among others) in addition to Rh_2 complexes, yielding a putative metallonitrenoid and a stoichiometric amount of aryl iodide waste (e.g. Scheme 2.8b).[122] In 1983, Breslow and Gellman identified that the combination of $Rh_2(OAc)_4$ and iminoiodinanes as an *N*-atom source, was a promsing C–H amination protocol. The efficiency of this reaction prompted the investigation of $Rh_2(OAc)_4$ and its derivatives, as well as isostructural Ru_2 complexes, as catalysts for C−H amination. Method development in the field of Rh_2-catalyzed C–H amination has been largely pioneered by Du Bois and co-workers in the early 2000s. Important advances included the generation of iminoiodinanes *in situ*,[127] the identification of competent *N*-atom sources, namely highly electron-withdrawing sulfamate esters (e.g. H_2NTces, Scheme 2.9c),[35,36,59,60,128-130] and the development of new catalysts, such as $Rh_2(esp)_2$ (see Figure 2.3 for structure),[59] which have allowed the development of intermolecular C–H amination reactions.

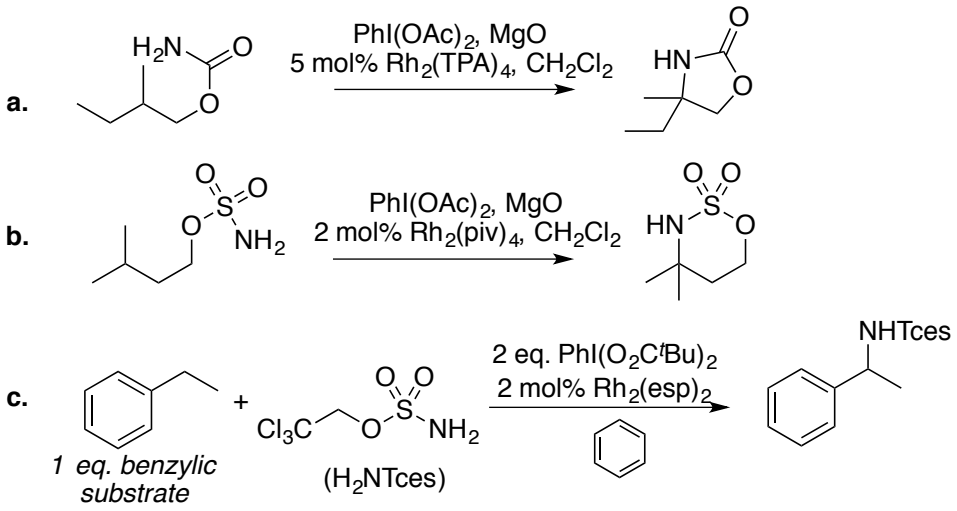

Scheme 2.9 Examples of efficient Rh_2-catalyzed amination reactions a) Intramolecular cyclization using a carbamate ester; b) Intramolecular cyclization using a sulfamate ester; c) Intermolecular oxidative amination of ethyl benzene using $Rh_2(esp)_2$.

Methodology development and catalyst design for C–H amination has been heavily reliant on mechanistic observations, which is why we discuss these topics together in the following sections. Nitrene chemistry has its roots in the decomposition of pre-oxidized *N*-atom sources such as iminoiodinanes or chloramine-T. Due to the similarity of these conditions with the decompostition of diazo compounds used to generate carbene intermediates, early mechanistic models of Rh_2-catalyzed nitrene reactivity were believed to proceed through two-electron steps similar to the atom transfer mechanism discussed for carbene transfer (Scheme 2.10).

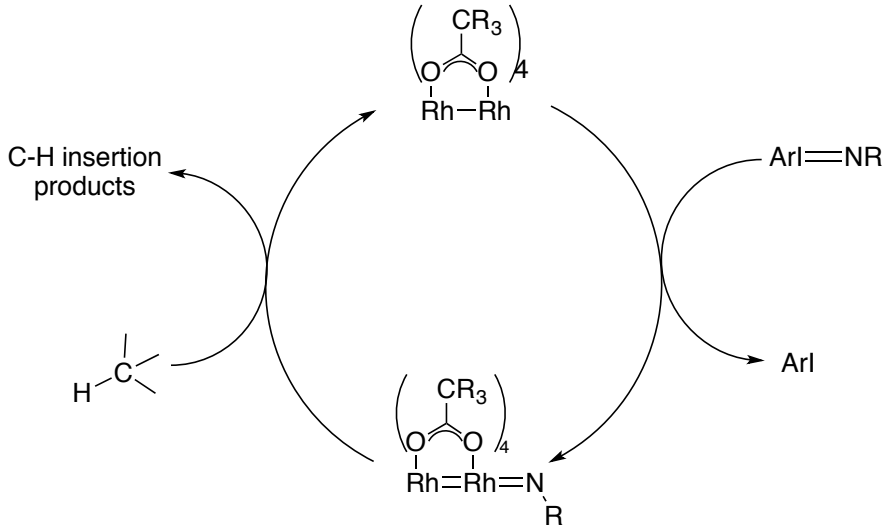

Scheme 2.10 Simplified mechanistic model for Rh_2-nitrene formation and concomitant C–H functionalization.

Carbene chemistry has been shown both experimentally and computationally to follow a mechanistic model like the one outlined for nitrene chemistry in Scheme 2.10 (*vide supra*) due to the fact that Rh_2-carbenes typically form and react on a singlet energy surface.[85] Nitrenes, on the other hand, have a more complicated electronic structure due to the fact that the triplet state for a free nitrene is typically close to, or lower than, the corresponding singlet state.[131,132] The accessibility of a triplet potential energy surface adds a complicating factor to the simple mechanism shown in Scheme 2.10. Modifying the electronics of the nitrene fragment to probe the participation of the triplet surface has not been heavily investigated, however, Schomaker and co-workers have observed differential stereochemical results when comparing sulfamate and carbamate sources in reactions with allenes and Rh_2 catalysts,[133] which suggests that mechanistic differences

can be imparted by the *N*-atom substrate. Due to the nature of nitrenes, radical chemistry is often implicated in nitrene transfer reactions (*vide infra*). An unusual feature of Rh_2-catalyzed C–H amination is that, while intramolecular C–H amination seems to follow the mechanism set forth in Scheme 2.10 closely, intermolecular amination is much more mechanistically complex, presumably because the nitrene intermediate is not immediately trapped by substrate once it is formed.[128] Du Bois and coworkers proposed that enhanced catalyst stability should improve the yield of intermolecular amination, and developed $Rh_2(esp)_2$, featuring chelating *bis*-carboxylates based on this proposal.[59] The emerging importance of one-electron chemistry in C–H amination will be further discussed in the following chapters as we develop a more modern mechanistic model for C–H amination.

Synthetic Scope

Intramolecular C–H amination chemistry is becoming a powerful tool for constructing complex molecular architectures.[121,134] The scope of this chemistry is quite broad, with several examples of atypical alkene/alkane substrates as well as cascade reactions. Schomaker and co-workers have reported intramolecular propargylic C–H amination from carbamate-derived nitrenes[133] and aziridination at allenes.[135] Blakey and co-workers have reported the construction of polycyclic scaffolds via vinyl-cation intermediate traps.[136,137] Intramolecular nitrene chemistry was recently reviewed by Dauban; the reader may find several examples of cascade reactions and heterocycle synthesis therein.[121]

Intermolecular C–H amination is not as well developed and is still mainly focused on the optimization of alkane C–H amination and olefin azirdination reactions. State of the art C–H insertions have been developed by Du Bois and co-workers.[59,128-130] Dodd and Dauban have also developed efficient intermolecular oxyamidations of indoles.[138] Oxidative amination chemistry poses unique challenges as compared to Rh_2-carbenoid chemistry because of the need for a suitable oxidizing agent; intermolecular C–H amination is a particularly challenging transformation. The Du Bois group has optimized intermolecular C–H amination reactions catalyzed by $Rh_2(esp)_2$ and identified that slow addition of hypervalent iodine oxidant ($PhI(O_2C^tBu)_2$) to a solution of substrate and 2,2,2-trichloroethylsulfamate ester is key (Scheme 2.9c).[128] This methodology is state-of-the-art in its reasonably low catalyst loading and efficient conversion of stoichiometric amounts (1 equivalent) of substrate.

A strategy for building the oxidant into the nitrogen substrate was recently developed by Lebel and co-workers. Unlike the conventional paradigm wherein nitrenes are formed by group transfer from iminoiodinane species, Lebel and co-workers show that intermolecular C–H insertion is possible via the decomposition of pre-oxidized 2,2,2-trichloroethyl-*N*-tosyloxycarbamate providing C–H functionalized products in good yields (Scheme 2.11).[139,140] This methodology has developed from the analogous intramolecular reactions.[139] Catalyst loadings for this transformation are somewhat higher than in iminoiodinane reactions (5 mol% as compared with ~2 mol%), however, simple addition of a base is sufficient for catalytic turnover. It is important to note that, similar to iminoiodinanes, the *N*-atom in *N*-tosyloxycarbamates is pre-oxidized, which limits the *N*-

atom source substrate scope. Although this transformation has not been mechanistically investigated, it suggests that nitrene formation need not come from iminoiodinane sources.

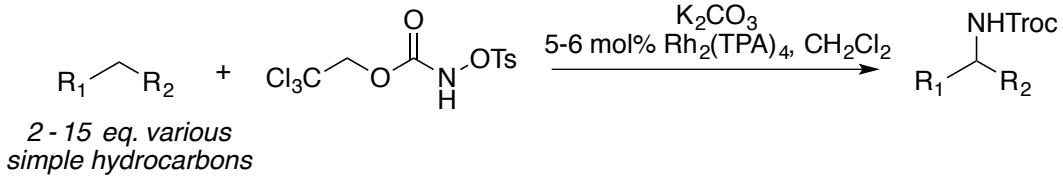

Scheme 2.11 Intermolecular amination from *N*-tosyloxycarbamates.

Rh_2-nitrenes can also be derived from azide precurors. Surprisingly few examples of azide activation using Rh_2 complexes have been reported. Recently, Driver and co-workers reported intramolecular cyclization reactions from organic azides (Scheme 2.12).[141] This work distinguishes itself from other examples of azide reactivity because it does not require a highly electron-withdrawing azide precursor. Isotope labeling studies support an H-atom abstraction/radical-recombination mechanism with an intramolecular KIE of ~6. Thus, an Rh_2-amido radical is a potential intermediate for this transformation. Being able to choose between a concerted or stepwise (radical) nitrene insertion mechanism will have important future applications in terms of site selectivity, and careful choice of both *N*-atom precursor and catalyst will likely play a large role in understanding this dichotomy.

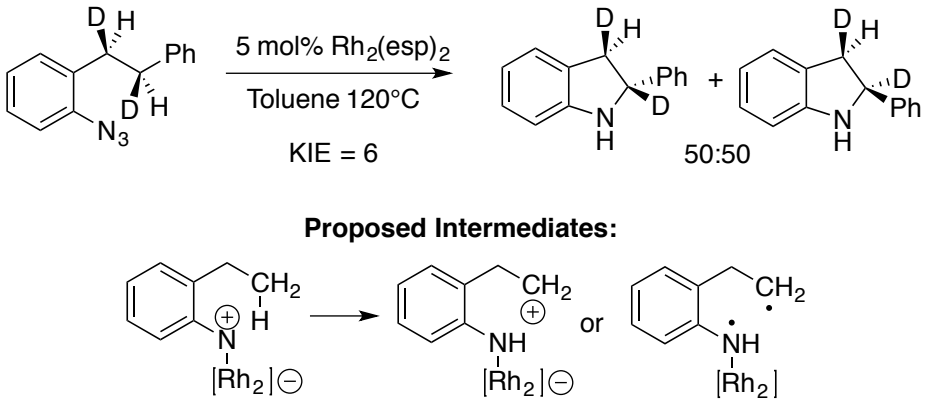

Scheme 2.12 Intramolecular amination using organic azides. Isolation of two diastereomers suggests the intermediacy of a radical (or cation) since scrambling of the C2-stereocenter must occur before recombination.

Current Mechanistic Understanding and its Impact on Catalyst Development

The most generally effective catalyst for intra- and intermolecular C–H amination is $Rh_2(esp)_2$ pioneered by Du Bois and co-workers.[59] This catalyst was initially developed with the idea that a chelating dicarboxylate ligand would prevent catalyst decomposition under the highly oxidizing conditions necessary for C–H amination (simple carboxylates such as $Rh_2(OAc)_2$ have low efficiency in C–H amination and typically decompose to Rh(III) species). Du Bois and co-workers have extensively studied the mechanism of both intra- and intermolecular C−H amination by $Rh_2(esp)_2$ as well as other Rh_2 complexes. Intramolecular amination is facile (compared to intermolecular amination) and can proceed using a variety of simple catalysts such as $Rh_2(OAc)_2$ or $Rh_2(TFA)_2$.

The mechanism of intramolecular C–H amination was investigated using a variety of catalysts: central reactivity patterns include the fact that the active oxidizing species is

an Rh_2-bound nitrene, and that C–H insertion is likely a concerted-asynchronous event based on small KIEs (1.9±0.2) and no observed ring opening in reactions using cyclopropane radical-clock substrates.[130] An interesting finding in the kinetic study of the intramolecular reaction was that the initial rate of product formation was independent of catalyst concentration. Consequently, it is proposed that the condensation of sulfamate ester and oxidant to form an iminoiodinane governs the reaction rate at early reaction times.[128] This is consistent with observations made by Berry and Kornecki who propose two separate mechanistic regimes for intermolecular C–H amination of ethylbenzene by $Rh_2(esp)_2$ that appear to be strongly dependent on the concentration of substrate in solution (see Chapter 3).[36]

The mechanism for intermolecular C–H amination has been shown to be similar to the intramolecular mechanism based on small KIE values, as well as Hammett analyses that indicate a small but discernable cationic charge stabilization in the transition state, which supports a concerted mechanism over radical abstracation/rebound.[128] Intermolecular radical clock experiments, like their intramolecular counterparts, do not show any ring opening. Du Bois and co-workers do note, however, that this does not completely discount a radical mechanism – should a radical mechanism be active, the lifetime of the radical species would have to be extremely short (on the order of 200 fs). The reason that a radical mechanism has not been discounted is that the chemoselectivity of intermolecular C–H amination is opposite to otherwise identical intramolecular conditions. Benzylic C–H bonds are strongly preferred in the intermolecular reaction, while 3° C–H centers are preferred sites for intramolecular amination.[128] This

discrepancy is explained by the fact that selectivity may be a function of the rate at which the Rh_2-nitrene is trapped by substrate versus the rate at which it decomposes via nonproductive pathways. A benzylic position has two equivalent C–H bonds, thus doubling the speed with which it can intercept the Rh_2-nitrene.

An important observation made by Du Bois and coworkers during the study of intermolecular C−H amination was the existence of mixed-valent Rh_2(II,III) species under amination conditions, as exemplified by a color change from green to red.[35,128] A pathway is proposed wherein carboxylic acid byproducts (from hypervalent iodine oxidant decomposition) can reduce the Rh_2(II,III) state back to Rh_2(II,II), which is the proposed active form of the catalyst. [35] It was hypothesized that $Rh_2(esp)_2$ is a better catalyst for the oxidative C–H amination reaction because the kinetic stability of the mixed-valent Rh_2(II,III) state is superior in $Rh_2(esp)_2$ as compared to non-chelating Rh_2-tetracarboxylate complexes.

$Rh_2(esp)_2$ is indeed a more robust catalyst, and interestingly, it has been shown that the resting state of this catalyst is likely a mixed-valent Rh_2(II,III)-amido species; the red color of the catalyst under the reaction conditions is not identical to $Rh_2(esp)_2^+$ free of axial ligation, shown in Chapter 3. Spectroelectrochemical studies on $Rh_2(esp)_2$ have led to the proposal that the Rh_2(II,III) state is accessed during catalysis via a putative proton-coupled electron transfer (PCET) reaction between a sulfamate ester and hypervalent iodine oxidant, which acts as both an oxidant and a base (outer cycle, Scheme 2.13).[36] A second PCET reaction from a putative Rh_2-amido species results in convergence with the two-electron nitrene transfer mechanism.[36] The proposed amido species may have

significant *N*-radical character and it is not yet clear if an Rh_2-amido species can itself be the active oxidant in lieu of a nitrene. This could explain mechanistic aspects of the later reaction stage typically observed for C–H amination vis-à-vis the fast initial reaction rates.

A recent study highlighting the use of desorption electrospray ionization mass spectrometry (DESI-MS) for the capture of reaction intermediates has shown evidence for both an Rh_2-nitrene and an Rh_2-amido in a prototypical C–H amination mixture, further implying that more than one mechanistic pathway may be operative at any given time.[142] More recently, diastereotopic-differentiation at the benzylic methylene position using $Rh_2(esp)_2$ as a C−H amination catalyst was studied; a DFT model that reproduces experimentally observed KIEs was also reported.[143] The study concluded that while *intra*molecular amination reactions proceed through a concerted mechanism,[144] *inter*molecular amination likely occurs via an H-atom abstraction/radical recombination on a singlet energy surface.[143] This conclusion is in agreement with the mechanistic discrepancies between intra- and intermolecular reactivity of $Rh_2(esp)_2$ that are described in Chapters 3 and 4 and noted by Du Bois and coworkers.

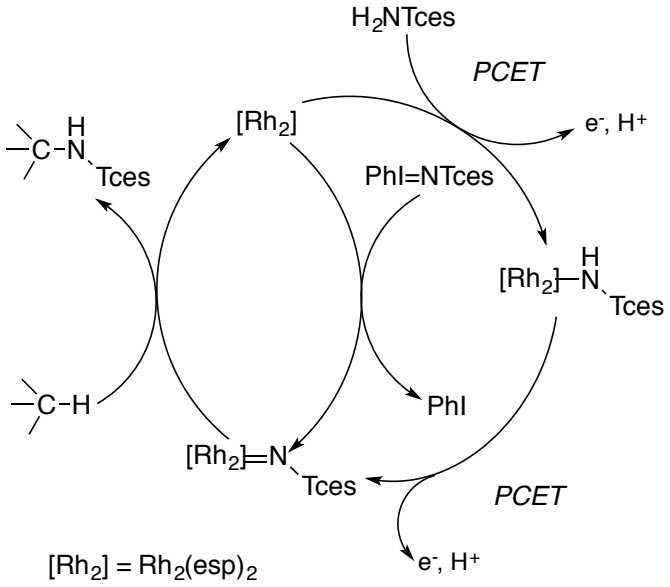

Scheme 2.13 Two possible limiting mechanisms for turnover catalyzed by $Rh_2(esp)_2$. The outer mechanism features the spectroscopically observable catalyst resting state, Rh_2(II,III)-amido.

The necessity of a mixed-valent Rh_2 complex in intermolecular C–H amination chemistry is further implicated in Chapter 4 through the synthesis of Rh_2 compounds with redox-active chelating carboxylates structurally analogous to H_2esp. These complexes are shown to be less effective C–H amination catalysts, presumably due to their inability to access an Rh_2(II,III) state as their resorcinol-based ligands are preferentially oxidized.[60] It is also worth noting that complexes such as Rh_2(S-biTISP)$_2$ (see Figure 2.3 for structure) are not effective at promoting intermolecular amination despite having chelating ligands.[128]

Chapter 5 describes a stable mixed-valent analogue of $Rh_2(esp)_2$ with chelating

diamidate ligands, $Rh_2(espn)_2Cl$ (espn = α,α,α',α'-tetramethyl-1,3-benzenedipropanamidate). This new Rh_2(II,III) catalyst is free of axial chloride in low concentrations as measured by CV, since Cl^- ligated and unligated complexes display different oxidation potentials. $Rh_2(espn)_2Cl$ displays intramolecular selectivity preferences that are similar to $Rh_2(esp)_2$, providing indirect support for a mixed-valent resting state in reactions using $Rh_2(esp)_2$. Furthermore, cationic catalyst $Rh_2(espn)_2Cl$ displays enhanced longevity in simple cyclization reactions compared to $Rh_2(esp)_2$, implying that the stability of the Rh_2(II,III) redox state may be key in designing robust amination catalysts.[64]

2.6 Outline

Chapters 3 – 5 will focus on identifying the factors that enable a catalyst to perform favorably in catalytic oxidative C–H amination reactions. Chapter 3 identifies an important one-electron oxidized catalyst resting state in reactions catalyzed by $Rh_2(esp)_2$. Chapter 4 investigates a series of new Rh_2 catalysts with ligand-based redox activity; it serves to isolate the importance of metal-centered redox activity in Rh_2-mediated nitrene transfer reactions. Chapter 5 describes the synthesis and reactivity of a new mixed-valent Rh_2 complex that is an effective C–H amination catalyst. Chapter 6 delves into carbenoid chemistry and demonstrates the generation and first spectroscopic evidence for an Rh_2-carbenoid intermediate stabilized by a donor/acceptor carbene fragment. Together, these

chapters stand as an advance in the current understanding of electronic structure and mechanism for Rh_2-mediated C−H functionalization.

References

(1) Bertrand, J. A.; Cotton, F. A.; Dollase, W. A. *J. Am. Chem. Soc.* **1963**, *85*, 1349.

(2) Cotton, F. A.; Curtis, N. F.; Harris, C. B.; Johnson, B. F. G.; Lippard, S. J.; Mague, J. T.; Robinson, W. R.; Wood, J. S. *Science* **1964**, *145*, 1305.

(3) Cotton, F. A.; Murillo, C. A.; Walton, R. A. *Multiple Bonds between Metal Atoms*; 3rd ed.; Oxford University Press, 2005.

(4) Lawton, D.; Mason, R. *J. Am. Chem. Soc.* **1965**, *87*, 921.

(5) Brencic, J. V.; Cotton, F. A. *Inorg. Chem.* **1969**, *8*, 7.

(6) Cotton, F. A.; Bratton, W. K. *J. Am. Chem. Soc.* **1965**, *87*, 921.

(7) Bennett, M. J.; Caulton, K. G.; Cotton, F. A. *Inorg. Chem.* **1969**, *8*, 1.

(8) Cotton, F. A.; Deboer, B. G.; Laprade, M. D.; Pipal, J. R.; Ucko, D. A. *J. Am. Chem. Soc.* **1970**, *92*, 2926.

(9) Muraveiskaya, G. S.; Kukina, G. A.; Orlova, V. S.; Evstafeva, O. N.; Poraikoshits, M. A. *Doklady Akademii Nauk Sssr* **1976**, *226*, 596.

(10) Collins, D. M.; Cotton, F. A.; Koch, S.; Millar, M.; Murillo, C. A. *J. Am. Chem. Soc.* **1977**, *99*, 1259.

(11) Cotton, F. A.; Thompson, J. L. *J. Am. Chem. Soc.* **1980**, *102*, 6437.

(12) Rasmussen, P. G.; Anderson, J. E.; Bailey, O. H.; Tamres, M.; Bayon, J. C. *J. Am. Chem. Soc.* **1985**, *107*, 279.

(13) Cotton, F. A.; Matonic, J. H.; Murillo, C. A. *J. Am. Chem. Soc.* **1997**, *119*, 7889.

(14) Umakoshi, K.; Sasaki, Y. *Adv. Inorg. Chem.* **1993**, *40*, 187.

(15) Cotton, F. A.; Gu, J. D.; Murillo, C. A.; Timmons, D. J. *J. Am. Chem. Soc.* **1998**, *120*, 13280.

(16) Peligot, E. *C. R. Acad. Sci.* **1844**, *19*, 609.

(17) Peligot, E. *Ann. Chim. Phys.* **1844**, *12*, 528.

(18) Cotton, F. A.; Poli, R. *Inorg. Chem.* **1987**, *26*, 3652.

(19) Cotton, F. A.; Daniels, L. M.; Murillo, C. A. *Angew. Chem. Int. Ed.* **1992**, *31*, 737.

(20) Cotton, F. A.; Daniels, L. M.; Falvello, L. R.; Murillo, C. A. *Inorg. Chim. Acta* **1994**, *219*, 7.

(21) Cotton, F. A.; Daniels, L. M.; Murillo, C. A. *Inorg. Chim. Acta* **1994**, *224*, 5.

(22) Harvey, M. E.; Musaev, D. G.; Du Bois, J. *J. Am. Chem. Soc.* **2011**, *133*, 17207.

(23) Lyons, T. W.; Sanford, M. S. *Chem. Rev.* **2010**, *110*, 1147.

(24) Davies, H. M. L.; Manning, J. R. *Nature* **2008**, *451*, 417.

(25) Dubicki, L.; Martin, R. L. *Inorg. Chem.* **1970**, *9*, 673.

(26) Norman, J. G.; Kolari, H. J. *J. Am. Chem. Soc.* **1978**, *100*, 791.

(27) Martin, D. S.; Webb, T. R.; Robbins, G. A.; Fanwick, P. E. *Inorg. Chem.* **1979**, *18*, 475.

(28) Bienek, G.; Tuszynski, W.; Gliemann, G. *Z. Naturforsch B Chem. Sci.* **1978**, *33*, 1095.

(29) Miskowski, V. M.; Schaefer, W. P.; Sadeghi, B.; Santarsiero, B. D.; Gray, H. B. *Inorg. Chem.* **1984**, *23*, 1154.

(30) Trexler, J. W.; Schreiner, A. F.; Cotton, F. A. *Inorg. Chem.* **1988**, *27*, 3265.

(31) Cotton, F. A.; Hillard, E. A.; Murillo, C. A. *J. Am. Chem. Soc.* **2002**, *124*, 5658.

(32) Chavan, M. Y.; Zhu, T. P.; Lin, X. Q.; Ahsan, M. Q.; Bear, J. L.; Kadish, K. M. *Inorg. Chem.* **1984**, *23*, 4538.

(33) Norman, J. G.; Renzoni, G. E.; Case, D. A. *J. Am. Chem. Soc.* **1979**, *101*, 5256.

(34) Kawamura, T.; Maeda, M.; Miyamoto, M.; Usami, H.; Imaeda, K.; Ebihara, M. *J. Am. Chem. Soc.* **1998**, *120*, 8136.

(35) Zalatan, D. N.; Du Bois, J. *J. Am. Chem. Soc.* **2009**, *131*, 7558.

(36) Kornecki, K. P.; Berry, J. F. *Chem. Eur. J.* **2011**, *17*, 5827.

(37) Lichtenberger, D. L.; Pollard, J. R.; Lynn, M. A.; Cotton, F. A.; Feng, X. J. *J. Am. Chem. Soc.* **2000**, *122*, 3182.

(38) Kawamura, T.; Katayama, H.; Nishikawa, H.; Yamabe, T. *J. Am. Chem. Soc.* **1989**, *111*, 8156.

(39) Das, K.; Kadish, K. M.; Bear, J. L. *Inorg. Chem.* **1978**, *17*, 930.

(40) Bear, J. L.; Han, B.; Wu, Z.; Van Caemelbecke, E.; Kadish, K. M. *Inorg. Chem.* **2001**, *40*, 2275.

(41) Bear, J. L.; Van Caemelbecke, E.; Ngubane, S.; Da-Riz, V.; Kadish, K. M. *Dalton Trans.* **2011**, *40*, 2486.

(42) Doyle, M. P.; Forbes, D. C. *Chem. Rev.* **1998**, *98*, 911.

(43) Davies, H. M. L.; Dick, A. R. In *Top. Curr. Chem.*; Yu, J.-Q., Shi, Z., Eds.; Springer-Verlag Berlin: Berlin, 2010; Vol. 292, p 303.

(44) Doyle, M. P.; Duffy, R.; Ratnikov, M.; Zhou, L. *Chem. Rev.* **2009**, *110*, 704.

(45) Davies, H. M. L.; Beckwith, R. E. J. *Chem. Rev.* **2003**, *103*, 2861.

(46) Rempel, G. L.; Legzdins, P.; Smith, H.; Wilkinson, G. *Inorg. Synth.* **1972**, *13*, 90.

(47) Winkhaus, G.; Ziegler, P. *Z. Anorg. Allgem. Chem.* **1967**, *350*, 51.

(48) Bear, J. L.; Kitchens, J.; Willcott, M. R. *J. Inorg. Nucl. Chem.* **1971**, *33*, 3479.

(49) Cotton, F. A.; Norman, J. G. *J. Am. Chem. Soc.* **1972**, *94*, 5697.

(50) Wilson, C. R.; Taube, H. *Inorg. Chem.* **1975**, *14*, 405.

(51) Roos, G. H. P.; McKervey, M. A. *Synth. Commun.* **1992**, *22*, 1751.

(52) Golubnichaya, M. A.; Baranovskii, I. B.; Mazo, G. Y.; Shchelokov, R. N. *Zhurnal Neorganicheskoi Khimii* **1981**, *26*, 2868.

(53) Bontcev, P. R.; Miteva, M.; Zhecheva, E.; Mechandjiev, D.; Pneumatikakis, G.; Angelopoulos, C. *Inorg. Chim. Acta* **1988**, *152*, 107.

(54) Koralewicz, M.; Pruchnik, F. P.; Szymaszek, A.; Wajda-Hermanowicz, K.; Wrona-Grzegorek, K. *Transition Met. Chem. (London)* **1998**, *23*, 523.

(55) Davies, H. M. L.; Bruzinski, P. R.; Lake, D. H.; Kong, N.; Fall, M. J. *J. Am. Chem. Soc.* **1996**, *118*, 6897.

(56) Berry, J. F.; Cotton, F. A.; Huang, P. L.; Murillo, C. A.; Wang, X. P. *Dalton Trans.* **2005**, 3713.

(57) Davies, H. M. L.; Kong, N. *Tetrahedron Lett.* **1997**, *38*, 4203.

(58) Davies, H. M. L.; Panaro, S. A. *Tetrahedron Lett.* **1999**, *40*, 5287.

(59) Espino, C. G.; Fiori, K. W.; Kim, M.; Du Bois, J. *J. Am. Chem. Soc.* **2004**, *126*, 15378.

(60) Kornecki, K. P.; Berry, J. F. *Eur. J. Inorg. Chem.* **2012**, 562.

(61) Bickley, J.; Bonar-Law, R.; McGrath, T.; Singh, N.; Steiner, A. *New J. Chem.* **2004**, *28*, 425.

(62) Doyle, M. P. *J. Org. Chem.* **2006**, *71*, 9253.

(63) Catino, A. J.; Nichols, J. M.; Choi, H.; Gottipamula, S.; Doyle, M. P. *Org. Lett.* **2005**, *7*, 5167.

(64) Kornecki, K. P.; Berry, J. F. *Chem. Commun.* **2012**, *48*, 12097.

(65) Catino, A. J.; Raymon, E. F.; Doyle, M. P. *J. Am. Chem. Soc.* **2004**, *126*, 13622.

(66) Ratnikov, M. O.; Farkas, L. E.; McLaughlin, E. C.; Chiou, G.; Choi, H.; El-Khalafy, S. H.; Doyle, M. P. *J. Org. Chem.* **2011**, *76*, 2585.

(67) Catino, A. J.; Nichols, J. M.; Forslund, R. E.; Doyle, M. P. *Org. Lett.* **2005**, *7*, 2787.

(68) Guthikonda, K.; Du Bois, J. *J. Am. Chem. Soc.* **2002**, *124*, 13672.

(69) Ackermann, L. *Chem. Rev.* **2011**, *111*, 1315.

(70) Borovik, A. S. *Chem. Soc. Rev.* **2011**, *40*, 1870.

(71) Davies, H. M. L.; Morton, D. *Chem. Soc. Rev.* **2011**, *40*, 1857.

(72) McDonald, R. I.; Liu, G. S.; Stahl, S. S. *Chem. Rev.* **2011**, *111*, 2981.

(73) Boorman, T. C.; Larrosa, I. *Chem. Soc. Rev.* **2011**, *40*, 1910.

(74) Che, C. M.; Lo, V. K. Y.; Zhou, C. Y.; Huang, J. S. *Chem. Soc. Rev.* **2011**, *40*, 1950.

(75) Hartwig, J. F. *Chem. Soc. Rev.* **2011**, *40*, 1992.

(76) Lu, H. J.; Zhang, X. P. *Chem. Soc. Rev.* **2011**, *40*, 1899.

(77) Wencel-Delord, J.; Droge, T.; Liu, F.; Glorius, F. *Chem. Soc. Rev.* **2011**, *40*, 4740.

(78) Zhang, S. Y.; Zhang, F. M.; Tu, Y. Q. *Chem. Soc. Rev.* **2011**, *40*, 1937.

(79) Zhou, M.; Crabtree, R. H. *Chem. Soc. Rev.* **2011**, *40*, 1875.

(80) Baudoin, O. *Chem. Soc. Rev.* **2011**, *40*, 4902.

(81) Cho, S. H.; Kim, J. Y.; Kwak, J.; Chang, S. *Chem. Soc. Rev.* **2011**, *40*, 5068.

(82) Meunier, B.; de Visser, S. P.; Shaik, S. *Chem. Rev.* **2004**, *104*, 3947.

(83) Bergman, R. G. *Nature* **2007**, *446*, 391.

(84) Canty, A. J.; Vankoten, G. *Acc. Chem. Res.* **1995**, *28*, 406.

(85) Bertrand, G. *Carbene Chemistry*; Marcel Dekker: New York, 2002.

(86) Buchner, E.; Feldmann, L. *Chem. Ber.* **1903**, *36*, 3509.

(87) Staudinger, H.; Kupfer, O. *Chem. Ber.* **1912**, *45*, 501.

(88) Maas, G. In *Organic Synthesis, Reactions and Mechanisms*; Springer Berlin Heidelberg: 1987; Vol. 137, p 75.

(89) Doyle, M. P. *Chem. Rev.* **1986**, *86*, 919.

(90) Doyle, M. P.; McKervey, M. A.; Ye, T. *Modern Catalytic Methods for Organic Synthesis with Diazo Compounds: From Cyclopropanes to Ylides*; 1 ed.; John Wiley & Sons, Inc.: New York, 1998.

(91) Yates, P. *J. Am. Chem. Soc.* **1952**, *74*, 5376.

(92) Greuter, F.; Kalvoda, J.; Jeger, O. *Proc. Chem. Soc., London* **1958**, 349.

(93) von E. Doering, W.; Roth, W. R. *Tetrahedron* **1963**, *19*, 715.

(94) Diaz-Requejo, M. M.; Belderrain, T. R.; Nicasio, M. C.; Trofimenko, S.; Perez, P. J. *J. Am. Chem. Soc.* **2002**, *124*, 896.

(95) Demonceau, A.; Noels, A. F.; Hubert, A. J.; Teyssie, P. *J. Chem. Soc., Chem. Commun.* **1981**, 688.

(96) Terada, M.; Toda, Y. *Angew. Chem. Int. Ed.* **2012**, *51*, 2093.

(97) Davies, H. M. L.; Lian, Y. *Acc. Chem. Res.* **2012**, *45*, 923.

(98) Wang, X. C.; Xu, X. F.; Zavalij, P. Y.; Doyle, M. P. *J. Am. Chem. Soc.* **2011**, *133*, 16402.

(99) Selander, N.; Fokin, V. V. *J. Am. Chem. Soc.* **2012**, *134*, 2477.

(100) Parr, B. T.; Green, S. A.; Davies, H. M. L. *J. Am. Chem. Soc.* **2013**, *135*, 4716.

(101) Nakamura, E.; Yoshikai, N.; Yamanaka, M. *J. Am. Chem. Soc.* **2002**, *124*, 7181.

(102) Pelphrey, P.; Hansen, J.; Davies, H. M. L. *Chem. Sci.* **2010**, *1*, 254.

(103) Berry, J. F. *Dalton Trans.* **2012**, *41*, 700.

(104) Doyle, M. P. *J. Am. Chem. Soc.* **1993**, *115*, 958.

(105) Padwa, A.; Austin, D. J.; Price, A. T.; Semones, M. A.; Doyle, M. P.; Protopopova, M. N.; Winchester, W. R.; Tran, A. *J. Am. Chem. Soc.* **1993**, *115*, 8669.

(106) Doyle, M. P.; Ren, T. In *Prog. Inorg. Chem.*; Karlin, K., Ed.; John Wiley & Sons, Inc.: New York, 2001, p 113.

(107) Nadeau, E.; Li, Z.; Morton, D.; Davies, H. M. L. *Synlett* **2009**, *2009*, 151.

(108) Davies, H. M. L.; Venkataramani, C. *Angew. Chem. Int. Ed.* **2002**, *41*, 2197.

(109) Hansen, J.; Autschbach, J.; Davies, H. M. L. *J. Org. Chem.* **2009**, *74*, 6555.

(110) Hansen, J.; Davies, H. M. L. *Coord. Chem. Rev.* **2008**, *252*, 545.

(111) Davies, H. M. L.; Panaro, S. A. *Tetrahedron* **2000**, *56*, 4871.

(112) Doyle, M. P.; Griffin, J. H.; Bagheri, V.; Dorow, R. L. *Organometallics* **1984**, *3*, 53.

(113) Qu, Z.; Shi, W.; Wang, J. *J. Org. Chem.* **2001**, *66*, 8139.

(114) Taber, D. F.; Malcolm, S. C. *J. Org. Chem.* **1998**, *63*, 3717.

(115) Nishiyama, H.; Itoh, Y.; Matsumoto, H.; Park, S.-B.; Itoh, K. *J. Am. Chem. Soc.* **1994**, *116*, 2223.

(116) Maxwell, J. L.; Brown, K. C.; Bartley, D. W.; Kodadek, T. *Science* **1992**, *256*, 1544.

(117) Dikarev, E. V.; Li, B.; Zhang, H. T. *J. Am. Chem. Soc.* **2006**, *128*, 2814.

(118) Hansen, J.; Li, B.; Dikarev, E.; Autschbach, J.; Davies, H. M. L. *J. Org. Chem.* **2009**, *74*, 6564.

(119) Timmer, G.; Berry, J. F. *Chem. Sci.* **2012**, *3*, 3038.

(120) Collet, F.; Dodd, R. H.; Dauban, P. *Chem. Commun.* **2009**, 5061.

(121) Dequirez, G.; Pons, V.; Dauban, P. *Angew. Chem. Int. Ed.* **2012**, *51*, 2.

(122) Zalatan, D.; Bois, J. In *Top. Curr. Chem.*; Yu, J.-Q., Shi, Z., Eds.; Springer Berlin / Heidelberg: 2010; Vol. 292, p 347.

(123) Kwart, H.; Khan, A. A. *J. Am. Chem. Soc.* **1967**, *89*, 1951.

(124) Abramovitch, R. A.; Bailey, T. D.; Takaya, T.; Uma, V. *J. Org. Chem.* **1974**, *39*, 340.

(125) Yamada, Y.; Yamamoto, T.; Okawara, M. *Chem. Lett.* **1975**, *4*, 361.

(126) Breslow, R.; Gellman, S. H. *J. Am. Chem. Soc.* **1983**, *105*, 6728.

(127) Espino, C. G.; Wehn, P. M.; Chow, J.; Du Bois, J. *J. Am. Chem. Soc.* **2001**, *123*, 6935.

(128) Fiori, K. W.; Du Bois, J. *J. Am. Chem. Soc.* **2007**, *129*, 562.

(129) Zalatan, D. N.; Du Bois, J. *J. Am. Chem. Soc.* **2008**, *130*, 9220.

(130) Fiori, K. W.; Espino, C. G.; Brodsky, B. H.; Du Bois, J. *Tetrahedron* **2009**, *65*, 3042.

(131) Lwowski, W. *Nitrenes*; Wiley: New York, 1970.

(132) Scriven, E. F. V. *Azides and nitrenes*; Academic Press: New York, 1984.

(133) Grigg, R. D.; Rigoli, J. W.; Pearce, S. D.; Schomaker, J. M. *Org. Lett.* **2011**, *14*, 280.

(134) Mulcahy, J. V.; Du Bois, J. *J. Am. Chem. Soc.* **2008**, *130*, 12630.

(135) Boralsky, L. A.; Marston, D.; Grigg, R. D.; Hershberger, J. C.; Schomaker, J. M. *Org. Lett.* **2011**, *13*, 1924.

(136) Thornton, A. R.; Blakey, S. B. *J. Am. Chem. Soc.* **2008**, *130*, 5020.

(137) Thornton, A. R.; Martin, V. I.; Blakey, S. B. *J. Am. Chem. Soc.* **2009**, *131*, 2434.

(138) Beaumont, S.; Pons, V.; Retailleau, P.; Dodd, R. H.; Dauban, P. *Angew. Chem. Int. Ed.* **2010**, *49*, 1634.

(139) Lebel, H.; Huard, K.; Lectard, S. *J. Am. Chem. Soc.* **2005**, *127*, 14198.

(140) Lebel, H.; Huard, K. *Org. Lett.* **2007**, *9*, 639.

(141) Nguyen, Q.; Sun, K.; Driver, T. G. *J. Am. Chem. Soc.* **2012**, *134*, 7262.

(142) Perry, R. H.; Cahill, T. J.; Roizen, J. L.; Du Bois, J.; Zare, R. N. *Proc. Natl. Acad. Sci. U. S. A.* **2012**, *109*, 18295.

(143) Norder, A.; Warren, S. A.; Herdtweck, E.; Huber, S. M.; Bach, T. *J. Am. Chem. Soc.* **2012**, *134*, 13524.

(144) Lin, X.; Zhao, C.; Che, C.-M.; Ke, Z.; Phillips, D. L. *Chem. Asian J.* **2007**, *2*, 1101.

Chapter 3

Evidence for a One-Electron Mechanistic Regime in Dirhodium Catalyzed Intermolecular C-H Amination

This chapter has been published:
Kornecki, K. P.; Berry, J. F. *Chem. Eur. J.* **2011**, *17*, 5827-5832.

3.1 Abstract

Swift and energy efficient conversion of chemical feedstocks to pharmaceuticals and agrochemicals requires the development of new methods to add nitrogen functionality to unfunctionalized organic substrates. Dirhodium-catalyzed insertion of nitrene species into C–H bonds is a promising new method, the main drawback of which is the currently limited understanding of the catalytic mechanism. Herein, cyclic voltammetry and controlled potential electrolysis measurements have enabled us to solve many of the mechanistic mysteries of intermolecular C–H amination catalyzed by $[Rh_2(esp)_2]$ (esp = α,α,α',α'-tetramethyl-1,3-benzenedipropanoate). The primary result is that, in addition to a simple nitrene-transfer mechanism that dominates the early stages of the reaction, another mechanism is available that relies on sequential proton-coupled electron transfer steps. Whereas the nitrene transfer mechanism requires the use of expensive, atom-inefficient oxidants, we show that simple one-electron oxidants such as Ce^{4+} may be used to achieve catalytic C–H amination via the one-electron mechanistic regime.

3.2 Introduction

The controlled catalytic oxidative functionalization of aliphatic C-H bonds to produce new C-N bonds is a transformative emerging method in organic synthesis that has the potential to facilitate the synthesis of complex molecules in an energy-efficient manner.[1] Although several transition metals have been shown to accomplish oxidative C-H amination,[3-12] metal-metal bonded dirhodium complexes are the best catalysts for this process in terms of their efficiency and selectivity, and are therefore utilized in a number of synthetic applications.[13,14] Despite the successful application of dirhodium-catalyzed C-H aminations, a major drawback is that very little is known about the mechanism of the reaction. The currently accepted mechanistic hypothesis for Rh_2-catalyzed C-H amination is highlighted in Regime A of Scheme 3.1. In this mechanism, the Rh_2 catalyst (**1**) intercepts a nitrene from an iminoiodinane species, in our studies, PhI=NTces (Tces = $SO_3CH_2CCl_3$). The resulting Rh_2-nitrenoid species (**1a**) is then responsible for the insertion of NTces into a substrate C-H bond. Such a species has never been observed or isolated, but is invoked in analogy to Rh-Rh=CR_2 carbenoid intermediates in the corresponding Rh_2-catalyzed carbene transfer chemistry, for which convincing indirect evidence has been provided.[15,16] Here, we provide evidence that a second mechanism, Regime B, which is based on successive proton coupled electron transfer (PCET) steps, is operative in Rh_2-catalyzed intermolecular aminations.

Current mechanistic understanding of Rh_2-catalyzed C-H amination stems from the work of Du Bois and coworkers. In initial work focusing on intramolecular amination reactions that yield cyclic amine products, kinetic data were found to be consistent with a

mechanism in which the rate-limiting step is the formation of an iminoiodinane, $PhI{=}NSO_3R$, from sulfamate ester and hypervalent iodine oxidant $PhI(OAc)_2$ (Equilibrium 1 in Scheme 3.1). Importantly, radical clock experiments provided no evidence for the involvement of radicals in these intramolecular reactions.[17]

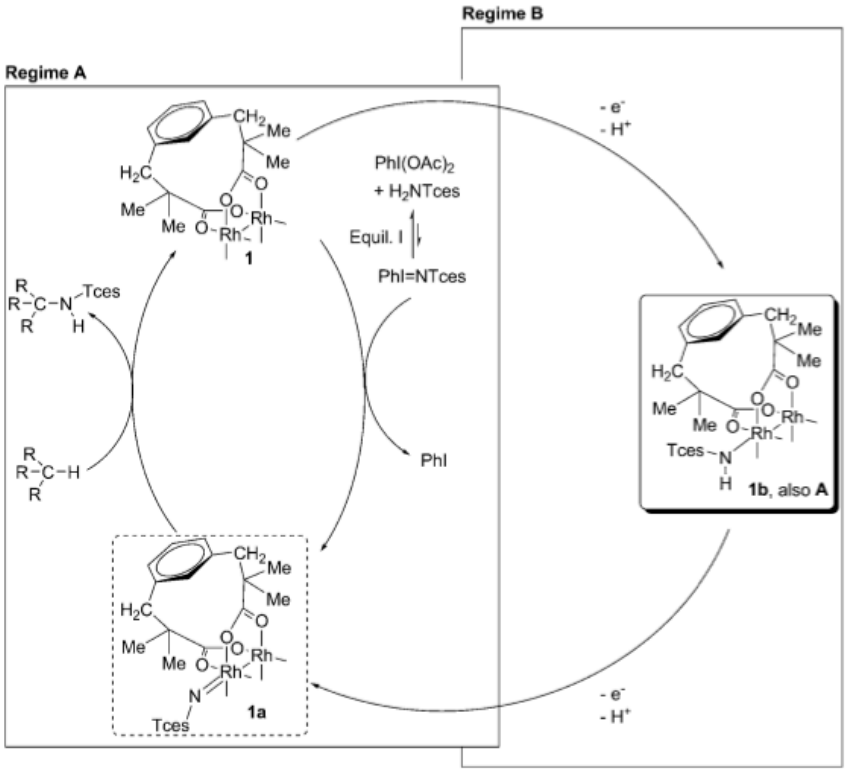

Scheme 3.1 Regime A: Currently hypothesized mechanism for C–H amination catalyzed by **1** (Tces = $SO_3CH_2CCl_3$). Regime B: Proposed observable Rh_2-amido intermediate in a mechanism that is driven by consecutive PCET steps to yield the same reactive Rh_2-nitrenoid species. The second esp ligand is omitted from each molecule for clarity.

In contrast to the intramolecular reactions described above, catalytic intermolecular reactions are mechanistically more complex, though they have a greater potential utility in synthesis. In 2004, the Du Bois group made a major breakthrough in intermolecular C-H amination through the introduction of the new catalyst $Rh_2(esp)_2$, **1** (Scheme 3.1); its robustness is believed to be due to the chelating dicarboxylate ligand, esp, which disfavors ligand dissociation.[18] The mechanism of intermolecular C-H amination catalyzed by **1**, as investigated by Du Bois and coworkers, appears to depend strongly on the concentration of C-H substrate. At high substrate concentrations, a reaction profile similar to that of intramolecular cyclizations is observed. However, at lower C-H substrate concentrations, strong evidence for a one-electron oxidized $Rh_2^{II,III}$ species of unknown composition (hereafter referred to as **A**) as well as free radical derived products are observed.[19,20] Importantly, product formation occurs under both mechanistic regimes. The current hypothesis put forth to explain these results is that C-H amination arises by an exchange reaction of the $Rh_2^{II,II}$ catalyst **1** with iminoiodinanes to produce nitrenoid species **1a**, which inserts the nitrene equivalent into a C-H bond via a concerted asynchronous transition state.[21] Under the highly oxidizing reaction conditions, catalyst **1** is believed to be in equilibrium with the $Rh_2^{II,III}$ species **A**, which is postulated to lead to decomposition of the catalyst.[20] However, the experiments reported here show that species **A** is indeed catalytically active.

A goal of our research is to explore the fundamental coordination chemistry and mechanistic underpinnings for the activity of dirhodium catalysts such as **1**, and we have recently reported the preparation of the first metal-metal/metal-ligand multiply bonded

species analogous to **1a**, a diruthenium nitride,[22] and its remarkable reactivity towards proximal C-H bonds.[23] Here, we report an investigation of the electrochemical oxidation of $Rh_2(esp)_2$ to its $Rh_2^{II,III}$ form and show that a) $Rh_2^{II,III}$ species are catalytically relevant and b) intermolecular C-H functionalization can occur without iminoiodinane transfer reagents, validating the one-electron mediated mechanistic regime proposed as Regime B in Scheme 3.1. Significantly, this work opens the door for the future use of cheaper and more atom economical oxidants in catalytic C-H amination.

3.3 Results and Discussion

We chose to examine the amination of ethylbenzene with H_2NTces as a model intermolecular C-H functionalization reaction for the work reported here. $Rh_2(esp)_2$, **1**, is used as a catalyst, and $PhI(OAc)_2$ is employed as an oxidant, as shown in equation (1). Under typical amination conditions, the reactions proceed to completion in roughly 48h in roughly 70% yield. A plot of product concentration as a function of time (Figure 3.1) is illuminating. In the first 2h, there is an initial burst of reactivity that results in conversion of roughly 30% of the starting material. After this preliminary reactivity surge, the amination product continues to form, albeit at a slower rate. These data are consistent with the two rate regimes proposed by Du Bois.[19] Moreover, a significant amount (up to 10% yield) of the acetoxylated byproduct, a-methylbenzyl acetate, is identified in these reactions, suggesting the action of acetoxy radicals, which have recently been exploited in the oxyamination of indoles reported by Dauban.[24] Under the conditions of equation (1), the red species **A** is observed, and its electronic spectrum is shown in Figure 3.2b.

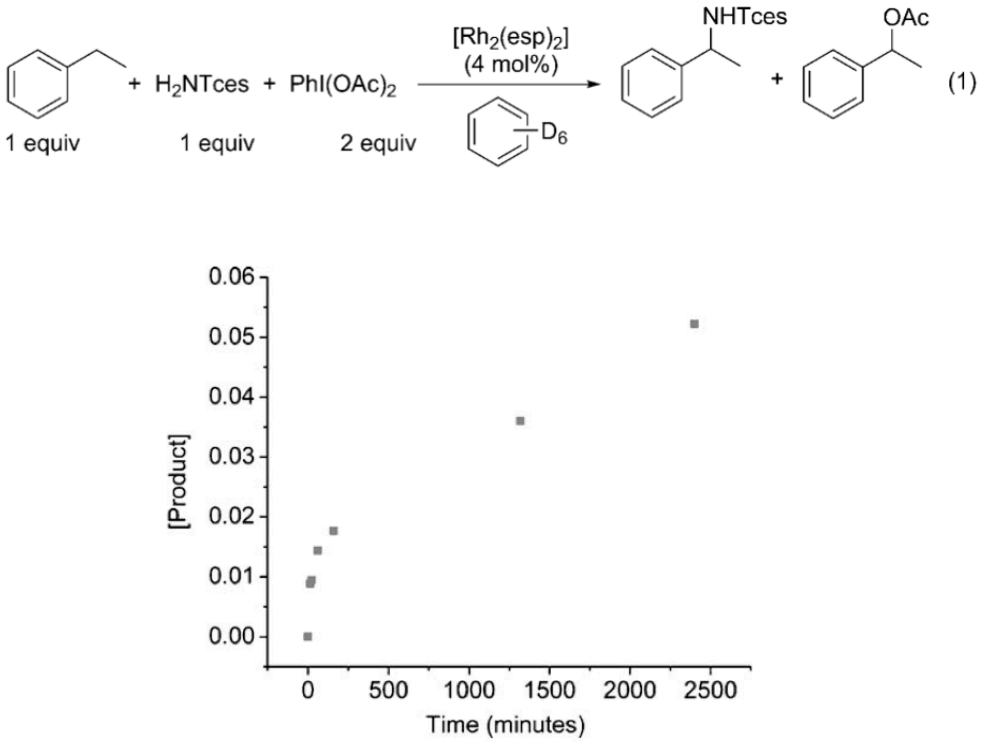

Figure 3.1 Catalytic reactivity of **1** with $PhI(OAc)_2$ as the oxidant, recorded as a plot of product concentration versus time. Yields are based on ^1H NMR integration versus an internal 0.01 M naphthalene standard.

Since product formation occurs in the presence of **A**, this red species is potentially an intermediate in the reaction. Thus, the identity of **A** is of paramount importance for a complete understanding of the catalytic C-H amination reaction. We have used electrochemical one-electron oxidation of **1** in CH_2Cl_2 to address this problem. Cyclic voltammetry experiments show that **1** undergoes reversible one-electron oxidation at $E_{½}$ = 1095 mV vs. $Ag/AgNO_3$. Upon controlled potential electrolysis (CPE) of **1** at an applied potential of 1550 mV vs. $Ag/AgNO_3$, the characteristic Rh_2 $\pi^* \rightarrow \sigma^*$ transition of

1 at 640 nm disappears, and is replaced by new bands at 500 and 810 nm, hereafter called Bands 1 and 2, respectively (Figure 3.2a), as the charge necessary for one-electron oxidation is lost from the electrochemistry solution (calc'd: 1.92 C vs. 1.95 C, observed experimentally). Although the visible spectrum of this brilliant red solution, $\mathbf{1^{ox}}$, is qualitatively similar to that measured *in situ* for **A** during catalytic amination (Figure 3.2b), Band 2 in the latter is shifted bathochromically by 80 – 100 nm to appear at ~890 – 910 nm. Thus $\mathbf{1^{ox}}$ and **A** show different spectroscopic characteristics and are therefore not the same chemical species.

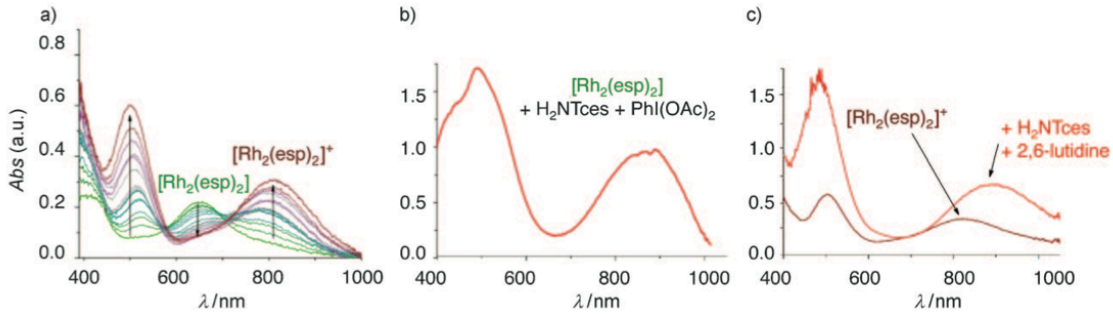

Figure 3.2 a) Conversion of **1** to $\mathbf{1^{ox}}$ via CPE. b) UV-Vis spectrum of species **A** generated under catalytic reaction conditions. c) Shift observed upon addition of 2,6-lutidine to an electrochemically generated solution of $\mathbf{1^{ox}}$ with added sulfamate.

Du Bois has noted that **1** can be chemically oxidized in CH_2Cl_2 by H_2NTces and $PhI(OAc)_2$ to produce a catalytically inactive red species formulated on the basis of its mass spectrum as $Rh_2(esp)_2Cl$.[19] The chloride ligand is proposed to originate from CH_2Cl_2. We report crystallographic characterization of such a chloride-ligated red

species, which we generated by chemical oxidation of **1** with tris(4-bromophenyl)aminium hexachloroantimonate in the presence of H_2NTces and the base 2,6-lutidine. This complex is actually a $Rh_2^{II,III}$ bis-axial chloro adduct, $[Rh_2(esp)_2Cl_2]^-$(**2**, crystallographic data available from the CCDC). Both axial sites are effectively blocked by the presence of the chloro ligands, which explains the stability and catalytic inactivity of this species. However, the UV-visible spectrum of this inactive compound more closely resembles that of electrochemically generated $\mathbf{1^{ox}}$ (Band 2, l = 810 nm), and does not share the band at ~900 nm observed *in situ* for Band 2 of **A**. We attribute the imperfect isosbestic behavior in Figure 3.2a to the reaction of $\mathbf{1^{ox}}$ with CH_2Cl_2 to form **2** in small quantities.

It is well established that the energy of the Rh_2 $\pi^* \rightarrow \sigma^*$ transition in $Rh_2^{II,II}$ species is strongly affected by the identity of axial ligands, so it is reasonable that Band 2 in $\mathbf{1^{ox}}$ would also be sensitive to the nature of axially coordinated ligands.[25] Thus, it is likely that $\mathbf{1^{ox}}$ and **A** exist in the $Rh_2^{II,III}$ oxidation state, but differ in their axial ligands. In order to identify species **A**, we have treated $\mathbf{1^{ox}}$ with potential catalytically relevant axial ligands. Addition of H_2NTces shifts Band 2 by only ~5 nm, which is consistent with coordination of sulfamate ester, but inconsistent with the spectral features of **A**.

Considering the relative acidity of H_2NTces protons, it seemed reasonable to consider a deprotonated $HNTces^-$ axial ligand. If a solution of electrochemically generated $\mathbf{1^{ox}}$ is treated with 100 eq. of H_2NTces and 100 eq. of the non-coordinating base 2,6-lutidine, Band 2 instantly shifts to lower energy (Figure 3.2c), closely mirroring the spectrum of species **A**. This result suggests that species **A** results from both one-

electron oxidation and deprotonation of H_2NTces coordinated to **1**, and we therefore propose that **A** has the the $Rh_2^{II,III}$ amido structure, **1b** (Scheme 3.1). One reason that we suggest the structure **1b** for species A is its similarity to Cu^{II}-amido species that have been shown by Warren and co-workers to be important intermediates in Cu-catalyzed C–H amination.[4] The Cu^{II} amido species are long-lived enough to be isolated and crystallographically characterized.[3] In contrast, we estimate the half-life of **1b** to be on the order of minutes under an inert atmosphere. Similarly, the role of an $Rh_2^{II,III}$ species as a tether for radical-like intermediates has been exploited by Doyle to achieve hydrocarbon oxidation with t-butyl hydroperoxide.[26]

In conjunction with the similarities to the above examples, several pieces of chemical evidence support this structural assignment of species **A** as **1b**. First, though electrochemical oxidation of **1** is possible, chemical oxidation of **1** requires H_2NTces and a base to be present. Thus, **1** does not react with $PhI(OAc)_2$ by itself, but it reacts with H_2NTces/$PhI(OAc)_2$ immediately to form **1b**. Similarly, chemical oxidation of **1** can be accomplished using tris(4-bromophenyl)aminium hexachloroantimonate only in the presence of H_2NTces and 2,6-lutidine as described above. **1** does not react with aminium oxidants by itself. Furthermore, the electrochemical features of **1** are significantly altered by the presence of H_2NTces and 2,6-lutidine, as evidenced by cyclic voltammetry (Figure 3.3). Addition of H_2NTces and 2,6-lutidine causes the $Rh_2^{II,II}/Rh_2^{II,III}$ half-wave potential of **1** ($E_{½}$= 0.80 V vs. Fc/Fc^+) to be ~200 mV more accessible than that for **1** without additives. The lowering of the redox potential in the presence of a base is a signature feature of a PCET process.

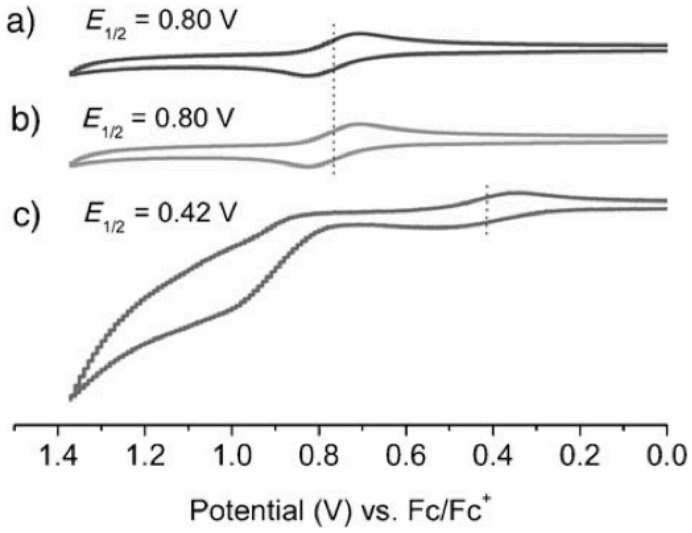

Figure 3.3 a) Cyclic voltammogram (CV) of **1** in CH_2Cl_2. B) CV of **1** plus H_2NTces and ethylbenzene. c) CV of **1** plus H_2NTces, ethylbenzene and 2,6-lutidine.

Interestingly, when H_2NTces is added to an electrochemically generated solution of $\mathbf{1}^{ox}$ in a 1:1 mole ratio, and a further 1 eq. of $PhI(OAc)_2$ is added in the presence of excess ethylbenzene, the solution instantly becomes green again, displaying the spectroscopic features of **1**, suggesting that one turnover occurs. When 2,6-lutidine is added in place of $PhI(OAc)_2$, however, **1b** is formed; further addition of 1 eq. of H_2O_2 (*aq.*) returns the catalyst to the $Rh_2^{II,II}$ state. These results clearly establish **1b** as a competent intermediate, showing that the pathway from **1b** to **1** via the intermediacy of **1a** is mechanistically viable (Scheme 3.1).

Our observation of the reduction of **1b** to **1** in the presence of oxidant prompted us to test the mechanism proposed for Regime B by performing catalytic C-H amination

using a one-electron oxidant. We were inspired by the recent report of Pd-catalyzed C-H amination using $Ce(SO_4)_2$ by Yu and coworkers.[27] This oxidant seemed advantageous to us in that the sulfate groups could act as a base for the necessary PCET steps. Thus, the reaction in equation (2) was carried out, which is readily comparable to equation (1), the analogous hypervalent iodine conditions. C-H amination was observed on a quantitative scale (40% yield) over 48 hours, and notably, in contrast to the results of $PhI(OAc)_2$-driven reactions, no radical byproducts were observed in crude ^1H NMR spectra.

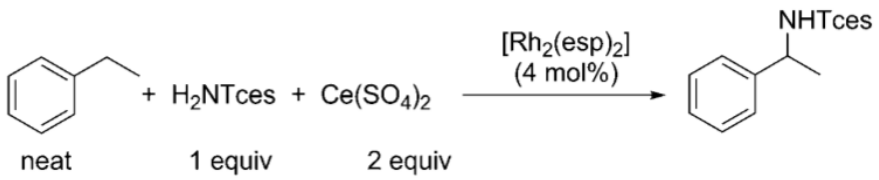

(2)

The double catalytic cycle in Scheme 3.1 can be used to rationalize the results presented here for catalytic intermolecular C-H amination. In Scheme 3.1, the inner cycle (Regime A) corresponds to the reactions that take place in the substrate-rich regime of the reaction (the initial burst of reactivity), which are presumed to be faster than those of the outer cycle, the substrate poor regime (Regime B). Regime A is essentially unchanged from that deduced by Du Bois for intramolecular amination. Notably, we propose that Regime B proceeds via two sequential PCET steps with the red species **1b** as an observable intermediate, and suggest that it converges with the substrate-rich mechanism

in the formation of the Rh-Rh=NTces nitrenoid species (**1a**), which inserts –NTces into C-H bonds. Interestingly, Regime B appears to be more robust over time than Regime A.

Several lines of evidence support the necessity and nature of the proposed substrate-poor mechanism. In intramolecular amination, for which only the substrate-rich mechanism appears to be operative, pre-formed iminoiodinanes (PhI=NR species) quantitatively insert the -NR group into C-H bonds in the presence of catalytic $Rh_2(esp)_2$. For intermolecular aminations, however, similar experiments give only ~33% of the C-H insertion product.[19] When monitoring product conversion by ^{1}H NMR using the hypervalent iodine oxidant (Figure 3.1), the initial burst of activity ends at a product concentration that corresponds to ~30% yield of product by ^{1}H NMR, nearly identical to the yield obtained with pre-formed PhI=NTces. Clearly, the substrate-rich mechanism in intermolecular amination reactions becomes inactive after a period of time for reasons that are currently unknown.

The yield for the reaction involving Ce^{4+} fits nicely in this context in reactions like equation (1), the overall yield from the reaction plateaus around 70%. If Regime A contributes roughly 30% to product formation, the remainder of the product formation must occur under Regime B (40%). In the reaction described by equation (2), only Regime B is operable, and a 40% yield is obtained. Clearly, Regime B exhibits an arrest at approximately 40% conversion, and therefore future work in new catalyst design must take into account the deficiencies of **1** in both mechanistic regimes.

The robust nature of **1** has been attributed to its chelating ligands, which may stabilize the one-electron oxidized intermediate. However, there have been examples of

dirhodium compounds with chelating ligands that do not perform favorably under amination conditions, but whose redox activity has not been reported.[19] This leads us to believe that Rh-centered redox activity may be a necessary requirement for mechanistic Regime B, another observation that may spur new catalyst design.

3.4 Summary

The results reported here have several important implications for Rh_2-catalyzed C-H amination. First, we outline features of a successful amination catalyst: the catalyst must exhibit reversible, Rh-centered redox chemistry and must be able to support a Rh-Rh-NHR linkage if Regime B is to be accessible. Second, the choice of oxidant may be addressed. Regime A strongly requires the use of expensive and chemically promiscuous hypervalent iodine oxidants,[28] but this requirement is lifted in Regime B, opening the door for the future development of methodology that utilizes more environmentally friendly and atom economical oxidants such as hydrogen peroxide, which is chemically compatible with the transformation from **1b** to **1**, but may not be able to affect conversion of **1** to **1b**. The improved selectivity of Regime B is also promising, suggesting that the possibility of eliminating radical-derived side-products is now an option, as we show to be the case when Ce^{4+} is used.

3.5 Acknowledgements

We are grateful to the University of Wisconsin for financial support for this project, as well as to the Chemical Sciences, Geosciences, and Biosciences Division, Office of Basic Energy Sciences, Office of Science, U.S. Department of Energy (DE-FG02-10ER16204).

3.6 Experimental

General. All reagents were obtained commercially unless otherwise noted, and anhydrous ethylbenzene and 2,6-lutidine were used without further purification. Reactions were performed using oven-dried glassware under an atmosphere of nitrogen, either in a glove box or using Schlenk techniques. Dichloromethane and dichloroethane were dried over CaH_2 and distilled before use. Benzene-d6 was dried on an activated alumina column prior to use. Catalyst **1** was prepared according to methods described by Du Bois and coworkers.[18] ^{1}H NMR spectra were collected on a 300 MHz Bruker spectrometer at room temperature.

Spectroelectrochemistry. All electrochemistry experiments were conducted in 10 mL 0.1 M solutions of tetrabutylammonium hexafluorophosphate in freshly distilled dichloromethane with a 0.001 M analyte concentration, under a nitrogen atmosphere. The reference electrode consisted of a silver wire immersed in a 10 mM silver nitrate solution contained by a Vycor tip. The auxiliary electrode was a platinum wire. For cyclic voltammetry, data was referenced to the ferrocene/ferrocenium redox couple, and the working electrode was made of glassy carbon. For controlled potential electrolysis, the working electrode was a 4 X 2 cm fine platinum net. UV-Visible spectra were obtained in

real-time using a Miniature BLUE-Wave UV-Vis dip probe with Tungsten-Krypton lightsource, 10 mm path length tip.

Monitoring equation (1) by ^{1}H NMR, (Figure 3.1). To a 10 mL Schlenk flask charged with **1** (4.5 mg, 4 mol%), sulfamate (34 mg , 0.15 mmol), and naphthalene (2.6 mg, 0.01 M internal standard), dry [D_6]benzene (2 mL) was added into the reaction, followed by the addition of ethyl benzene (18.5 mL, 0.15 mmol) via microsyringe. Finally, $PhI(OAc)_2$ (96 mg, 0.3 mmol) was added to the reaction – a color change to red is generally observed at this point. A portion of the reaction solution was transferred to a dry nitrogen-purged NMR tube, and spectra were collected every 30 minutes for four hours from the same tube. A final spectrum was collected after 40 hours. Growth of the product methyl doublet at 1.27 ppm is monitored.

Chemical oxidation to yield 2 (available from the CCDC). **1** (30 mg, 0.04 mmol) and H_2NTces (18 mg, 0.08 mmol) were added to a 25 mL Schlenk flask and dried under vacuum. Freshly distilled dichloroethane (10 mL) was added via cannula, followed by the addition of 2,6-lutidine (9 mL). In a separate Schlenk flask, tris-(4-bromophenyl)aminium hexachloroantimonate (magic blue) (32 mg, 0.04 mmol) was dissolved in another 10 mL of distilled dichloroethane. The magic blue solution was slowly added to the reaction via cannula at 0°C. A color change from green to brick red was observed. The solution was filtered into a second Schlenk flask through a medium filter frit to remove residual antimonate salts. The filtrate was then layered with hexanes and kept at -20°C until crystals formed.

Amination using Ce^{4+}, equation (2). A 25 mL Schlenk flask was charged with $Ce(SO_4)_2$ (398 mg, 1.2 mmol) and anhydrous ethylbenzene (3 mL) was added by syringe. A second flask was charged with **1** (18 mg, 4 mol%), H_2NTces (137 mg, 0.6 mmol) and ethylbenzene (3 mL), the contents of which were transferred to the slurry of $Ce(SO_4)_2$ by cannula. After a few minutes in these conditions, the reaction mixture changed color from green to red. After 48h, the reaction was filtered to remove cerium salts, rinsed with dichloromethane and concentrated. The amination product can be purified by column chromatography (9:1 hexanes:EtOAc), yielding a yellow oil (40%). ^{1}H NMR and ESI mass spectrometry agree with characterization data published in the literature.[19]

3.7 Supplementary Information

CCDC 809823 contains the supplementary crystallographic data for structure **2**. These data can be obtained free of charge from The Cambridge Crystallographic Data Centre via www.ccdc.cam.ac.uk/data_request/cif.

References

(1) H. M. L. Davies, J. R. Manning, *Nature* **2008**, *451*, 417-424.

(2) D. N. Zatalan, J. Du Bois, *Top. Curr. Chem.* **2010**, *292*, 347-378.

(3) S. Wiese, Y. M. Badiei, T. Raymond, S. Mossin, M. S. Varonka, M. M. Melzer, K. Meyer, T. R. Cundari, T. H. Warren, *Angew. Chem.* **2010**, *122*, 9034-9039; *Angew. Chem. Int. Ed. Engl.* **2010**, *49*, 8850-8855.

(4) Y. M. Badiei, A. Dinescu, X. Dai, R. M. Palomino, F. W. Heinemann, T. R. Cundari, T. H. Warren. *Angew. Chem.* **2008**, *120,* 10109-10112; *Angew. Chem. Int. Ed. Engl.* **2008**, *47*, 9961-9964.

(5) C. Liang, F. Collet, F. Robert-Peillard, P. Muller, R. H. Dodd, P. Dauban, *J. Am. Chem. Soc.* **2008**, *130*, 343-350.

(6) K. Huard, H. Lebel, *Chem. Eur. J.* **2008**, *14*, 6222-6230.

(7) E. Milczek, N. Boudet, S. Blakey, *Angew. Chem.* **2008**, *120*, 6931-6934; *Angew. Chem. Int. Ed. Engl.* **2008**, *47*, 6825-6828.

(8) S. Fantauzzi, E. Gallo, A. Caselli, F. Ragaini, N. Casati, P. Macchi, S. Cenini, *Chem. Commun.* **2009**, *26*, 3952-3954.

(9) Z. Wang, Y. Zhang, H. Fu, Y. Jiang, Y. Zhao, *Org. Lett.* **2008**, 1863-1866.

(10) J. D. Harden, J. V. Ruppel, G.-Y. Gao, X. P. Zhang, *Chem. Commun.* **2007**, 4644-4646.

(11) Y. Lu, V. Subbarayan, J. Tao, X. P. Zhang, *Organometallics* **2010**, *29*, 389-393.

(12) M. R. Fructos, S. Trofimenko, M. M. Dias-Requejo, P. J. Perez, *J. Am. Chem. Soc.* **2006**, *128*, 11784-11791.

(13) F. Collet, R. H. Dodd, P. Dauban, *Chem. Comm.* **2009**, 5061-5074.

(14) H. M. L. Davies, M. S. Long, *Angew. Chem.* **2005**, *117*, 3584-3586; *Angew. Chem. Int. Ed.* **2005**, *44*, 3518-3520.

(15) E. Nakamura, N. Yoshikai, M. Yamanaka, M. *J. Am. Chem. Soc.* **2002**, *124*, 7181-7192.

(16) M. P. Doyle, R. Duffy, M. Ratnikov, L. Zhou, *Chem. Rev.* **2010**, *110*, 704-724.

(17) K. W. Fiori, C. G. Espino, B. H. Brodsky, J. Du Bois, *Tetrahedron* **2009**, *65*, 3042-3051.

(18) C. G. Espino, K. W. Fiori, M. Kim, J. Du Bois, *J. Am. Chem. Soc.* **2004**, *126*, 15378-15379.

(19) K. W. Fiori, J. Du Bois, *J. Am. Chem. Soc.* **2007**, *129*, 562-568.

(20) D. N. Zatalan, J. Du Bois, *J. Am. Chem. Soc.* **2009**, *131*, 7558-7559.

(21) P. Dauban, R. H. Dodd, in, *Amino Group Chemistry* (Ed. A. Ricci) Wiley Online Library, **2008**, pp. 55-92.

(22) J. S. Pap, S. Debeer-George, J. F. Berry, *Angew. Chem.* **2008**, *120*, 10256-10259; *Angew. Chem. Int. Ed. Engl.* **2008**, *47*, 10102-10105.

(23) A. K. Musch Long, R. Yu, G. H. Timmer, J. F. Berry, *J. Am. Chem. Soc.* **2010**, *132*, 12228-12230.

(24) S. Beaumont, V. Pons, P. Retailleau, R. H. Dodd, P. Dauban, *Angew. Chem.* **2010**, *122*, 1678-1681; *Angew. Chem. Int. Ed. Engl.* **2010**, *49*, 1634-1637.

(25) S. A. Johnson, H. R. Hunt, H. M. Neuman, *Inorg. Chem.* **1963**, *2*, 960-962.

(26) E. C. McLaughlin, H. Choi, K. Wang, G. Chiou, M. P. Doyle, *J. Org. Chem.* **2009**, *74*, 730-738.

(27) T.-S. Mei, X. Wang, J.-Q. Yu, *J. Am. Chem. Soc.* **2009**, *131*, 10806-10807.

(28) V. V. Zhdankin, P. J. Stang, *Chem. Rev.* **2008**, *108*, 5299-5358.

Chapter 4

Dirhodium Catalysts Bearing Redox Non-Innocent Chelating Dicarboxylate Ligands and their Performance in Intra- and Intermolecular C-H Amination

This chapter has been published:
Kornecki, K. P.; Berry, J. F. *Eur. J. Inorg. Chem.* **2012**, 562-568.

4.1 Abstract

We report two new analogues of the well-known C–H amination catalyst $[Rh_2(esp)_2]$ (**1**) (esp = α,α,α',α'-tetramethyl-1,3- benzenedipropanoate) that bear redox-active supporting li- gands that are structurally similar to esp. The redox-active ligands are 2-[3-(1-carboxy-1-methylethoxy)phenoxy]-2- methylpropanoic acid (H_2**L1**) and (3-methoxycarbonyl-2,5- di-*tert*-butylphenoxy)ethanoic acid (H_2**L2**), which react with $Rh_2(OAc)_4$ to form the catalysts $[Rh_2($**L1**$)_2]$ (**2**) and $[Rh_2($**L2**$)_2]$ (**3**). Both **2** and **3** have been characterized by X-ray crystallography and cyclic voltammetry, inter alia. Compounds **2** and **3** are structurally similar to **1** but show more complex electrochemical features. Whereas **1** has a single reversible redox wave that corresponds to the $Rh_2^{II,II}/Rh_2^{II,III}$ couple, **2** and **3** show multiple oxidations that are characteristic of ligand-centered oxidation. Catalysts **1**, **2**, and **3** perform well in a model intramolecular C–H amination reaction, and all three catalysts perform equally well during the first four hours of a model intermolecular reaction. After this point, **2** and **3** cease to function, whereas **1** continues to be active. These results support the hypothesis that intermolecular C– H amination utilizes two distinct mechanisms: (1) a nitrene interception/insertion mechanism that is fast but ceases to be operative after four hours, and (2) a one-electron

mechanism that is more robust over extended time periods, but requires the catalyst to be able to undergo Rh_2-centered oxidation.

4.2 Introduction

Catalytic C-H amination via nitrene transfer mediated by dirhodium paddlewheel compounds has become an important synthetic tool.[1] This reaction is outlined in Scheme 4.1, and involves oxidative transformation of a nitrogen containing substrate (typically a sulfamate or carbamate ester) into a nitrene equivalent, with subsequent insertion of this nitrene into a substrate C-H bond. The nitrene insertion can either be intramolecular, yielding cyclized products, or intermolecular. While intramolecular reactions are well established, it has been shown that not every Rh_2 catalyst can efficiently accomplish intermolecular reactions.[2] $Rh_2(esp)_2$ (esp = α,α,α',α'-tetramethyl-1,3-benzenedipropanoate) (**1**) has been shown to be the best catalyst for the intermolecular amination transformation,[3] a fact that has been attributed to the added stability of the catalyst due to the chelate effect of the bridging dicarboxylate ligands. Current mechanistic information on intramolecular C-H amination by **1** is consistent with the mechanism shown on the left side of Scheme 1 whereby an iminoiodinane intermediate (formed in the rate-limiting reaction of sulfamate ester with $PhI(OAc)_2$) transfers the nitrene to the dirhodium catalyst, yielding the dirhodium nitrene intermediate **A**.[2] Intermediate **A** is then able to insert the nitrene directly into substrate C-H bonds to reform the original catalyst. For intermolecular C-H amination reactions, the iminoiodinane transfer mechanism appears to account for only ~30% of the product

formation. The majority of the product has been proposed to form via the outer mechanism in Scheme 4.1, which involves single-electron redox steps.[4] The formation of C–H amination products using the one-electron oxidant Ce^{4+} verifies the one-electron nature of this mechanism.[4]

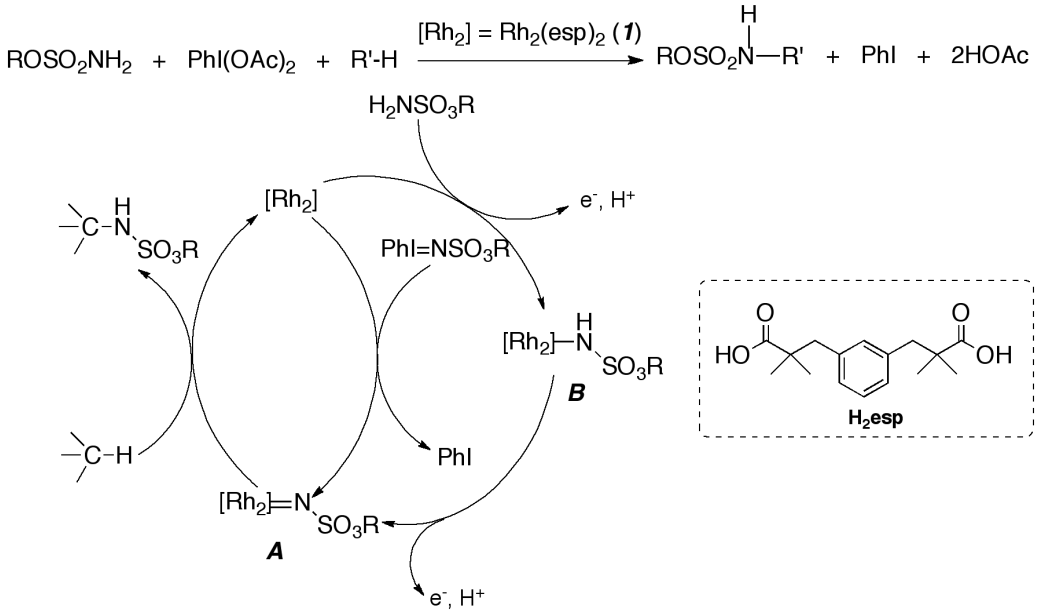

Scheme 4.1 Proposed catalytic cycle for dirhodium-catalyzed C-H amination: the inner mechanism involves direct nitrene transfer, and the outer mechanism (with amido intermediate **B**) corresponds to the one-electron pathway that dominates the intermolecular amination mechanism.

Redox non-innocent ligands that are strongly coupled to a transition metal center have been employed with success in catalytic reactions involving redox transformations.[5] To our knowledge, redox non-innocence has never been studied in the context of

dirhodium complexes, or the possible implications to catalysis. Ferrocene-based redox auxilliaries in dirhodium complexes have been reported, but only their electrochemistry has been studied.[6] Because of the one-electron transformations involved in the outer mechanism for intermolecular C-H amination catalyzed by Rh_2 complexes, we have prepared Rh_2 catalysts bearing redox non-innocent ligands and describe their performance in intra- and intermolecular amination in this article.

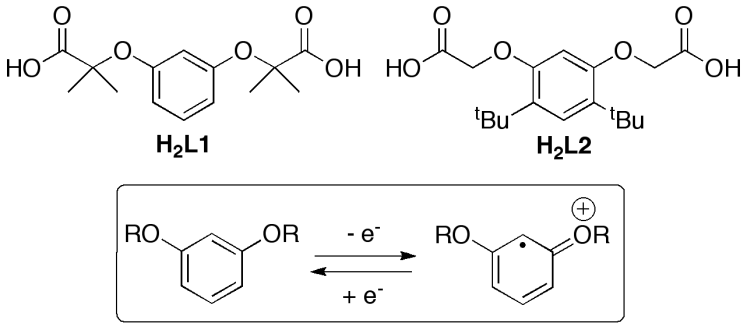

Scheme 4.2 Chelating dicarboxylate ligands and the redox capabilities of resorcinol-based compounds.

Since the chelate effect is touted for the increased stability and selectivity of **1** as an intermolecular amination catalyst, we decided to study catalysts that are close structural analogs of **1**. The ligands **L1** (2-(3-(1-carboxy-1-methylethoxy)phenoxy)-2-methylpropanoate) and **L2** ((3-carboxymethoxy-2,5-di-tert-butylphenoxy)ethanoate) (previously reported in the context of metallomacrocycle assembly)[7] have the same backbone chain-length as **esp**, however the backbones of **L1** and **L2** contain a redox-active resorcinol-derived component (Scheme 4.2). Like the more well known 1,2- or

1,4-dialkoxy-substituted benzenes,[8] 1,3-dialkoxybenzenes may be oxidized to the corresponding radical cations, as shown in Scheme 4.2.[9] The *meta*-disubstituted radical species are significantly less stable than their *ortho*- or *para*- congeners.[9,10] To our knowledge, the *meta*-dialkoxybenzene motif has not yet been investigated as a redox-noninnocent ligand in coordination complexes, which futher prompted this study.

4.3 Results and Discussion

Synthesis. Both **H_2L1** and **H_2L2** were previously reported by Bonar-Law and coworkers,[6] and were prepared simmilarly herein with slight modifications to the synthesis of **H_2L2** (outlined in the experimental section). Reacting the dicarboxylate ligands with dirhodium tetraacetate at 150°C in dichlorobenzene affords the loss of acetic acid, and the formation of complexes **1** – **3** in good yields (60 – 75%). Complex formation and purity were established by ^{1}H NMR spectroscopy, MALDI-MS and elemental analysis. Crystals suitable for X-ray diffraction were obtained for complexes **2** and **3** as their diaquo and bis-acetone adducts, respectively (Figures 4.1 and 4.2, vide infra). The axial ligands were removed under vacuum prior to the use of these compounds as catalysts.

Crystallography. Crystal data for **2** and **3** are given in Table 4.1. The solid state structures of **1**, **2** and **3** are similar showing chelation of the dicarboxylate ligands to the metal-metal bonded dirhodium core. The Rh-Rh distances in all three catalysts range from 2.3817(9) Å to 2.3910(6) Å, which are effectively the same (see Table 4.2), and fall within the

normal range for bond distances in simpler $Rh_2^{II,II}$ carboxylate complexes.[10] The Rh-O bond distances to the carboxylate ligands and axial ligands are all normal. An interesting difference between the three structures presents itself in a comparison of the $O_{bound\ carboxylate}$-C-C-$O_{phenolate}$ torsion angles. There are two of these torsion angles in **1** that are crystallographically inequivalent; one is 57.301° on one side of the bound carboxylate, and 59.238° on the other, which are very close values and may not be considered to be significantly different in a chemical sense. This torsion angle in **3** is significantly smaller at only 18.79°. Interestingly, **2** differs from **1** and **3** in that its two crystallographically inequivalent smallest torsion angles on either side of the bound dicarboxylate are very different: 99.341° and 37.912°. If this difference in torsion angles is retained in solution, the nearly 90° torsion angle could play a role in facilitating hyperconjugation effects between the oxygen atom of the meta-dialkoxybenzene backbone and the carboxylate π orbitals, thus allowing for direct electronic communication to the rhodium center.

Table 4.1 Crystallographic parameters for **2** and **3**.

Compound	**2**•$2H_2O$	**3**• 2acetone
Space Group	$P\bar{1}$	*I4/m*
Crystal System	Triclinic	Tetragonal
a, Å	12.520(3)	19.3634(5)
b, Å	12.637(3)	19.3634(5)
c, Å	14.577(4)	12.1982(4)
a, °	91.372(4)	90
b, °	100.240(4)	90
g, °	101.962(4)	90
V,	2215.8(10)	4573.69(2)
Z	2	4
R1, *w*R2 (I>2σ)	0.0398, 0.0911	0.0302, 0.0736
R1, *w*R2 (all)	0.0510, 0.0995	0.0446, 0.0793

Table 4.2 Selected bond distances and angles in **1**, **2** and **3**.

Compound	**1**• 2acetone[16]	**2**•2H_2O	**3**• 2acetone
Rh-Rh, Å	2.3817(9)	2.3873(6)	2.3910(6)
Rh-$O_{carboxylate}$, Å	2.0386[18]	2.0355[2]	2.036[2]
Rh-O_{axial}, Å	2.3042(19)	2.298[7]	2.286(4)
O-C-C-O (torsion), °	57.301	37.912	18.79
	59.238	99.341	

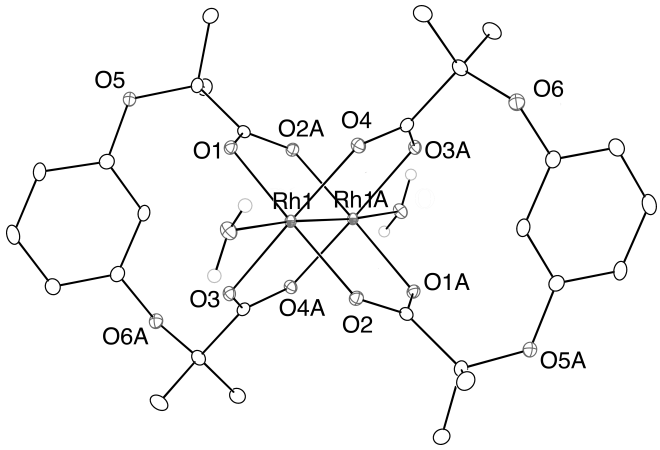

Figure 4.1 Thermal ellipsoid plot of catalyst **2**•2H_2O, with thermal ellipsoids drawn at the 30% probability level. Hydrogen atoms are omitted for clarity.

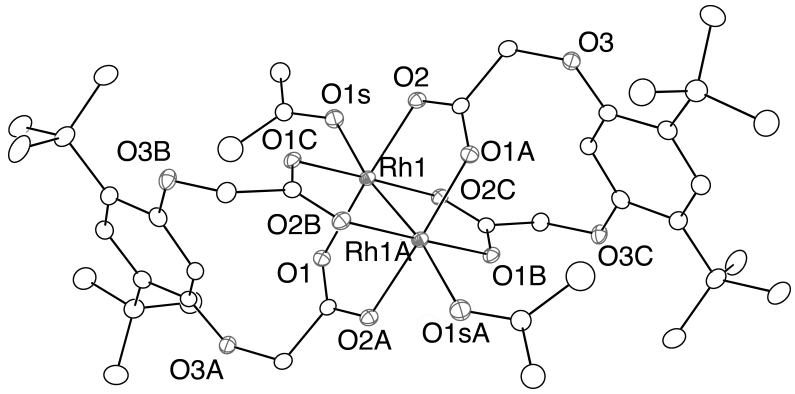

Figure 4.2 Thermal ellipsoid plot for **3**•2acetone, with thermal ellipsoids drawn at the 30% probability level. Hydrogen atoms are omitted for clarity.[11]

Electrochemistry. To test the redox activity of the ligands **L1** and **L2**, cyclic voltammetric measurements have been performed (Figures S4.1 and S4.2). The **H_2esp** ligand, lacking the *meta*-dialkoxybenzene moiety, shows no redox behavior in THF up to 2.1 V versus Fc/Fc^+. Under reducing conditions, an irreversible wave at -1.4 V is observed. Similar reductive waves are observed in THF for **H_2L1** and **H_2L2**, and it is thus reasonable to conclude that these waves correspond to electrochemical reduction and subsequent decarboxylation of the carboxylic acid functionalities. In addition to these reductive events, **H_2L1** and **H_2L2** show waves at positive potentials corresponding to oxidations that are absent in **H_2esp**. For **H_2L1**, multiple irreversible oxidation events are observed at potentials > 1.2 V. In contrast, two discrete irreversible waves are observed for **H_2L2** at 0.9 and 1.1 V. The oxidations in **H_2L1** and **H_2L2** are safely assigned to the oxidation of the *meta*-dialkoxybenzene unit. The irreversibility of the oxidations is

consistent with a fast decomposition process that occurs after the radical cation is generated.

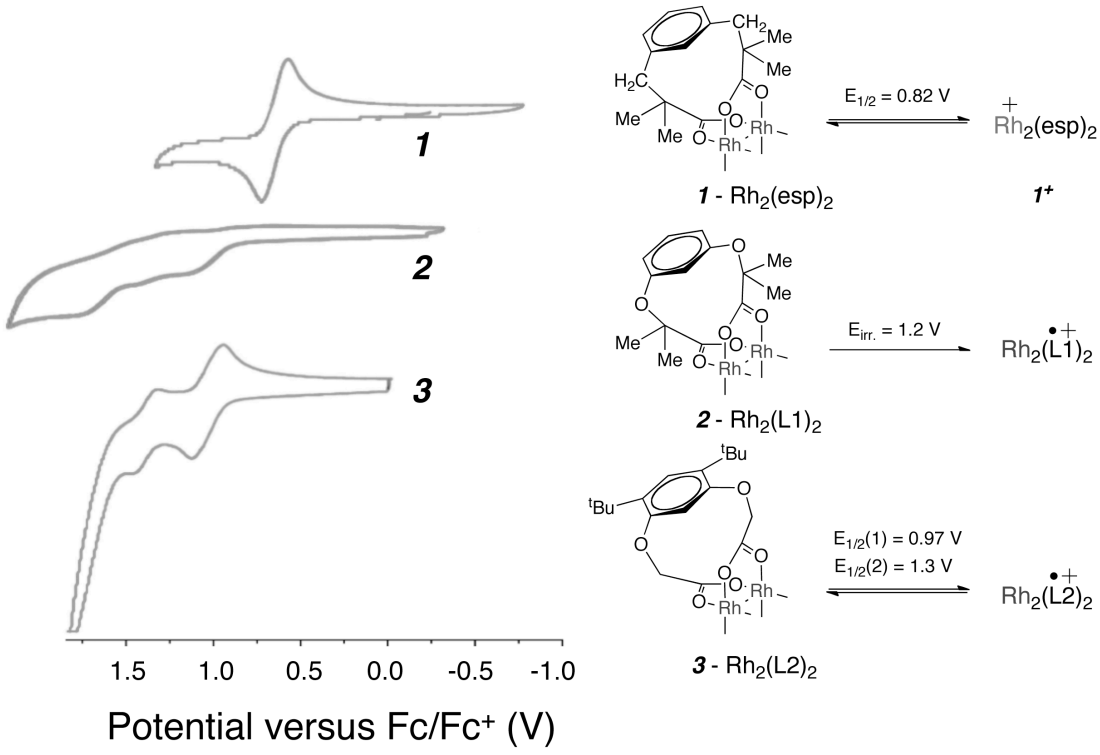

Figure 4.3 Redox features of chelate catalysts **1**, **2** and **3**.

The majority of dirhodium carboxylate paddlewheel complexes exhibit one reversible redox event corresponding to the $Rh_2^{II,II}/Rh_2^{II,III}$ couple.[12] $Rh_2(esp)_2$ (**1**) exhibits a perfectly reversible Rh-centered redox couple at $E_{1/2}$ = 0.82 V (vs. Fc/Fc^+ in dichloromethane). Chemical oxidation and spectroelectrochemistry results indicate that this wave is centered at the Rh_2 unit, and is assigned as the $Rh_2^{II,II}/Rh_2^{II,III}$ redox couple.[4] Compounds **2** and **3** feature more complexity in their cyclic voltammograms than does **1**.

In contrast to the single, reversible wave observed for **1**, **2** displays multiple irreversible features at >1.2 V. The irreversibility of these features and their higher redox potential as compared to **1** suggest that these oxidation events have a different origin than the $Rh_2^{II,II}/Rh_2^{II,III}$ couple of **1**. Since these redox events closely mirror the irreversible electrochemical behavior of the **H_2L1** ligand, it is reasonable to assign these as oxidations of the *meta*-dialkoxyphenylene moiety of the ligand backbone. Much like in the case of the free ligand itself, the radical cationic species resulting from these oxidations are unstable and undergo a fast chemical reaction, likely radical/radical coupling, that renders the electrochemical signal irreversible. Like **2**, **3** shows multiple redox waves in its cyclic voltammogram. Unlike the irreversible behavior of **2**, the redox waves of **3** are reversible, and appear at lower potentials. The CV of **3** shows a reversible two-electron wave at 0.97 V, and a further reversible one-electron wave at 1.3V.

It is well established that phenoxyl radicals and phenoxyl radical complexes can be stabilized when bulky substituents protect the *ortho*- and *para*- positions of the aryl ring.[13] In a similar manner, addition of two *t*Bu substituents to the aryl ring of the ligands of **2** so as to form **3** leads to a greater stabilization of the corresponding radical cation $[\mathbf{L2}]^{\bullet+}$. This stabilization is both a thermodynamic effect (reflected in the more accessible oxidation potential of **3**, 0.9 V, as compared to **2**, >1.2 V) and a kinetic effect (the reversibility of the redox waves for **3** indicates that the chemical process responsible for rendering the **2** waves irreversible is now slower than the scan time of the cyclic voltammogram) (Figure 4.3). It is not possible to tell if one of the multiple redox waves displayed by **2** or **3** is centered at the Rh_2 unit. However, in comparing the

electrochemical data of **1**, **2**, and **3** we may note that any $Rh_2^{II,II}/Rh_2^{II,III}$ oxidations of **2** or **3** occur at substantially higher potential than in **1**, and that such an oxidation for **2** is not reversible. Given the general structural similarities between **1**, **2**, and **3**, it is not obvious why the $Rh_2^{II,II}/Rh_2^{II,III}$ couple would be less accessible in the latter two compounds, but this is certainly what happens.

Catalysis. As mentioned above, catalytic amination of C-H bonds is one of the primary applications of dirhodium complexes in which their redox chemistry is proposed to play an important role. Thus the catalytic activity of **1**, **2**, and **3** in intra- and intermolecular C-H amination reactions is of interest. The reaction shown in Scheme 4.3 has been a useful test reaction for the performance of dirhodium catalysts in intramolecular C-H aminations targeting the benzylic C-H position.[15] Simple Rh_2 carboxylates such as $Rh_2(oct)_4$ (oct = octanoate) perform well as catalysts for this reaction with reported yields of ~84%.[15] Thus, chelating dicarboxylate ligands such as **esp** are not absolutely necessary for this transformation. Catalysts **1**, **2**, and **3** nevertheless perform intramolecular amination very well, particularly **1** and **3**. It is not entirely obvious why **2** gives a lower yield; however, catalyst **2** is not recoverable after the course of the reaction, implying that radical reactions at the ligand may initiate catalyst degradation.

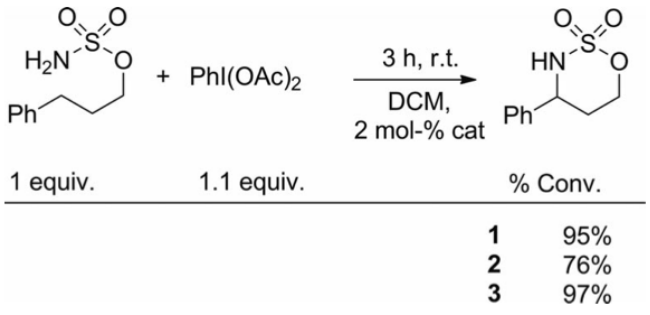

Scheme 4.3 Intramolecular reactivity of chelate catalysts. Percent conversion based on ^{1}H NMR spectroscopic integration versus concentration of uncyclized substrate.

To test the catalytic competence of **1** – **3** under intermolecular C-H amination conditions, conversion of ethyl benzene to the corresponding amination product using H_2NTces (Tces = trichloroethylsulfamate) and $PhI(OAc)_2$ was used as a representative amination reaction (Scheme 4.4). Ethylbenzene is a particularly appropriate substrate, since it presents benzylic C-H bonds similar to those in the intramolecular substrate described above. At four hours under these conditions, the three catalysts show comparable activity. However after this short time span, **2** and **3** cease to function, whereas **1** continues to perform until a significant portion of the ethyl benzene is consumed. These results complement the report from Du Bois that Rh_2(S-biTISP)$_2$ (S-biTISP = 1,3-[N,N'-di(2,4,6-triisopropylbenzenesulfonyl)-(2S,2'S),(5R,5'R)-prolinate]benzene), despite having chelating dicarboxylate ligands, is a poor intermolecular C-H amination catalyst.[2] Due to the structural analogy between **1**, **2**, and **3**, the poor catalytic performance of the latter two can be attributed to electronic rather

than steric properties. Another important piece of information regarding these reactions is that the brilliant red color ascribed to one-electron oxidized $Rh_2^{II,III}$ species appears when catalyst **1** is used, but is absent for reactions involving **3**, and appears but is short-lived for reactions involving **2**.

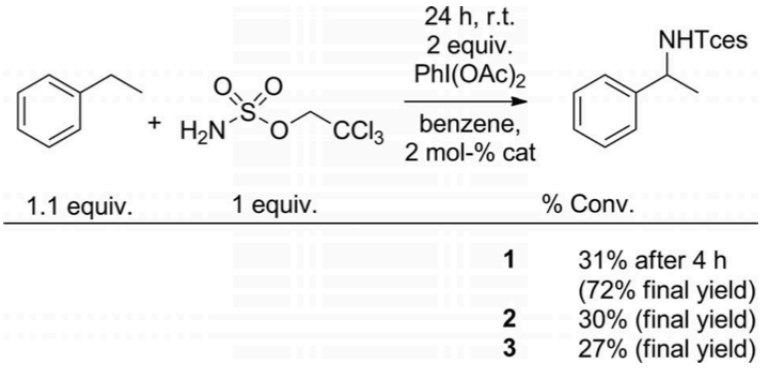

Scheme 4.4 Intermolecular reactivity of chelate catalysts. Percent conversion based on ^{1}H NMR spectroscopic integration versus an internal standard.

The catalytic results presented here can be rationalized in terms of the mechanism shown in Scheme 4.1 and provide further evidence supporting this mechanism. Mechanistic data[15] on intramolecular C-H amination reactions are consistent with nitrene transfer from an iminoiodinane to the dirhodium catalyst, thereby forming the dirhodium nitrene complex **A**, which, in turn, is extremely electrophilic[16] and inserts the nitrene into the substrate C-H bond. This nitrene interception/insertion mechanism does not require any change in the oxidation state of the Rh_2 core, as long as **A** is considered to be an adduct of a neutral nitrene to an $Rh_2^{II,II}$ carboxylate core.[17]

At a 2 mol-% catalyst loading in the intramolecular cyclization reaction (Scheme 3), catalysts **1**, **2** and **3** all seem to perform equally well, affording high yield of product (> 75%).

Magnesium oxide is an important additive that can affect the outcome of the reaction.[16] Table 4.3 gives a comparison of the yields of intramolecular C-H amination reactions catalyzed by 1 mol-% of **1**, **2** and **3** (listed as turnover numbers) for the first 24h of the reaction in the presence or absence of MgO. In general, catalyst performance is enhanced by this additive. We may expect that the function of MgO is to neutralize the acetic acid reaction byproduct, and that excessive amounts of acetic acid may be an important cause of catalyst arrest, particularly for **2** and **3**. Indeed, when no MgO is present, the initial green color of the dirhodium catalysts **2** and **3** quickly dissipates. Instead, the color of the reaction mixture becomes yellow, reminicent of mononuclear Rh^{III} species. This is not the case when **1** is used as a catalyst, indicating that some facet of its structure makes it more robust under the reaction conditions. In fact, when 1 equivalent of **1** is reacted with 2 equivalents each of a sulfamate ester and $PhI(OAc)_2$ in dichloromethane, crystalline **1**•2HOAc can be isolated after several days, indicating that the catalyst is unchanged by acidic conditions. Acetic acid is clearly more detrimental to catalysts **2** and **3**, possibly implicating a protonation of the resorcinol-derived O atoms and subsequent destruction of the ligand, which is not feasible when **1** is used. Notwithstanding, when MgO is present, the reaction mixture will maintain its initial green color for **2** and **3**, allowing all three catalysts to remain active until complete

product formation is achieved, which occurs at ~20h for catalyst **1**, and after ~50h for catalysts **2** and **3**.

Table 4.3 Turnover numbers (TON) for the intramolecular cyclization depicted in Scheme 3 using 1 mol-% catalyst loading after 24 h.

Catalyst	TON (3 equiv. MgO)	TON (MgO-free)
1	99	91
2	86[a]	56
3	69[a]	60

[a] > 90 after about 50 h.

We[4] and Du Bois[2,3] have noted that the nature of intermolecular C-H amination catalyzed by **1** is different at the beginning of the reaction than during the reaction's later stages. Our current hypothesis for this behavior is that intermolecular C-H amination initially occurs via the interception/insertion mechanism described above, but after conversion of roughly 30% of the substrate this mechanism becomes inactive and the reaction continues following a slower one-electron mechanism. This mechanism, which dominates product formation late in the reaction, involves oxidation of **1** in the presence of sulfamate ester substrate to yield a one-electron oxidized $Rh_2^{II,III}$-amido-type species **B**. **B** has a brilliant red color and is observable as an intermediate in the reaction, and undergoes a further one-electron oxidation to yield the nitrene intermediate **A**, which inserts the nitrene into the substrate C-H bond.

The hypothesis that the nitrene interception/insertion mechanism and the one-electron mechanism operate contemporaneously is supported by results we report here. Since the nitrene interception/insertion mechanism does not involve Rh_2-centered oxidation, we expect catalysts **1**, **2** and **3** to perform equally well in the first stage of the catalytic reaction, just as the three catalysts all perform well in intramolecular C-H amination. Indeed, this is what happens. In the first four hours of the reaction, catalysts **1**, **2** and **3** convert ~30% of the ethylbenzene to product. The one-electron mechanism for intermolecular C-H amination requires the catalyst to be oxidized to form **B**. Both **2** and **3** are more difficult to oxidize than **1** by at least 100 mV. Moreover, one-electron oxidation of **2** or **3** does not necessarily involve oxidation of the Rh_2 center from $Rh_2^{II,II}$ to $Rh_2^{II,III}$, but may instead involve oxidation of the *meta*-dialkoxybenzene ligand fragment. Neither **2** nor **3** is active in C-H amination beyond the initial four hour period dominated by the nitrene interception/insertion mechanism. There are two possible explanations for this observation that are consistent with the working mechanistic hypothesis. First, it is possible that the one-electron oxiation of **2** or **3** occurs at such a high potential that these catalysts cannot be oxidized to **B** under the reaction conditions. The other possibility is that **2** or **3** can be oxidized under the reaction conditions, but that this oxidation is centered on the chelating dicarboxylate ligand rather than on the Rh_2 unit. If the ligand oxidation is strongly coupled to the metal center, we may anticipate that **B** could still be formed under these conditions. However, there is no π conjugation pathway between the *meta*-dialkoxybenzene group and the Rh_2 center and a hyperconjugation pathway is doubtful, so the electronic coupling here is anticipated to be weak, resulting in a one-

electron oxidized species resembling an uncoupled $Rh_2^{II,II}$ unit appended to an organic radical cation. Such a species would not be chemically equivalent to **B**, and therefore may not take part in the one-electron C-H amination mechanism. There is some indication that both of these possibilities are, in fact, occurring. When **2** is used as a catalyst, the red color characteristic of **B** appears briefly at the beginning of the reaction, then disappears. This observation is consistent with the first possibility outlined above where, initially the concentration of oxidant is high enough that **B** can be produced, but as the concentration of the oxidant wanes, the reaction mixture no longer has sufficient oxidizing power to utilize the one-electron mechanism. In contrast, when **3** is used as a catalyst, the red color of **B** is never observed. Thus, if **3** is oxidized under these conditions, then the oxidation must be ligand-centered and there must be little electronic coupling between the *meta*-dialkoxybenzene ligand fragment and the Rh_2 center. We interpret these results to mean that Rh_2-centered oxidation is necessary for the success of the one-electron intermolecular mechanism, and thereby for complete conversion of substrate.

4.4 Summary

For the first time, we have introduced redox non-innocent ligands as supporting ligands for metal-metal bonded compounds specifically to investigate their catalytic behavior. The *meta*-dialkoxybenzene motif in ligands **L1** and **L2** has been shown to engender the corresponding dirhodium complexes **2** and **3** with complex ligand-centered redox properties that are absent from the structurally analogous **1**. By assessing the differences in performance for catalysts **1** – **3**, it is evident that rhodium-centered oxidation is

essential to the performance of dirhodium carboxylate catalysts in intermolecular C-H amination. Catalyst **1**, which has a reversible rhodium-centered redox couple, can access intermediate **B**, an $Rh_2^{II,III}$-amido species; catalysts **2** and **3** are more difficult to oxidize and are not successful in this one-electron mechanistic regime.

For the first time, we have introduced redox non-innocent ligands as supporting ligands for metal-metal bonded compounds specifically to investigate their catalytic behavior. The *meta*-dialkoxybenzene motif in ligands **L1** and **L2** has been shown to engender the corresponding dirhodium complexes **2** and **3** with complex ligand-centered redox properties that are absent from the structurally analogous **1**. By assessing the differences in performance for catalysts **1** – **3**, it is evident that rhodium-centered oxidation is essential to the performance of dirhodium carboxylate catalysts in intermolecular C-H amination. Catalyst **1**, which has a reversible rhodium-centered redox couple, can access intermediate **B**, an $Rh_2^{II,III}$-amido species; catalysts **2** and **3** are more difficult to oxidize and are not successful in this one-electron mechanistic regime.

4.5 Experimental Section

General. All reagents were obtained commercially unless otherwise noted. Reactions were performed using oven-dried glassware under an atmosphere of nitrogen, either in a glove box or using Schlenk techniques. Dichloromethane was dried over CaH_2 and distilled before use. Benzene-d^6 was dried on an activated alumina column prior to use. All other solvents were collected anhydrous from a Vacuum Atmospheres solvent system. The structures of known compounds were confirmed by ^{1}H NMR spectroscopy

and ESI-MS. ^{1}H NMR spectra were collected on a 300 MHz Bruker spectrometer at room temperature.

Electrochemistry. All electrochemistry experiments were conducted under a nitrogen atmosphere in 10 mL 0.1 M solutions of tetrabutylammonium hexafluorophosphate in freshly distilled dichloromethane with a 0.001 M analyte concentration. The reference electrode consisted of a silver wire immersed in a 10 mM silver nitrate solution contained by a Vycor tip. The auxiliary electrode was a platinum wire. For cyclic voltammetry, data was referenced to the ferrocene/ferrocenium redox couple, and the working electrode was made of glassy carbon.

Ligands. **H_2esp** was prepared according to the synthesis described by Du Bois and coworkers.[18] **H_2L1** was prepared according to the synthesis reported by Bonar-Law and coworkers.[7] **H_2L2** was prepared similarly to the synthesis described by Bonar-Law and coworkers;[7] the differences are outlined below:

Synthesis of H_2L2. **Et_2L2**: A 100 mL Schlenk flask was charged with potassium carbonate (1.6 g, 11.6 mmol) and 4,6-di-tertbutyl-resorcinol (1.04 g, 4.7 mmol). Acetonitrile (50 mL) was added into the reaction, followed by the addition of a-iodo ethyl acetate (1.1 mL, 9.3 mmol). The reaction was stirred at room temperature for 40 h. Solvent was removed in vacuo and the residue was dissolved in dichloromethane. Particulates were filtered from the dichloromethane solution, which was subsequently concentrated. Purification was achieved via column chromatography on silica gel with

gradient elution from 5 – 20% ethyl acetate in hexanes to yield a clear crystalline solid (0.9 g, 24%), the ethyl ester, **Et_2L2**. ^{1}H NMR ($CDCl_3$): d= 7.229 (s, 1H), 6.199 (s, 1H), 4.576 (s, 4H), 4.281 (q, 4H), 1.387 (s, 18H), 1.315 (t, 6H). ESI/EMM $(M+Na)^+$ Calc'd: 417.2248, Obs: 417.2243. **H_2L2**: In a 25 mL round bottom flask charged with 0.4 g diester (1.0 mmol), 7 mL 1 M NaOH, 5 mL ethanol and 2 mL acetone were added. The flask was equipped with a reflux condenser and heated to 70˚C for 12 h. Any remaining ethanol was removed by rotary evaporation. A solution of 1.0 M HCl was added to the remaining reaction mixture, resulting in a creamy white precipitate that was extracted into ethyl acetate (3 X 50 mL). The organic layer was dried over sodium sulfate, filtered and concentrated. An off-white solid was isolated (0.31 g, 96%). ^{1}H NMR (acetone-d^6): d= 7.212 (s, 1H), 6.563 (s, 1H), 4.730 (s, 4H), 1.392 (s, 18H). ^{13}C NMR (acetone-d^6): d= 29.79, 34.32, 65.11, 99.24, 124.88, 129.78, 155.57, 169.55. ESI/EMM $(M-H)^-$ Calc'd: 337.1656, Obs: 337.1657.

Synthesis of dirhodium chelate complexes 1, 2 and 3. Dirhodium tetracetate bis-methanol (100 mg, 0.197 mmol, 1 eq.) and chelate ligand (2.5 eq.) were added to an Erlenmeyer flask with anhydrous dichlorobenzene (30 mL). The flask was heated to 150°C for 4h, then allowed to cool completely. The solvent was removed by rotary evaporation, and the resulting green residue was chromatographed on silica gel, gradient elution with acetone in dichloromethane, 0 % – 25 %. The complexes were afforded in 60 – 75% yields, as microcrystalline green/green-blue solids.

Compound 1: characterization data matched values previously reported by Du Bois and coworkers.[18]

Compound 2: ^{1}H NMR ($CDCl_3$ + 3 vol.-% acetone-d^6): d= 7.033 (t, 2H), 6.464 (dd, 4H), 6.108 (t, 2H), 1.358 (s, 24H); MALDI-MS (m/z) Calc'd: 766.000, Obs: 765.910; IR (n, cm^{-1}) 2978.91, 2962.29, 1727.29, 1596.67, 1201.36, 961.30; Elemental Analysis (CHN) (**2** was dried at 100°C under vacuum to afford the complex with no axial ligation), Calc'd: %C 43.88, %H 4.21, %N 0.00, Obs: %C 43.83, %H 4.55, %N 0.09. Crystals suitable for X-ray diffraction were obtained by dissolving the purified material in hot dichlorobenzene and allowing the solution to cool slowly (~70h). Crystallographic data is available from the CCDC (837373).

Compound 3: ^{1}H NMR (acetone-d^6 + 3 vol.-% $CDCl_3$): d= 7.137 (s, 2H), 5.202 (s, 2H), 4.614 (s, 8H), 1.343 (s, 36H); MALDI-MS (m/z) Calc'd: 878.126, Obs: 877.980; IR (n, cm^{-1}) 2958.67, 2914.94, 2873.92, 1592.91, 1414.18, 919.83; Elemental Analysis (CHN) (**3** was dried at 100°C under vacuum to afford the complex with no axial ligation), Calc'd: %C 49.21, %H 5.51, %N 0.00, Obs: %C 49.28, %H 5.79, %N 0.13. Crystals suitable for X-ray diffraction were obtained by dissolving the purified material in a 1:1 mixture of acetone and dichloromethane followed by slow evaporation of the solvents. Crystallographic data is available from the CCDC (837374).

Compound 1•2HOAc: Crystals suitable for X-ray diffraction were isolated from the

reaction of **1** (30 mg, 0.039 mmol) with trichloroethylsulfamate (18 mg, 0.078 mmol) and $PhI(OAc)_2$ (25 mg, 0.078 mmol) in dichloromethane (5 mL). The red reaction mixture was layered with hexanes; after several days, blue-green crystals were harvested.

Amination reactions. Each of the three catalysts was tested in a prototypical intermolecular C-H amination reaction, as well as an intramolecular cyclization. For the intramolecular reaction, a prototypical reaction using the substrate depicted in Scheme 3 was performed in dichloromethane with the addition of 1.1 equivalents of hypervalent iodine oxidant, as reported in the literature.[15] The intramolecular reaction was typically complete after 4h, as monitored by TLC. TONs were measured internally by ^1H NMR using a 1 mol % catalyst loading over a 24h period, conducting the reaction described above in CD_2Cl_2. Product concentrations were determined versus an internal cyclooctane standard.

Intermolecular reactions were performed in deuterated solvent and product formation was monitored over the course of 24 h in the presence of two equivalents of hypervalent iodine oxidant, as reported previously.[4] Final product conversion was based off of ^1H NMR integration.

4.6 Supporting Information

CCDC-837373 (for **2**), -837374 (for **3**), and -846682 (for **1**·2HOAc) contain the supplementary crystallographic data for this paper. These data can be obtained free of charge from The Cam- bridge Crystallographic Data Centre via www.ccdc.cam.ac.uk/ data_request/cif.

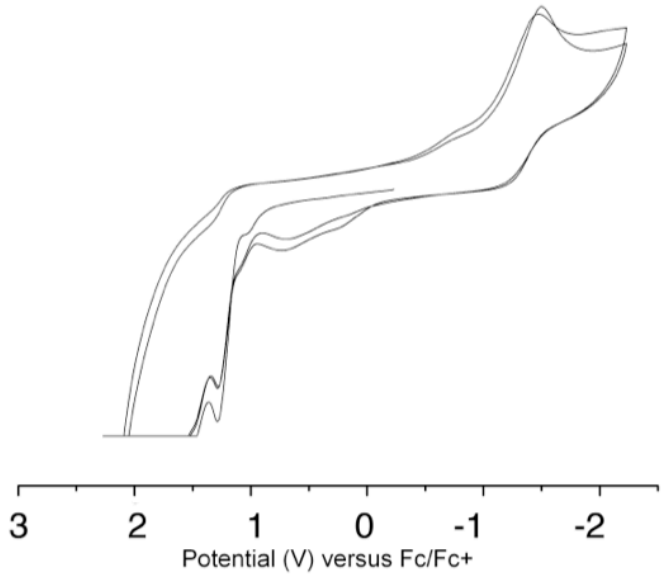

Figure S4.1 Cyclic voltammogram for the ligand **H_2L1**.

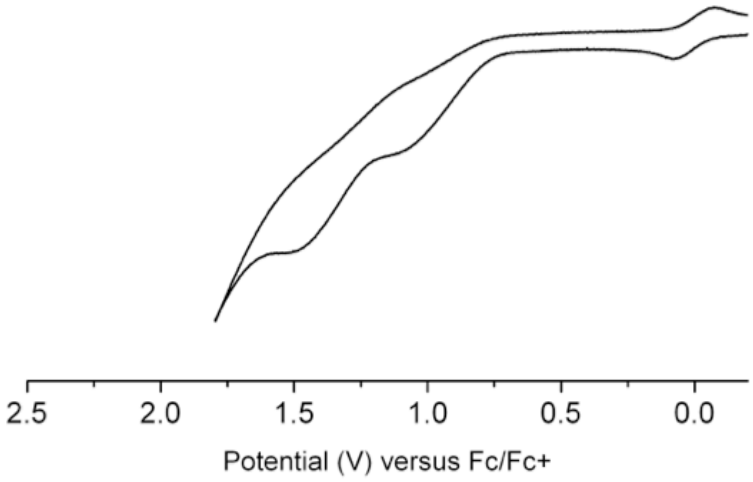

Figure S4.2 Cyclic voltammogram for the ligand **H_2L2**.

4.7 Acknowledgments

We thank the Chemical Sciences, Geosciences, and Biosciences Division, Office of Basic Energy Sciences, Office of Science, U.S. Department of Energy for support under DE-FG02-10ER16204.

References

(1) a) D. N. Zatalan, J. Du Bois, *Top. Curr. Chem.* **2010**, *292*, 347– 378; b) H. M. L. Davies, J. R. Manning, *Nature* **2008**, *451*, 417– 424; c) H. M. L. Davies, M. S. Long, *Angew. Chem.* **2005**, *117*, 3584–3586; *Angew. Chem. Int. Ed.* **2005**, *44*, 3518–3520.

(2) K. W. Fiori, J. Du Bois, *J. Am. Chem. Soc.* **2007**, *129*, 562–568.

(3) D. N. Zatalan, J. Du Bois, *J. Am. Chem. Soc.* **2009**, *131*, 7558– 7559.

(4) K. P. Kornecki, J. F. Berry, *Chem. Eur. J.* **2011**, *17*, 5827–5832.

(5) a) P. J. Chirik, K. Wieghardt, *Science* **2010**, *327*, 794–795; b) W. Kaim, *Inorg. Chem.* **2011**, *50*, 9752–9765.

(6) F. Estevan, P. Lahuerta, J. Latorre, E. Peris, S. Garcia-Granda, F. Gomez-Beltran, A. Aguirre, M. A. Salvado, *J. Chem. Soc., Dalton Trans.* **1993**, 1681–1688.

(7) J. Bickley, R. Bonar-Law, T. McGrath, N. Singh, A. Steiner, *New J. Chem.* **2004**, *28*, 425–433.

(8) J. K. Kochi, *Angew. Chem.* **1988**, *100*, 1331; *Angew. Chem. Int. Ed. Engl.* **1988**, *27*, 1227–1266, and references therein.

(9) a) M. Jonsson, J. Lind, T. Reitberger, T. E. Eriksen, *J. Phys. Chem.* **1993**, *97*, 11278–11282; b) J. Pavlinac, M. Zupan, S. Stavber, *Org. Biomol. Chem.* **2007**, *5*, 699–707; c) J. Pavlinac, M. Zupan, S. Stavber, *J. Org. Chem.* **2006**, *71*, 1027–1032.

(10) F. Marchetti, G. Pampaloni, C. Pinzino, *J. Organomet. Chem.* **2011**, *696*, 1294–1300.

(11) H. T. Chifotides, K. R. Dunbar, in: *Multiple Bonds Between Metal Atoms* (Eds.: F. A. Cotton, C. A. Murillo, R. A. Wal- ton), Springer, New York, **2005**, pp. 465–567.

(12) The structure of **3** crystallizes with both acetone and dichloro- methane as axial ligands with disorder 84% acetone/16% dichloromethane. The CH_2Cl_2 ligand was omitted from the thermal ellipsoid plot for clarity.

(13) K. Das, K. M. Kadish, J. L. Bear, *Inorg. Chem.* **1978**, *17*, 930– 934.

(14) P. Chaudhuri, K. Wieghardt, *Prog. Inorg. Chem.* **2001**, *50*, 151– 216.

(15) C. G. Espino, P. M. Wehn, J. Chow, J. Du Bois, *J. Am. Chem. Soc.* **2001**, *123*, 635–6936.

(16) K. W. Fiori, C. G. Espino, B. H. Brodsy, J. Du Bois, *Tetrahe- dron* **2009**, *65*, 3042–3051.

(17) J. F. Berry, *Dalton Trans.* **2012**, *41*, 700-713.

(18) C. G. Espino, K. W. Fiori, M. Kim, J. Du Bois, *J. Am. Chem. Soc.* **2004**, *126*, 15378–15379.

Chapter 5

Introducing a Mixed-Valent Dirhodium(II,III) Catalyst with Increased Stability in C-H Functionalization

This chapter has been published:
Kornecki, K. P.; Berry, J. F. *Chem. Commun.* **2012**, *48*, 12097-12099.

5.1 Abstract

A new mixed-valent $Rh_2^{II,III}$ dimer, $[Rh_2(espn)_2Cl]$ ($espn^{2-}$ = α,α,α',α'-tetramethyl-1,3-benzenedipropanamidate), is reported. This compound readily dissociates Cl^- at low concentrations in solution to form the active $[Rh_2(espn)_2]^+$ catalyst, which performs intramolecular C–H amination with TONs > 1400. This work expands the scope of $Rh_2^{II,III}$ dimers to nitrenoid chemistry.

5.2 Introduction

Selective and efficient amination of C−H bonds is an increasingly important synthetic tool for introducing complex functionality into simple hydrocarbons. [1] Breakthroughs in C−H amination technology have come largely as a function of catalyst design: simple $Rh_2(OAc)_4$ derivatives have been shown to be decent catalysts for intramolecular C−H amination,[2] but one of the top catalysts for performing both intra- and intermolecular C−H amination is $[Rh_2(esp)_2]$ (**1**) (esp = α,α,α',α'-tetramethyl-1,3-benzenedipropanoate), which was developed by Du Bois and coworkers in 2004.[3] Two important factors contribute to the success of **1** as a catalyst. First, the chelating dicarboxylate ligands provide added thermodynamic stability to **1** via the chelate effect. Similar catalyst design principles have been employed in Rh_2-carbenoid catalysts.[4]

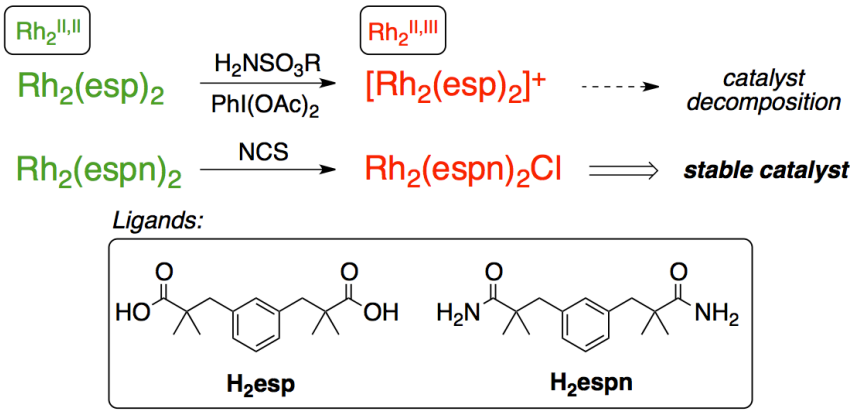

Scheme 5.1 Designing a purposefully mixed-valent $Rh_2^{II,III}$ catalyst.

Accessibility of the $Rh_2^{II,III}$ state under catalytic conditions is another key feature of **1**; both Du Bois and we have recognized that the catalyst resting state in intermolecular amination reactions is an $Rh_2^{II,III}$ species. However, the oxidized $Rh_2^{II,III}$ complex of **1** degrades rapidly (~5 minutes in solution), which is believed to be the major cause of catalyst arrest.[5]

We have therefore been interested in purposefully designing complexes that are stable in the $Rh_2^{II,III}$ oxidation state to examine their performance as catalysts for C−H amination (Scheme 5.1). It is well known that N-donor ligands provide greater stabilization of metal-metal bonded compounds in high oxidation states than do O-donor ligands.[6] Doyle and coworkers have capitalized on this concept by using Rh_2 complexes with carboxamidate ligands as catalysts.[6c] One such catalyst, $[Rh_2(cap)_4]$ (cap = caprolactamate), has been shown to be active in its $Rh_2^{II,III}$ oxidation state for allylic oxidation of C−H bonds, as well as aziridination.[7] To apply this idea to C-H amination chemistry we chose to modify the H_2esp ligand to form the corresponding chelating

diamide (H_2espn), and report the catalytic activity of its $Rh_2^{II,III}$ complex [Rh_2(espn)$_2$Cl], **2a** (Figure 5.1). It was recently reported that $Ru_2^{II,III}$ complexes preferentially catalyze allylic intramolecular amination under conditions nearly identical to Rh_2 amination chemistry,[8] as well as other reactions.[9] Since the $Ru_2^{II,III}$ manifold contains fewer electrons than $Rh_2^{II,III}$ species, it follows that modifying metal oxidation states may allow for fine tuning of the reactivity and selectivity profile of C−H amination.

5.3 Results and Discussion

The ligand H_2espn is conveniently prepared in 56% yield from H_2esp by converting to the diacid chloride followed by a reaction with aqueous ammonia. Rh_2(espn)$_2$Cl is readily accessed in two steps from [Rh_2(OAc)$_4$•2MeOH] and H_2espn by first refluxing the two in chlorobenzene using a Soxhlet extraction apparatus having the thimble filled with K_2CO_3 and sand. This reaction yields an insoluble lime-green amorphous powder that is not isolated but is instead oxidized *in situ* by adding 1.1 equivalents of *N*-chlorosuccinimide to the reaction mixture. The desired catalyst **2a** is then isolated in moderate yield (50%). The initial ligand exchange reaction results in two structural isomers: *cis*-[2,2] Rh_2(espn)$_2$Cl (**2a**) and [4,0] Rh_2(espn)$_2$Cl (**2b**). These isomers are named following the convention for metal-metal bonded compounds with mixed donor equatorial ligands, i.e., the [4,0] isomer has all of the amidate N atoms bound to one Rh atom and all the O atoms bound to the other. The *cis*-[2,2] isomer has a mix of two O and two N donor atoms on each Rh atom in a cis arrangement. The **2a** isomer is favored (4:1 ratio) and readily crystallizes from methylene chloride/acetone

solutions, following chromatographic purification, to yield analytically pure material.

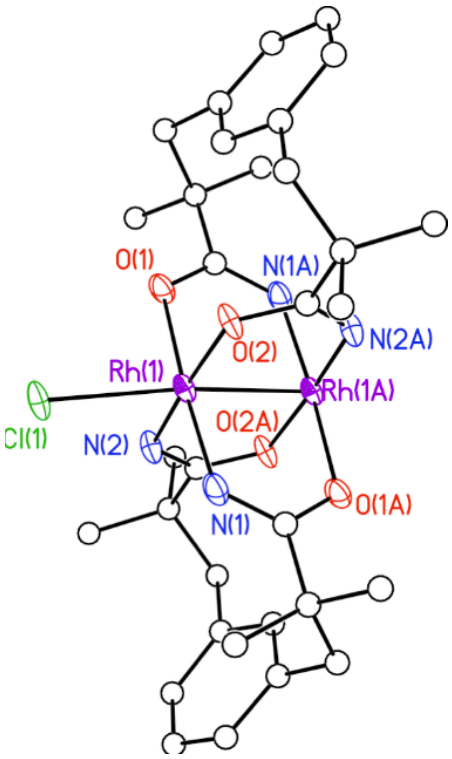

Figure 5.1 Crystal structure of **2a**, the [2,2] isomer of $Rh_2(espn)_2Cl$. Thermal ellipsoids are drawn at 50% probability. Hydrogen atoms are omitted for clarity. The Rh−Rh bond distance is 2.4155(9) Å.

We have tested both isomers in catalytic aminations (and both are equally active catalysts in terms of turnover number, see Supplementary Information, Table S5.2), but the experiments reported herein have been done exclusively with the *cis*-[2,2] isomer (**2a**) since it is readily obtained in macroscopic quantities. The two isomers differ in their solid-state structures: **2b** is a distinct molecular species in the solid state (see

Supplementary Information, Figure S5.2), whereas **2a** forms a coordination polymer with bridging chlorides (Figure S5.1).

Cyclic voltammetry (CV) experiments on **2a** show interesting electrochemical behavior (Figure 5.2). The CV of **2a** shows three redox waves: $E_{1/2}(1)$ at -334 mV, $E_{1/2}(2)$ at 604 mV and $E_{1/2}(3)$ at 1005 mV (versus Fc/Fc^+ in CH_3CN) (Figure 2a). $E_{1/2}(1)$ and $E_{1/2}(3)$ are reversible and become less intense as Cl^- concentration is increased. $E_{1/2}(2)$ is not perfectly reversible and is the dominant signal in the presence of excess Cl^- ions (see supplementary information, Figure S5.3). Furthermore, when the CV solution is doped with two equivalents of non-coordinating counterion, $K[B(Ar^f)_4]$ ($Ar^f = (3,5\text{-}CF_3(C_6H_3))$ and filtered through celite, $E_{1/2}(2)$ is no longer present (Figure 5.2b). We therefore suggest that $E_{1/2}(1)$ and $E_{1/2}(3)$ correspond to chloride-free $[Rh_2(espn)_2]^{0/+}$ and $[Rh_2(espn)_2]^{+/2+}$ waves, respectively, and that $E_{1/2}(2)$ may be assigned to the $[Rh_2(espn)_2Cl]^{0/+}$ wave.

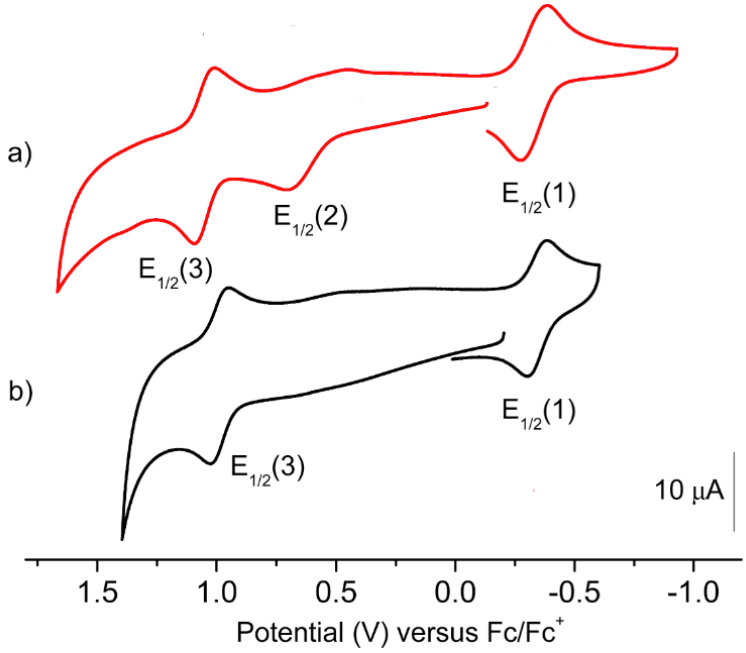

Figure 5.2 a) CV of **2a** (1mM in 0.1M tetrabutylammonium 20 hexafluorophosphate in CH_3CN) b) CV of **2a** plus two equivalents of non-coordinating counterion, BAr^f.

Dissociation of the Cl^- ion may cause the irreversibility of $E_{1/2}(2)$. A dissociation constant of ~2.5 M was estimated based on CV data, which is quite large and therefore indicative of weak chloride binding in solution. Importantly, lowering the concentration of **2a** in the CV solution also diminishes the $E_{1/2}(2)$ signal relative to the $E_{1/2}(1)$ and $E_{1/2}(3)$ signals, implying that the free $[Rh_2(espn)_2]^+$ cation is likely the only species present at the high dilutions relevant to catalysis.

The catalytic activity of compound **2a** has been tested with simple substrates in cyclization reactions with one equivalent of $PhI(OAc)_2$ as the oxidant in dichloromethane at room temperature (Table 5.1). To our surprise, **2a** catalyzed the cyclization of **S1** in

dichloromethane at room temperature with remarkable efficiency.

Table 5.1 Simple cyclization reactions at 0.05 mol% loading for catalysts **1** and **2a**.

	Substrate	Product	Catalyst *1* TON (Yield)	*Catalyst 2a* TON (Yield)
S1	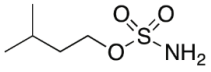	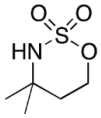	580 (29%)	1400 (70%)
S2	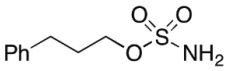	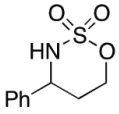	490 (25%)	1450 (72%)

The cyclizations of **S1** and **S2** proceed to 100% conversion with loadings as low as 0.07 mol%. Under identical conditions, catalyst **1** achieves TONs nearing 600, which is quite remarkable within the scope of C−H amination chemistry. However, catalyst **2a** is able to perform many more turnovers prior to catalyst arrest. The enhanced longevity of **2a** in cyclizing simple substrates suggests that the enhanced stability of the $Rh_2^{II,III}$ oxidation state serves to prevent catalyst arrest. Unsurprisingly, using catalytic amounts of the reduced $Rh_2^{II,II}$ powder form of **2a** in the cyclization of **S1** and **S2** results in catalyst oxidation and identical TONs. However, it is worth noting that using the amorphous powder requires a significant induction period (~40 minutes) for the catalyst to solubilize. This induction period, in addition to a lack of structural information for the reduced species, render the use of the oxidized compound **2a** more favorable. The importance of **2a** lies in its structural similarity to **1**, and the fact that it is both stable and isolable in the

$Rh_2^{II,III}$ state. These results refute the idea that Rh_2 dimers in only the (II,II) redox state can be active amination catalysts, and will allow for a discrete study of oxidation state influence on mechanism. Interestingly, the mixed-valent complex $Rh_2(cap)_4Cl$ was tested for competence in the cyclization of **S1** and no conversion was observed. This result implies that mixed-valency is not the only factor important in amination chemistry – the chelate effect may be critical as well.

To probe the selectivity of the nitrene oxidant in C−H amination reactions using **2a**, competition substrates **S3**-**S5** were examined (Table 5.2). Catalyst **1** is largely unselective in the cyclization of **S3** and **S4**, giving a 1:1 ratio of products in both cases.[8] Conversely, **2a** is more sensitive to the electronics of the substrate, perhaps implicating a greater degree of electrophilicity for **2a** versus **1**. However, this conclusion requires a more rigorous set of selectivity experiments than the few that are reported here. Competition between the 3° C−H bond and the benzylic C−H position in **S5** gives a profile that identically mirrors that of **1** with a 1:7 ratio preferring the 3° center: this selectivity is indicative of a concerted transition state.[3c] The recently reported $Ru_2(hp)_4Cl$ catalyst (**3**, with hp = 2-hydroxypyridinate) has opposite selectivity, and has been the subject of experimental and computational studies that indicate a two-step mechanism.[8]

Table 5.2 Intramolecular competition reactions using 0.1 mol% of catalyst **2a**.

Substrate	Product	%Conv.	A:B Ratio
S3 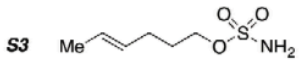	*A* 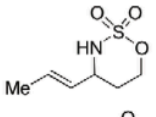 *B* 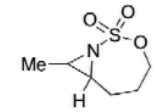	100%	1 : 4
S4 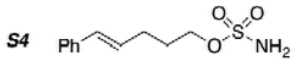	*A* 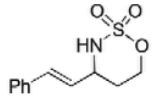 *B* 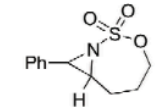	100%	1.4 : 1
S5 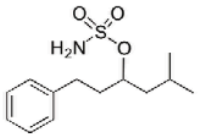	*A* 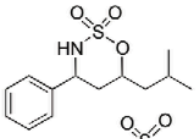 *B* 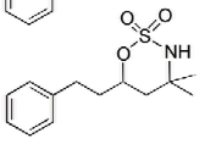	100%	1 : 7

The two limiting mechanisms for C−H amination via a dimetal nitrenoid that may be contemplated are shown in Scheme 5.2. A concerted, but asynchronous reaction mechanism has a great deal of experimental and computational support in $Rh_2^{II,II}$ catalyzed carbenoid reactions,[1a] and $Rh_2^{II,II}$ nitrenoid reactions are proposed to behave similarly.[3b] Alternatively, a two-step C−H abstraction/radical recombination mechanism may be considered that is similar to the classic mechanistic profile of Cytochrome P450.[10] We note that the selectivity of **2a** towards **S3** and **S5** is opposite that of **3**, and that we obtain identical selectivity for **S5** to that observed for **1**. These preliminary data suggest that **2a** likely utilizes a concerted asynchronous mechanism as in **1**, though the

selectivity differences seen in **S4** suggest that the nitrene in **2a** is more electron deficient than the **1**-nitrene, consistent with the cationic nature of the former. We should note, however, that the concerted mechanism may be considered a special case of the C−H abstraction/radical rebound mechanism in which the rate of the radical rebound is infinitely faster than the rate of abstraction. Further experiments to determine where on the continuum between these two limiting cases catalyst **2a** lies are needed.

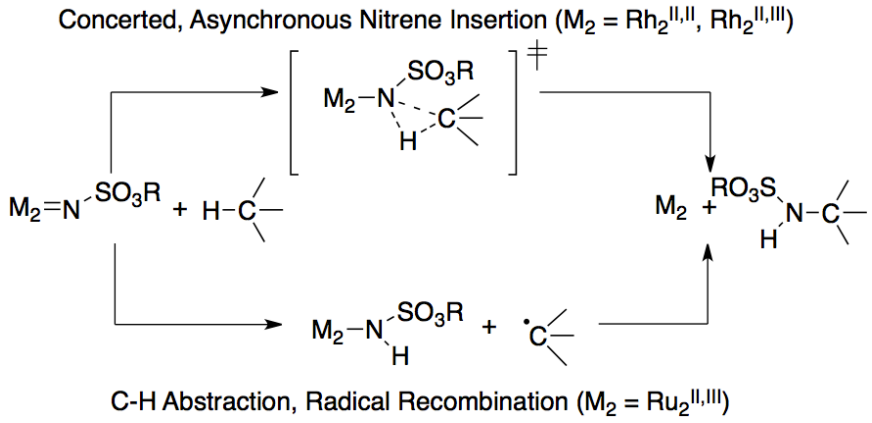

Scheme 5.2 Possible pathways for C−H amination.

We have made some attempts to perform intermolecular C−H amination reactions using **2a**. Experiments were conducted using the highly activated H_2NTces (1,1,1-trichloroethylsulfamate ester) as the nitrogen atom source and diacetoxyiodobenzene as the oxidant in either dichloromethane or benzene. With several substrates, **2a** can achieve full conversion to the C−H amination products with catalyst loadings as low as 0.1 mol%, but the yield of the reaction depends critically on the concentration of the C−H substrate (see supporting information, Table S5.1). Unlike with catalyst **1**, which offers superior

performance in intermolecular C−H amination, **2a** appears to catalyze a fast background reaction between H_2NTces and PhI(OAc)$_2$, yielding 2,2,2-trichloroethanol and sulfamic acid, among other unidentified and undesired products. Optimum yields with catalyst **2** are therefore only obtained when the reaction is carried out in neat hydrocarbon substrate.

5.4 Summary

In conclusion, $Rh_2(espn)_2Cl$ (**2a**) is a new effective and highly efficient catalyst for intramolecular C−H amination reactions. This complex is unique because it is a mixed-valent $Rh_2^{II,III}$ species when it is introduced to catalytic reactions, unlike its predecessor $Rh_2(esp)_2$ (**1**), which becomes oxidized *in situ*. The effectiveness of **2a** suggests that cationic $Rh_2^{II,III}$ species may be key in designing even better catalysts for C−H amination. The parallels between $\mathbf{1}^+$ and **2a** are striking; given the indefinite stability of **2a** as a mixed-valent dimer, studies are ongoing in our lab to better understand the mechanistic groundwork that allows cationic complexes $\mathbf{1}^+$ and **2a** to perform so favorably in the C−H amination transformation.

5.5 Acknowledgment

We thank the Chemical Sciences, Geosciences, and Biosciences Division, Office of Basic Energy Sciences, Office of Science, U.S. Department of Energy for support (DE-FG02-10ER16204). We also wish to acknowledge helpful discussions with Justin Du Bois and other members of the CCI Center for Selective C−H Functionalization supported by NSF (CHE-1205646).

5.6 Supplementary Information

General. All reagents were obtained commercially and used without further purification unless otherwise noted. Acetonitrile (CH_3CN), ether (Et_2O), tetrahydrofuran (THF) and toluene were obtained from a VAC solvent system and degassed prior to use. Dichloromethane was dried over CaH_2 and distilled prior to use. Reactions were performed using oven-dried glassware under an atmosphere of nitrogen. 4Å sieves used in catalytic reactions were activated in a 400°C oven overnight prior to use. Thin layer chromatography (TLC) was performed using EM Reagent 0.25 mm silica gel 60-F plates. Visualization was performed by UV absorbance or cerium ammonium molybdate. Flash chromatography was performed using EM Silica Gel 60 in the indicated solvents. ^1H NMR spectra were recorded in $CDCl_3$, unless otherwise noted, on a Bruker AV-300 spectrometer at room temperature. Chemical shifts are reported on a ppm scale referenced to TMS at 0.0 ppm. Electrochemical measurements were performed with a 1 mM analyte concentration and 0.1 M concentration of tetrabutylammonium hexafluorophosphate supporting electrolyte. The reference electrode was a non-aqueous $Ag/AgNO_3$ cell contained by a Vycor tip; the working electrode was a glassy carbon disk, and the auxiliary electrode was a platinum wire. All cyclic voltammetry data is referenced to the ferrocene/ferrocenium couple with $E_{1/2} = 0$ V. UV-Visible spectra were obtained using a StellarNet miniature BLUE-wave UV-Vis dip probe with Tungsten-Krypton lightsource and a 10 mm path length tip. X-Ray crystal diffraction was performed on a Bruker APEX diffractometer with a Mo-Ka radiation. Elemental analyses were measured at Midwest Microlab, LLC.

H_2espn

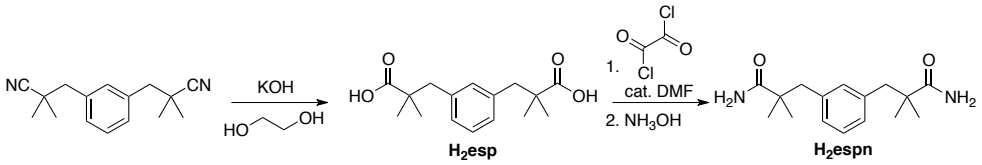

H_2espn is made by converting the previously reported dicarboxylate ligand, H_2esp, to the diamide. H_2esp was synthesized according to the literature[1] from a dinitrile precursor. The procedure for the dinitrile was modified in two ways: the formation of lithium diisopropylamide was performed at -78°C rather than at 0°C. Also, once the a,a,a',a'-dichloroxylene solution was added to deprotonated isobutyronitrile, the reaction was quenched after 5 minutes rather than after 10h. Additionally, the dinitrile was purified by recrystallizing from a 98:2 solution of hexanes:DCM rather than by column chromatography. Hydrolysis of the dinitrile was unmodified.

Converting the diacid to the diamide was done by forming the diacylchloride *in situ*. H_2esp (1.80 g, 6.47 mmol, 1 eq) was added to a Schlenk flask and freshly distilled DCM (30 mL) was added via syringe. Oxalyl chloride (1.65 mL, 19.4 mmol, 3 eq.) was added by syringe, followed by 3 drops of dry DMF. Vigorous bubbling occurred and the solution slowly became a homogenous clear yellow. The reaction was stopped after 4h, and the solvent was removed *in vacuo*. The flask was kept under vacuum for an additional 1h to ensure that excess oxalyl chloride was removed. The residue was redissolved in fresh DCM and the reaction was cooled to 0°C. Concentrated aqueous NH_3OH (7 mL) was added to the reaction and a white precipitate immediately precipitated from solution, which was collected by filtration. The residue was extracted

with acetone until only NH_4Cl remained on the filter. The filtrate was dried over $MgSO_4$ and filtered a second time. The filtrate was concentrated by rotary evaporation, and the residue recrystallized from chloroform. Filtering yields a bright white paper-like solid (1 g, 56%). d_H(300 MHz; $CDCl_3$; TMS) 1.198 (12H, s), 2.803 (4H, s), 5.417 (4H, br s), 7.024 (3H, m), 7.194 (1H, t). ESI EMM^+ m/z: (calc.) 267.1838; (found) 299.3610 (M+Na). mp 172 °C. CHN Elemental Analysis (calc.) C 69.53, H 8.75, N 10.14; (found) C 68.96, H 8.50, N 10.14.

$Rh_2(espn)_2Cl$ (Catalyst **2**)

H_2espn (450 mg, 1.6 mmol, 4 eq.) and crystalline $Rh_2(OAc)_4$□2MeOH (210 mg, 0.40 mmol, 1 eq.) were added to a 250 mL Schlenk flask, which was evacuated for 1h. Anhydrous, degassed chlorobenzene (150 mL) was added to the starting materials and the flask was equipped with a Soxhlet extraction head containing a thimble with a 3:1 mixture of $NaCO_3$ and sand that had been oven-dried overnight, and reflux condenser. The reaction was slowly heated to 140°C. The solution became a homogeneous clear indigo at ~90°C, but eventually became opaque and lime green at higher temperatures. The reaction was heated for 12h before being cooled to 80°C. The Soxhlet head was removed and N-chlorosuccinimide (54 mg, 0.40 mmol, 1 eq.) was added to the reaction. The reaction mixture was heated for 20 minutes at 80°C until the solution became bright red. The solution was then cooled to room temperature and the solvent was removed by rotary evaporation. The residue was dissolved in acetone and subjected to column chromatography with gradient elution (5% to 30% acetone in DCM) yielding two distinct

bands. The first to elute is orange (the [4,0] isomer, **2b**, ~9% yield), the second is red (the [2,2] isomer, **2a**). Both isomers can be recrystallized from their DCM/acetone solutions. Recrystallization of **2a** gives burgundy twinned crystals, (Figures 1 and SI-1) (125 mg, 39%). $\lambda_{max}(CH_3CN)$/nm 472, 1004 (see Figure S5). MALDI-MS m/z (calc.) 789.116 (found) 789.211. CHN Elemental Analysis (calc.) C 48.65, H 5.61, N 7.09; (found) C 48.52, H 5.40, N 7.01.

Competition substrates

Sulfamate esters used for intramolecular catalytic cyclization reactions are readily obtained from corresponding alcohols using Procedure A described in Espino et al.[2] Each sulfamate ester and C−H functionalization product described herein has previously been reported and fully characterized in the literature (respective references below). Thus, sulfamate ester and product ^{1}H NMR spectra were compared with known literature values to confirm identity. Starting alcohols for sulfamate esters **S1**, **S2** and **S3** are commercially available from Sigma-Aldrich and were used without further purification. Preparations for starting alcohols **S4-alcohol** and **S5-alcohol** are described below.

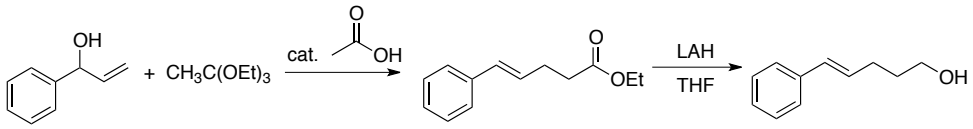

S4-alcohol

***S4*-alcohol**. Triethyl orthoacetate (14 mL, 74.5 mmol), a-vinyl benzyl alcohol (5 g, 37.2 mmol) and acetic acid (0.1 mL) were added to a flask equipped with a short-path distillation head and heated to 160°C for 3h. Ethanol was distilled out of the reaction at

~140°C after ~3h. The reaction mixture was then cooled to room temperature and diluted with an equal volume of ethyl acetate. An equal volume of 1 M aqueous HCl was added and the mixture was stirred vigorously for 1h. The phases were separated and the organic phase was washed with brine (~30 mL). The organic phase was then dried over $MgSO_4$ and concentrated. The **ethyl-ester** of **S4-alcohol** was purified by vacuum distillation. Yield = 3.5 g (46%) d_H(300 MHz; $CDCl_3$; TMS) 1.55 (3H, t), 2.49 (4H, m), 4.16 (2H, q), 6.18-6.33 (1H, m), 6.42 (1H, dt), 7.31-741 (5H, m). ESI EMM^+ m/z: (calc.) 204.1150; (found) 204.1161.

The ethyl ester of **S4-alcohol** was then reduced by reacting the neat oil with a 1 M THF solution of lithium aluminum hydride (10 eq.) at 0°C. The reaction was allowed to warm up to room temperature and react for 2h. The reaction was quenched by cooling to 0°C and slowly adding cold water dropwise. Once bubbling ceased, the reaction was poured into a beaker with 200 mL of water and acidified w/ 50 mL of 2 M aqueous HCl. The mixture was extracted into ethyl acetate three times, followed by a wash with brine. The organic phase was dried over $MgSO_4$ and concentrated. **S4-alcohol** was purified by column chromatography on silica gel with gradient elution 0 → 20% EtOAc in hexanes, R_f = 0.15. Purification yields a clear oil, 1.3 g (50%). d_H(300 MHz; $CDCl_3$; TMS) 1.68-1.82 (2H, m), 1.85-1.96 (2H, m), 2.71 (1H, t), 3.63-3.75 (2H, m), 6.23 (1H, dt), 6.36-6.45 (1H, m), 7.14-7.37 (5H, m). ESI EMM^+ m/z: (calc.) 162.1045; (found) 162.1050.

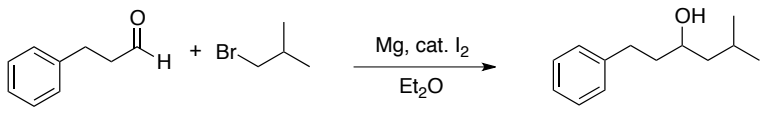

S5-alcohol

***S5*-alcohol**. A solution of 1-bromo-2-methyl propane (1.42 mL, 0.013 mmol) in 20 mL Et_2O was slowly added to a Schlenk flask containing magnesium turnings (350 mg, 0.014 mmol, 1.1 eq.) that had been activated with a crystal of iodine. Once the magnesium was consumed, a solution of hydrocinnemaldehyde (1.7 mL, 0.013 mmol) in 20 mL Et_2O was added dropwise over twenty minutes. The reaction was heated to reflux for 3h and monitored by TLC. Once the hydrocinnemaldehyde was consumed, the reaction mixture was cooled to 0°C and then quenched with 2 M aqueous HCl (20 mL) and extracted into ~50 mL of Et_2O three times. The organic layer was washed with saturated $NaHCO_3$ (20 mL), followed by a wash with brine (20 mL). The organic layer was dried over $MgSO_4$ and concentrated. The **S5**-alcohol was purified by column chromatography using isocratic elution 10% ethyl acetate in hexanes, $R_f = 0.48$. Purification yields a clear oil, 1 g (40%). d_H(300 MHz; $CDCl_3$; TMS) 0.906 (6H, d), 1.28-1.31 (2H, m), 1.39-1.47 (1H, m), 1.565 (2H, m), 1.72-1.81 (2H, m), 2.67-2.80 (1H, m), 3.7 (1H, br s), 7.19-7.31 (5H, m). ESI EMM^+ m/z: (calc.) 192.1514; (found) 192.1519.

Sulfamate Esters

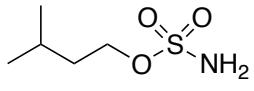 (S1)

δ_H(300 MHz; $CDCl_3$; TMS) 0.945 (6H, d), 1.64 (2H, q), 1.71-1.82 (1H, m), 4.25 (2H, m), 4.81 (2H, br d). Lit. ref[1]

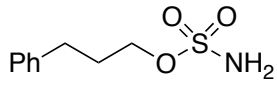 (S2)

δ_H(300 MHz; $CDCl_3$; TMS) 2.04-2.13 (2H, m), 2.75 (2H, t), 4.21 (2H, t), 4.86 (2H, br s), 7.16-7.35 (5H, m). Lit. ref[2]

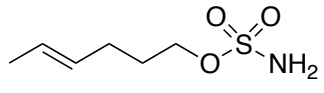 (S3)

δ_H(300 MHz; $CDCl_3$; TMS) 1.65 (3H, ddd), 1.80 (2H, tt), 2.14-2.08 (2H, m), 4.21 (2H, t), 4.68 (2H, br s), 5.32-5.52 (2H, m). Lit. ref[3]

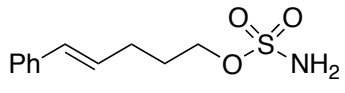 (S4)

δ_H(300 MHz; $CDCl_3$; TMS) 1.95 (2H, tt), 2.36 (2H, dtd), 4.28 (2H, t), 4.64 (2H, br s), 6.18 (1H, dt), 6.44 (1H, dt), 7.19-7.36 (5H, m). Lit. ref[3]

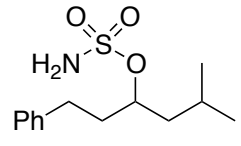 (S5)

δ_H(300 MHz; $CDCl_3$; TMS) 0.92 (3H, d), 0.95 (3H, d), 1.46-1.55 (1H, m), 1.75-1.81 (2H, m), 2.09-2.03 (m, 2H), 2.75 (2H, t), 4.59 (2H, br s), 4.73 (1H, tt), 7.18-7.32 (5H, m). Lit. ref[3]

***Prototypical catalytic conditions*.** All catalytic reactions were conducted on a 20 mg (sulfamate ester) scale in 2 mL of freshly distilled DCM or benzene with ~20 mg of 4 Å molecular sieves. Stock solutions of **2** were prepared and the appropriate catalyst loading was delivered by micropipette. In intermolecular reactions, C-H substrate was also delivered by micropipette, unless the reaction was run neat in substrate. $PhI(OAc)_2$ was added last as a solid (one equivalent in intramolecular reactions, two equivalents in intermolecular reactions). Reactions were stopped after 12h and the solvent was evaporated. The reaction mixture was then redissolved in $CDCl_3$ with and product conversion was determined by ^1H NMR integration of starting materials versus products. Product ratios were also determined by this method. Relaxation delays were increased to 10 seconds for the acquisition of spectra related to catalytic reactions to ensure integration accuracy.

Amination Products

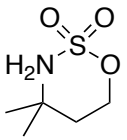

δ_H(300 MHz; $CDCl_3$; TMS) 1.42 (6H, s), 1.77 (2H, t), 4.46 (1H, br s), 4.67 (2H, t). Lit. ref [1]

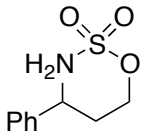

δ_H(300 MHz; $CDCl_3$; TMS) 1.99-2.09 (1H, m), 2.18-2.32 (1H, m), 4.34 (1H, d), 4.66 (1H, ddd), 4.87 (2H, td), 7.31-7.46 (5H, m). Lit. ref[2]

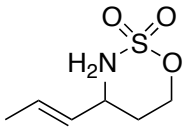

δ_H(300 MHz; $CDCl_3$; TMS) 1.73 (3H, ddd), 1.75-1.92 (2H, m), 3.92 (1H, br d), 4.20-4.32 (1H, m), 4.55 (1H, ddd), 4.75 (1H, dt), 5.44 (1H, m), 5.78 (1H, m). Lit. ref[3]

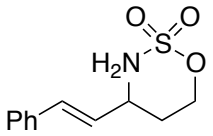

δ_H(300 MHz; $CDCl_3$; TMS) 1.90-2.05 (2H, m), 4.04 (1H, br d), 4.49-4.57 (1H, m), 4.62 (1H, ddd), 4.79-4.85 (1H, m), 6.12 (1H, dd), 6.66 (1H, dd), 7.28-7.39 (5H, m). Lit. ref[3]

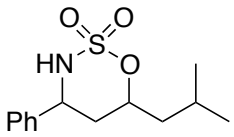

δ_H(300 MHz; $CDCl_3$; TMS) 0.96 (3H, d), 0.98 (3H, d), 1.42 (1H, ddd), 1.76-1.84 (1H, m), 1.86-1.96 (1H, m), 2.06 (1H, ddd), 4.12 (1H, br d), 4.82 (1H, ddd), 4.93-5.00 (1H, m), 7.33-7.43 (5H, m). Lit. ref[3]

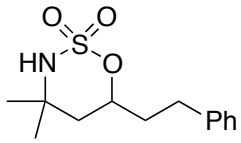

δ_H(300 MHz; $CDCl_3$; TMS) 1.30 (3H, s), 1.47 (3H, s), 1.62 (1H, d), 1.63 (1H, s), 1.84-1.93 (1H, m), 2.02-2.11 (1H, m), 2.75 (1H, ddd), 2.86 (1H, ddd), 3.94 (1H, br s), 4.81-4.87 (1H, m), 7.17-7.34 (5H, m). Lit. ref[3]

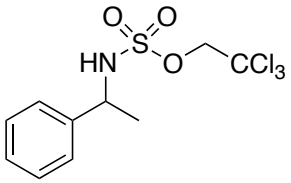

δ_H(300 MHz; $CDCl_3$; TMS) 1.63 (3H, d), 4.43 (1H, d), 4.44 (1H, d), 4.74 (1H, quint), 4.89 (1H, br d), 7.30-7.41 (5H, m). Lit. ref[4]

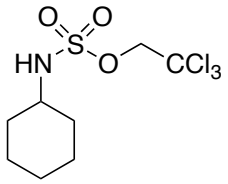

δ_H(300 MHz; $CDCl_3$; TMS) 1.12-1.41 (5H, m), 1.56-1.64 (1H, m), 1.71-1.79 (2H, m), 2.04-2.12 (2H, m), 3.39-3.49 (1H, m), 4.46 (1H, br d), 4.63 (2H, s). Lit. ref[4]

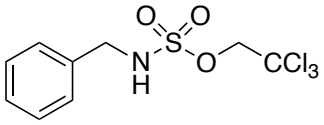

δ_H(300 MHz; $CDCl_3$; TMS) 4.38 (2H, d), 4.56 (2H, s), 4.92 (1H, br s), 7.32-7.35 (5H, m). Lit. ref [5]

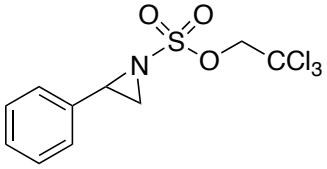

δ_H(300 MHz; $CDCl_3$; TMS) 2.63 (1H, d), 3.09 (1H, d), 3.88 (1H, dd), 4.81 (1H, d), 4.88 (1H, d), 7.29 – 7.39 (5H, m). Lit. ref[6]

Table S5.1. Intermolecular reactivity of **2a**.

R-**H** + H_2NTces —(***2*** (1 mol %), 2 eq. $PhI(OAc)_2$, DCM, 3h, RT)→ R-N**H**Tces

Substrate	*Product*	*Yield**
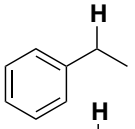	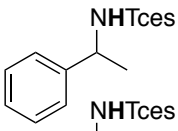	8% (47%)(100%)
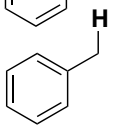	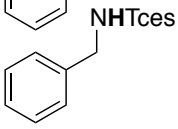	0% (20%)(92%)
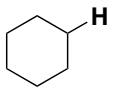	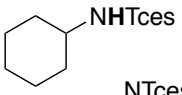	10% (50%)(100%)
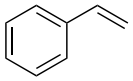	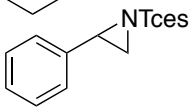	0% (18%)(48%)

*1 equivalent in DCM (10 equivalents in DCM) (neat)

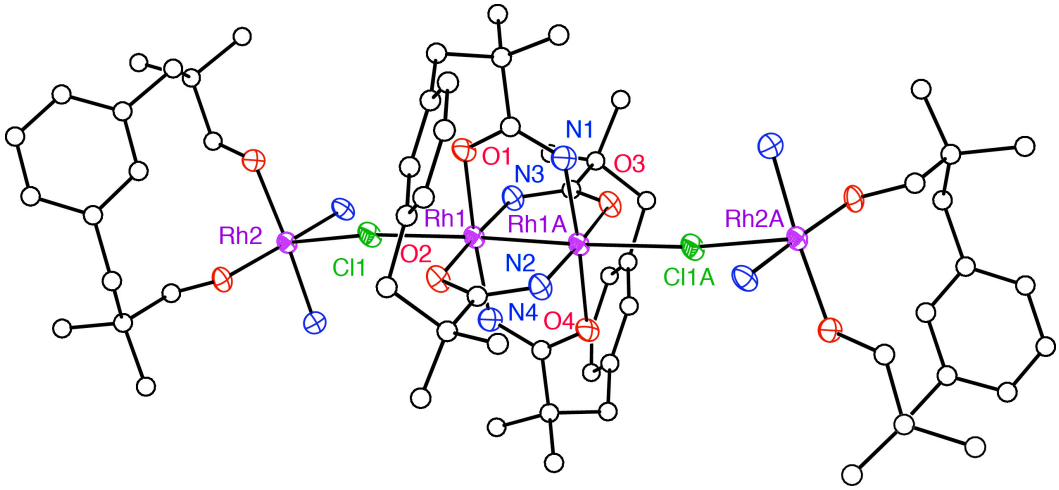

Figure S5.1 Grown structure of **2a**. This complex crystallizes in polymeric chains with three dichloromethane molecules (not shown for clarity). $C_{35}H_{50}Cl_{17}N_4O_4Rh_2$, M = 1044.76, triclinic, a = 12.6948(6), b = 13.6859(6), c = 14.8577(7), U = 2129.04(18) Å^3, T

= 100 K, space group *P-1*, *Z* = 2, R = 0.0613, *w*R2 = 0.1857. Relevant bond distances (Å): Rh-Rh = 2.4155(9), Rh-Cl = 2.617(2), Rh-N = 1.970[6], Rh-O = 2.033[5]. These data can be obtained free of charge from the Cambridge Crystallographic Data Centre via www.ccdc.cam.ac.uk/data_request/cif with CCDC#900048.

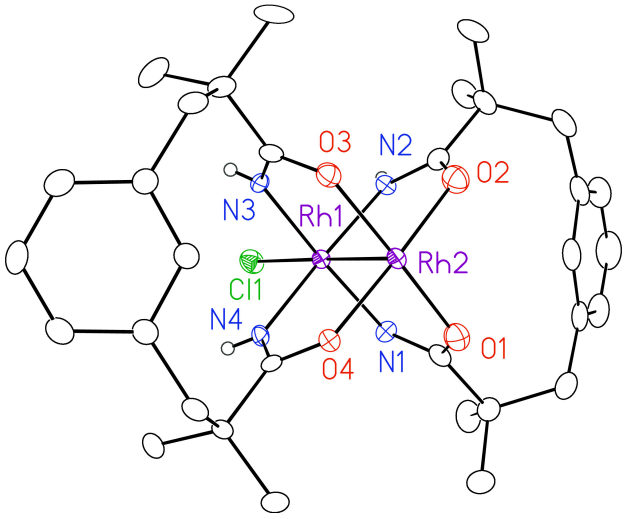

Figure S5.2 The [4,0] isomer of $Rh_2(espn)_2Cl$, **2b**. Thermal ellipsoids drawn at 50% probability. Hydrogen atoms omitted for clarity. This compound crystallizes with two dichloromethane molecules in the asymmetric unit (not shown for clarity). $C_{34}H_{44}Cl_{15}N_4O_4Rh_2$, *M* = 959.83, monoclinic, *a* = 13.2750(3), *b* = 12.8783(3), *c* = 23.4841(5), *U* = 3884.71(15) $Å^3$, T = 100 K, space group $P2_1/c$, *Z* = 4, R = 0.0296, *w*R2 = 0.0568. Relevant bond distances (Å): Rh-Rh = 2.4136(4), Rh-Cl = 2.4165(9), Rh-N = 2.003[3], Rh-O = 1.998[2]. These data can be obtained free of charge from the

Cambridge Crystallographic Data Centre via www.ccdc.cam.ac.uk/data_request/cif with CCDC#900049.

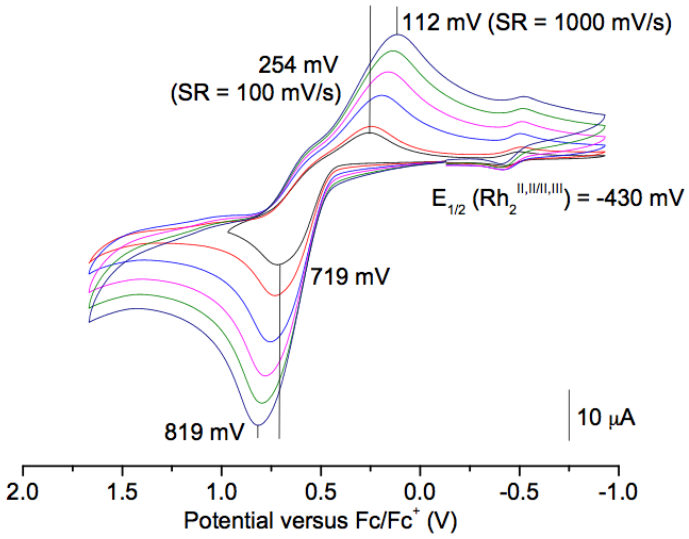

Figure S5.3. **2** (1 mM in CH_3CN/100 mM tetrabutylammonium hexafluorophosphate) in the presence of 10 mM tetrabutylammonium chloride at different scan rates.

Table S5.2 Simple cyclization reaction at 0.05 mol% loading for catalysts **2a** and **2b**.

	Substrate	Product	Catalyst ***2a*** **TON (Yield)**	*Catalyst* ***2b*** **TON (Yield)**
S1	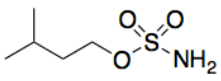	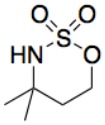	1400 (70%)	1460 (73%)
S2	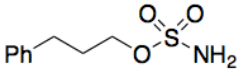	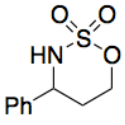	1450 (72%)	1420 (71%)

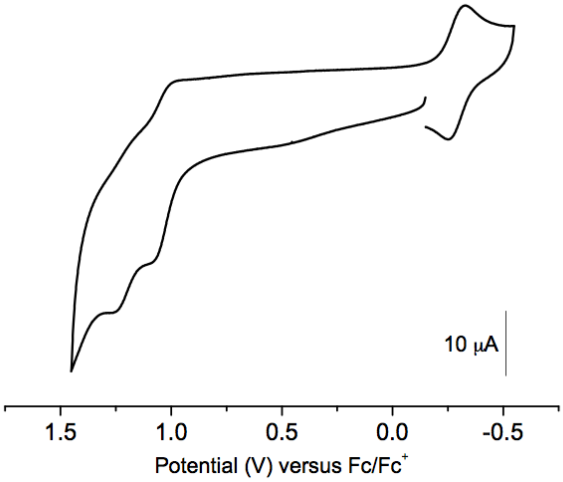

Figure S5.4. **2** (1 mM in CH_3CN/100 mM tetrabutylammonium hexafluorophosphate) with two equivalents $K(BAr^f)$ (Figure 2 in manuscript), plus 2 equivalents $PhI(OAc)_2$. The oxidant causes changes in the electrochemistry of **2**; this is not the case when $PhI(OAc)_2$ is added to **1**. [7]

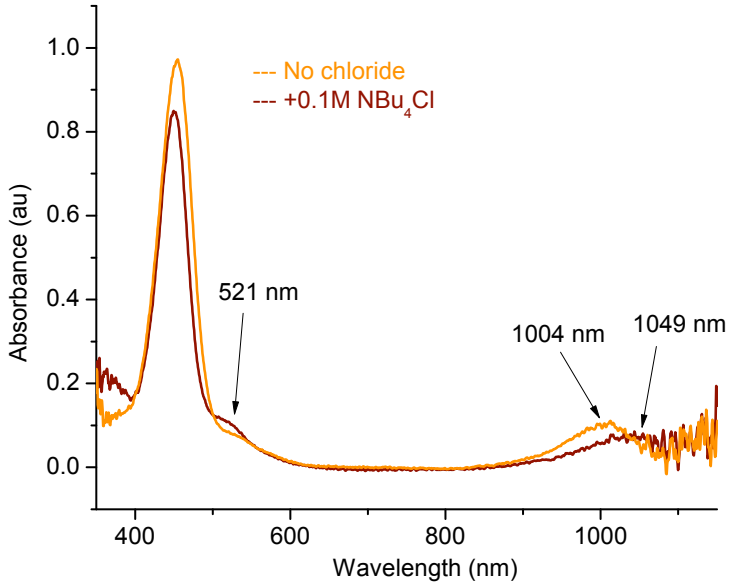

Figure S5.5 UV-Visible spectrum of **2** (orange); in the presence of excess chloride (red).

A slight bathochromic shift is observable upon chloride addition.

References

(1) a) H. M. L. Davies and J. R. Manning, *Nature*, 2008, **451**, 417-424; b) J. Du Bois, *Organic Process Research & Development*, 2011, **15**, 758-762.

(2) a) R. Breslow and S. H. Gellman, *J. Am. Chem. Soc.*, 1983, **105**, 6728-6729; b) C. G. Espino and J. A. DuBois, *Angew. Chem. Int. Edn Engl.*, 2001, **40**, 598-600.

(3) a) C. G. Espino, K. W. Fiori, M. Kim and J. Du Bois, *J. Am. Chem. Soc.*, 2004, **126**, 15378-15379; b) K. W. Fiori and J. Du Bois, *J. Am. Chem. Soc.*, 2007, **129**, 562-568; c) K. W. Fiori, C. G. Espino, B. H. Brodsky and J. Du Bois, *Tetrahedron*, 2009, **65**, 3042-3051.

(4) H. M. L. Davies and S. A. Panaro, *Tetrahedr. Lett.*, 1999, **40**, 5287-5290.

(5) a) D. N. Zalatan and J. Du Bois, *J. Am. Chem. Soc.*, 2009, **131**, 7558-7559; b) K. P. Kornecki and J. F. Berry, *Chem.-Eur. J.*, 2011, **17**, 5827-5832; c) K. P. Kornecki and J. F. Berry, *Eur. J. Inorg. Chem.*, 2012, 562-568.

(6) a) J. L. Bear, B. Han, Z. Wu, E. Van Caemelbecke and K. M. Kadish, *Inorg. Chem.*, 2001, **40**, 2275-2281; b) M. P. Doyle, R. Duffy, M. Ratnikov and L. Zhou, *Chem. Rev.*, 2009, **110**, 704-724; c) M. P. Doyle, *J. Org. Chem.*, 2006, **71**, 9253-9260; d) M. P. Doyle and T. Ren, in *Prog. Inorg. Chem.*, John Wiley & Sons, Inc., 2007, pp. 113-168.

(7) a) A. J. Catino, E. F. Raymon and M. P. Doyle, *J. Am. Chem. Soc.*, 2004, **126**, 13622-13623; b) A. J. Catino, J. M. Nichols, R. E. Forslund and M. P. Doyle, *Org. Lett.*, 2005, **7**, 2787-2790.

(8) M. E. Harvey, D. G. Musaev and J. Du Bois, *J. Am. Chem. Soc.*, 2011, **133**, 17207-17216.

(9) L. Villalobos, Z. Cao, P. E. Fanwick and T. Ren, *Dalton Transactions*, 2012, **41**, 644-650.

(10) B. Meunier, S. I. P. de Visser and S. Shaik, *Chem. Rev.*, 2004, **104**, 3947-3980.

Supplementary References

(1) C. G. Espino, K. W. Fiori, M. Kim and J. Du Bois, *J. Am. Chem. Soc.*, 2004, **126**, 15378-15379.

(2) C. G. Espino and J. A. DuBois, *Angew. Chem. Int. Edn Engl.*, 2001, **40**, 598-600.

(3) M. E. Harvey, D. G. Musaev and J. Du Bois, *J. Am. Chem. Soc.*, 2011, **133**, 17207-17216.

(4) K. W. Fiori and J. Du Bois, *J. Am. Chem. Soc.*, 2007, **129**, 562-568.

(5) L. J. Ingram, A. Desoky, A. M. Ali and S. D. Taylor, *The Journal of Organic Chemistry*, 2009, **74**, 6479-6485.

(6) K. Guthikonda and J. Du Bois, *J. Am. Chem. Soc.*, 2002, **124**, 13672-13673.

(7) K. P. Kornecki and J. F. Berry, *Chem.-Eur. J.*, 2011, **17**, 5827-5832.

Chapter 6

Spectroscopic Characterization of a Donor/Acceptor-Stabilized Dirhodium Carbenoid Intermediate

This chapter has been submitted for publication.

Authors: Katherine P. Kornecki,[1] John F. Briones,[2] Vyacheslav Boyarskikh,[2] Felicia Fullilove,[2] Jochen Autschbach,[3] Kaitlin E. Schrote,[4] Kyle M. Lancaster,[4] Huw M. L. Davies[2] and John F. Berry[1]

[1]Department of Chemistry, University of Wisconsin – Madison, 1101 University Avenue, Madison WI 53706 [2]Department of Chemistry, Emory University, 1515 Dickey Drive, Atlanta GA 30322 [3]Department of Chemistry, University of Buffalo, The State University of New York, Buffalo, NY 14226 [4]Department of Chemistry and Chemical Biology, Cornell University, Baker Laboratory, Ithaca NY 14853

Contributions: J. Briones prepared the ^{13}C-labeled diazo precursor. V. Boyarskikh, J. Autschbach performed DFT calculations. K. E. Schrote and K. M. Lancaster performed XAS measurements. F. Fullilove performed catalytic tests (Figure 6.2, right). All other experimental work was done by K. P. Kornecki.

6.1 Abstract

A multitude of organic transformations catalyzed by complexes of Rh, Cu and other metals are thought to proceed *via* the intermediacy of highly reactive, electrophilic, and to date unobservable carbenoid intermediates. Herein we report the generation of an Rh_2-carbenoid intermediate stabilized through the use of a donor/acceptor carbene fragment. This newly observed intermediate is stable for a period of ~20h in $CHCl_3$ solution at 0°C, allowing for an exploration of its physical and chemical properties. The Rh=C bond, which is established by vibrational and nuclear magnetic resonance spectroscopy, as well as extended X-ray absorption fine structure analysis, has weak sigma and pi components. This intermediate performs stoichiometric cyclopropanation

and C−H functionalization reactions to give products that are identical to those obtained from analogous Rh_2-mediated catalysis. This important breakthrough provides unequivocal experimental evidence for the previous theoretically-based catalytic reactivity of Rh_2-carbenoid intermediates.

6.2 Introduction

Isolation of reactive intermediates has historically provided a great deal of insight into the mechanisms of chemical reactions,[1] and great progress has been made in the synthesis of stable analogs of reactive species such as carbenes and nitrenes.[2] Carbenoids, or metal-carbene species, first postulated in 1952,[3] vary widely in their stability and reactivity. N-heterocyclic carbenes (**A**, Scheme 6.1), stabilized by two N atoms that flank the carbene C atom, serve well as unreactive spectator ligands to metals.[4,5] When only one heteroatom is present to stabilize the carbene, the resulting compounds are known as Fischer-type carbenes (**B**), which can be employed as stoichiometric reagents in reactions such as cyclopropanation.[6] Schrock-type carbene complexes (**C**) have no stabilizing heteroatoms on the carbene carbon and promote catalytic olefin metathesis.[7] Addition of one or more electron-accepting groups (such as esters) to the carbene center destabilizes it even further (**D**). Acceptor carbenes are thus often proposed as key intermediates in a broad range of organic reactions. Although some examples of mononuclear metal complexes of acceptor carbenes exist,[8-11] examples of the most efficient [12] and synthetically versatile system, the Rh_2 carbenoid, have never been observed. Rh_2 tetracarboxylate-catalyzed reactions of donor/acceptor diazocarbonyl compounds result

in a wide range of synthetically useful transformations [12-22] (e.g., Scheme 6.1, bottom). Additionally, the initial products of these reactions are often themselves highly reactive and can engage in domino sequences that lead to the rapid construction of complex products.[21] These systems are currently capable of achieving turnover numbers in excess of 1,000,000 at rates of up to 300 turnovers per second.[12]

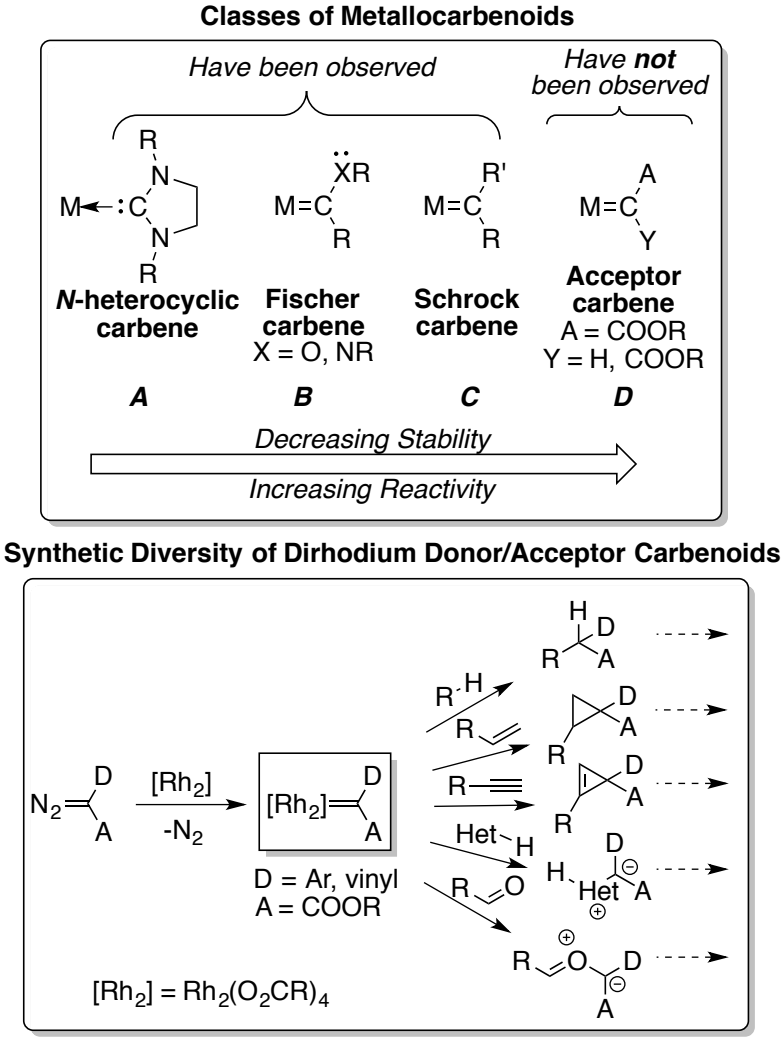

Scheme 6.1 (Top) Classes of metallocarbenoids. (Bottom) Synthetic diversity of Rh_2-carbenoids.

These transformations are thought to proceed *via* a highly electrophilic Rh_2-carbenoid intermediate that prior to this study has defied characterization. Our limited understanding of this intermediate has therefore relied on models that rationalize product distributions, computational studies and limited kinetic studies.[17,23] This type of carbenoid intermediate has remained elusive because in most instances its formation is the rate-determining step in the catalytic cycle.[23] The only known example of an isolated Rh_2 carbene complex is that of the stable nucleophilic Arduengo carbene,[24] which does not engage in reactivity equivalent to Rh_2-catalyzed reactions of a-diazo esters.

6.3 Results and Discussion

In order to observe an Rh_2-carbenoid intermediate, we have turned to donor/acceptor diazo esters, in which the donor group is typically aryl or vinyl.[16,25,26] Both chemical and computational studies indicate attenuated reactivities for donor/acceptor carbenoids compared to conventional acceptor-only carbenoids, so much so that C–H functionalization is predicted to be rate-limiting.[26] This attenuation not only leads to more selective transformations, but also implies substantial stabilization of the donor/acceptor carbenoid intermediate, suggesting that this intermediate has an excellent chance of being observed.

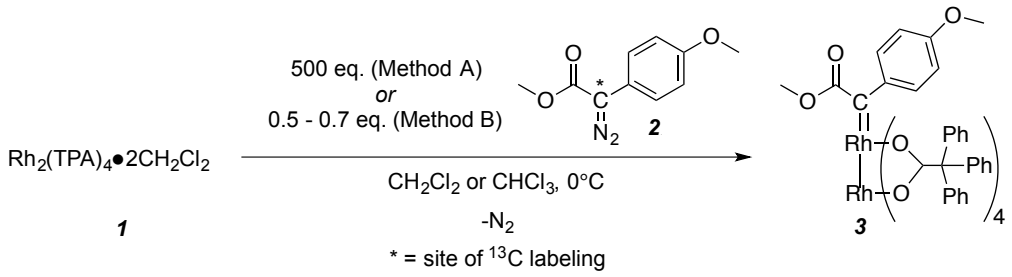

(**Eq. 1**)

To quickly screen for a metastable carbenoid intermediate, a number of Rh_2-carboxylate catalysts were subjected to a 500-fold excess of methyl 2-diazo-2-(4-methoxyphenyl)acetate (**2**) at 0°C (Method A). These conditions allow for the generation of a steady-state concentration of the carbenoid intermediate, detectable by UV-Vis spectroscopy. When $Rh_2(tpa)_4$ (**1**, Figures 6.1a and S6.1; tpa = triphenylacetate) was used in this test, a new 700 nm UV-Vis feature attributed to carbenoid intermediate **3** was observed, having a half-life of approximately 30 seconds under ambient conditions (Figure 6.1c). A second stoichiometric method to form a metastable solution of **3** was subsequently discovered (Method B). In Method B, rigorously dry, deoxygenated dichloromethane or chloroform solutions of **1** and **2** were combined in a 1 : 0.5 stoichiometry, respectively, producing an immediate effervescence. Methods A and B are summarized in Eq. 1; formation of **3** under both conditions is confirmed by similarity of the UV-Vis and Raman features of the intermediates formed by both methods (Figure 6.1c, Figure S6.4). Intermediate **3** can also be formed under conditions amenable to observation by mass spectrometry. When a mixture of solids **1** and **2** is exposed to a MALDI-MS laser source, a signal at m/z = 1532/1533 that corresponds to ^{12}C **3**/^{13}C **3** is

observed (see Eq. 1 for the site of ^{13}C labeling). Carbene complex **3** is readily distinguished from light green precursor **1** by its intensely dark ocean blue-green color is consistent with the higher molar absorptivity of **3** (e ~ 1300 at 700 nm) versus that of **1** (e ~ 500 at 670 nm). Solutions of **3** are stable under inert atmosphere at 0°C for up to 20 hours in chloroform or dichloromethane.

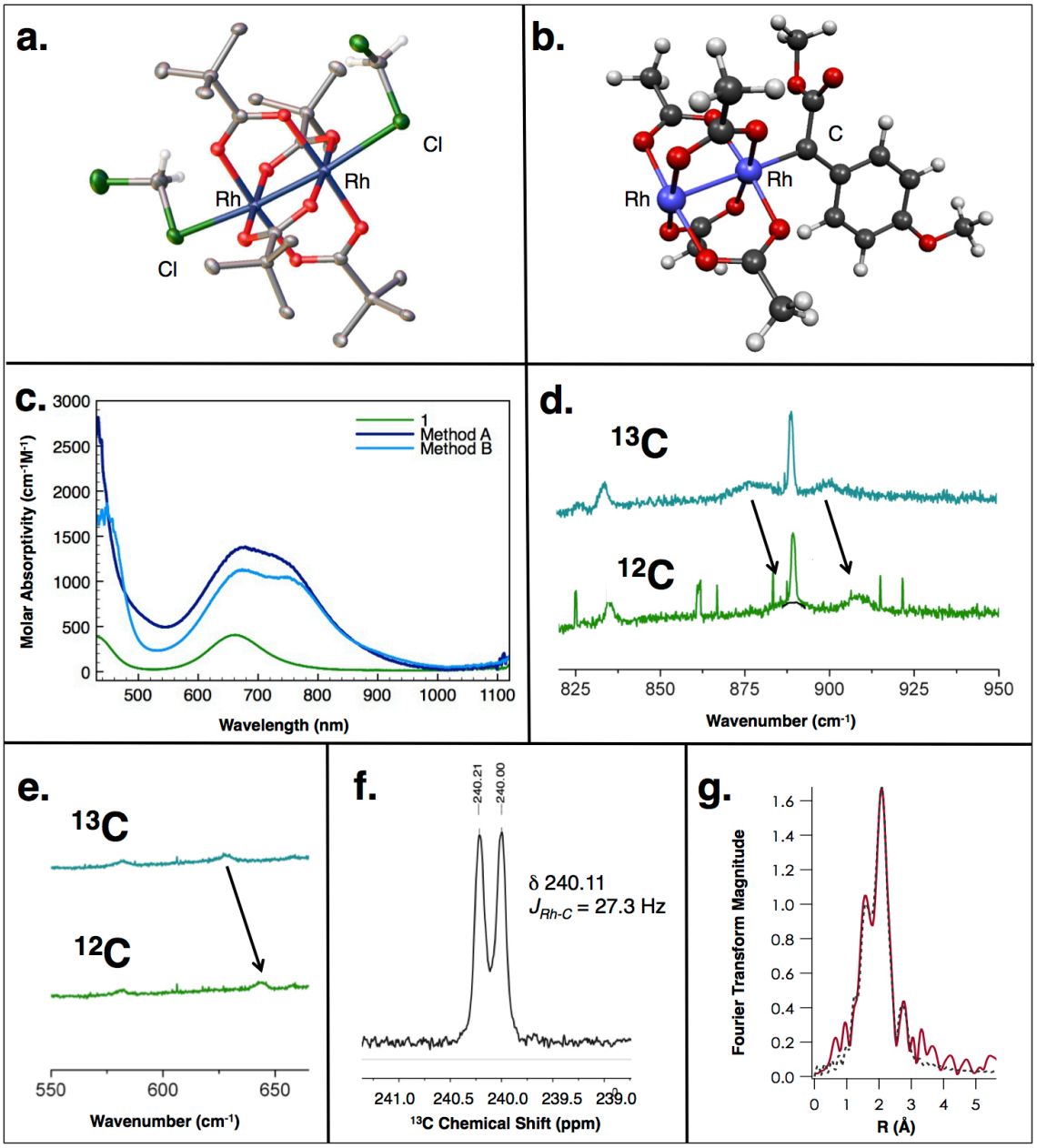

Figure 6.1 a) X-Ray crystal structure of **1** with axially bound dichloromethane molecules. Only the *ipso*-carbon of each phenyl group of the tpa ligands is shown for clarity; thermal ellipsoids are each drawn at a 50% probability level. b) Computational model **3a**. c) UV-Vis spectra of **3** in chloroform at –78°C generated by Method A (dotted

line) and Method B (dashed); the spectrum of starting complex **1** (room temperature) is shown as a solid line. d/e) Regions of the rR spectrum of **3** where isotopic shifts are observed by use of 647 nm laser irradiation. The position of the peak centered at 889.9 cm^{-1} in d) is marked with an arc for clarity. Arrows indicate isotopically shifted modes. f) ^{13}C NMR trace of a 0°C solution of **3** in $CDCl_3$. g) Rh K-edge EXAFS for **3**; experimental data are in red, fits are in dashed gray.

The intense absorption features of **3** allow for characterization of this intermediate by resonance Raman (rR) spectroscopy. Excitation of **3**, prepared by either Method A or B and immediately frozen at −196°C, yields three vibrational stretches that display substantial $^{12}C/^{13}C$ isotope shifts (Figures 6.1d,e, S6.2, and S6.3). These vibrations match well with computationally predicted Rh−C stretching and O−Rh−C bending modes, all due to an Rh=C interaction (Table 6.1). These data are comparable to those reported for Group VI Fischer carbene complexes, which exhibit carbene-based vibrational modes in the 700 – 900 cm^{-1} range.[27]

Table 6.1 Comparison of experimental and calculated properties of **3**/**3a**.

		Experiment (**3**)			DFT (**3**)			DFT (**3a**)		
	Rh–Rh	2.434(2)			2.412			2.459		
	$Rh–O_{carboxylate}$	--[a]			2.041			2.062		
EXAFS	$Rh–C_{carbene}$	--[a]			1.972			2.018		
(Å)	avg. Rh–C/O	2.037(2)[a]			2.027			2.040		
		Experiment (**3**)			DFT (**3a**)					
		^{12}C	^{13}C	Δ[b]	^{12}C	^{13}C	Δ[b]			
RR	Mode 1	643.8	628.3	15.5	656.4	641.7	14.7			
Vibrations	Mode 2	889.9	876.5	13.4	913.0	898.8	14.2			
(cm^{-1})	Mode 3	909.2	900.1	9.1	924.5	916.4	8.1			
		Experiment (**3**)			DFT (**3a**)					
^{13}C NMR	δ	240 ppm			218–270 ppm[c]					
($CDCl_3$)[d]	$J_{Rh–C}$	27.3 Hz; not observed[c]			26 Hz; 12 Hz[c]					

[a]Only an average Rh-O/C distance could be refined from EXAFS data.
[b]$\Delta = \nu(^{12}C)-\nu(^{13}C)$
[c]The calculated chemical shift is highly sensitive to the choice of functional (SI). The second predicted coupling constant of 12 Hz is to the distal Rh atom, but this coupling is too small to be observed under our experimental conditions.

The ^1H NMR spectrum of a $CDCl_3$ solution of **3** (Method B), shown in Figure S6.5, clearly shows the presence of unreacted **1** (multiplets at δ = 6.625, 6.87 and 7.08 ppm) as well as a new species (**3**) having slightly more upfield aryl proton resonances (δ = 6.575, 6.82 and 7.04 ppm) in addition to signals due to the methoxy groups of the carbene fragment at δ = 2.75 ppm (ester) and δ = 3.92 ppm (*p*-OMe). The ester methoxy signal is drastically shifted from its original position in **2** (3.85 ppm), due to proximity to the aryl rings of the tpa ligands, as established by the observation of NOE between the methyl peak at δ = 2.75 ppm and the aryl resonances of **3** at δ = 6.575 and 6.82 ppm (Figure S6.6).

Preparation of **3** using ^{13}C-labeled **2** allowed for observation of the highly deshielded carbenoid carbon by ^{13}C NMR at 242 ppm (Figures 6.1f and S6.8). This signal with δ > 200 ppm is the hallmark of a transition metal carbene complex.[28] Moreover, this signal is conspicuously split into a doublet (J_{Rh-C} = 27.3 Hz), indicating a bond between this C atom and a single I = ½ ^{103}Rh nucleus (100% natural abundance). Importantly, this data is in stark contrast to the previously reported Rh_2 Arduengo carbene complex,[24] which exhibits a carbene carbon resonance at 153.73 ppm, indicative of a lesser degree of electrophilicity, consistent with its lack of carbene transfer reactivity. Furthermore, the increased J_{Rh-C} of 41.5 Hz in the Arduengo carbene compared to **3** implies a stronger Rh=C interaction in the former. A mononuclear Rh phenyl carbene complex reported by Milstein and coworkers also displays an increased J_{Rh-C} at 38.3 Hz and attenuated electrophilicity with a ^{13}C chemical shift at 173 ppm.[29]

To obtain structural information for **3**, we have measured Rh K-edge X-ray absorption (XAS) including extended X-ray absorption fine structure (EXAFS) for **1**, **3** and a spent solution of **3** (**3-dec**). Samples of **1**, **3** and **3-dec** show no difference in their Rh K-edge energy, implying that intermediate **3** is best formulated as an Rh_2(II,II) species (Figure S6.9). Notably, EXAFS-derived bond distances for **1** show excellent agreement with corresponding distances determined for **1** by X-ray crystallography (Table S6.1).

The EXAFS data for **3** reveal two important changes from the structure of **1**. First, the Rh−Rh bond distance in **3** elongates to 2.43 Å from 2.38 Å in **1**. Second, whereas the average number of light atom (C or O) scatterers per Rh atom in **1** is 4, the EXAFS data

for **3** indicate 4.5 C/O scatterers bound per Rh, which is consistent with a linear Rh−Rh=C structure in which one carbene ligand binds to the axial site of the $Rh_2(tpa)_4$ molecule. Models with 4, 5, or 6 C/O scatterers bound per Rh led to poorer fits to the data.

A computational model of **3**, **3a**, was made for investigation of its electronic structure using DFT. In this model, the bulky triphenylacetate ligands have been replaced by acetates to increase computational efficiency; modeling the tpa ligands by DFT does not significantly change interatomic distances. Geometry optimization of **3a** yields a structure in good agreement with the experimental data available for **3** (Table 6.1). Greater molecular detail is available from **3a**. For example, the EXAFS data can only be refined with an average Rh−C/O distance of 2.037(2) Å, whereas the optimized structure of **3a** indicates individual Rh−O and Rh=C distances of 2.04 Å and 1.97 Å, respectively. Importantly, the weighted average of these distances, 2.03 Å, is in excellent agreement with the EXAFS result (2.037(2) Å).

Other experimental observables that have been calculated for **3a** include the vibrations observed for **3** by rR spectroscopy, and the ^{13}C NMR information for the carbene C atom. As seen in Table 1, these calculated data agree well with the experimentally observed values. Notably, the calculated vibrations are uniformly ~10-15 cm^{-1} higher than the observed values, which appears to be a systematic overestimation by the DFT methods. More importantly, the magnitude of the isotopic shifts are reproduced to within 1 cm^{-1}. The UV-Vis feature shown experimentally in Figure 2c is also reproduced reasonably well by TD-DFT (Figure S6.10).

Bonding within the Rh−Rh=C framework has been discussed in previous reports[23,30-33], although never before could the electronic structure be substantiated by comparison to direct experimental data. Sigma bonding along the Rh−Rh−C chain follows the three-center orbital paradigm described by Nakamura[23] and Berry[33]. Weak Rh_2=C π bonding is accomplished by the formation of in-phase (π_1, filled) and out-of-phase (π_2, empty) combinations of the Rh_2 π* orbital with the empty π orbital of the carbene unit. The π_2 orbital is the LUMO of **3a** and its polarization towards the carbene carbon is the basis of the electrophilicity of **3a**. An electronic transition that promotes an electron from π_1 to π_2 is responsible for the low energy absorption feature at ~720 nm that is characteristic of **3** (Figure S6.11). Importantly, **3a** is electronically distinct from other more stable carbene complexes in that both the σ and π bonding components are significantly weakened by the electronic effects of the Rh−Rh bond (calculated Rh=C bond orders are ~ 0.7-0.8).

The catalytic reactivity of **1** is subdued compared to other Rh_2 catalysts (i.e., it does not readily promote C-H functionalization of substrates such as cyclohexane, cyclopentane or ethyl benzene), although it does exhibit both cyclopropanation and C−H functionalization reactivity as exemplified by its reactions with styrene and THF, respectively (Figure 6.2). Importantly, the stoichiometric reactivity of intermediate **3** with these substrates is comparable to the respective catalytic reactions of **1**, supporting the proposed intermediacy of **3** in catalysis.

We also have been able to identify products of stoichiometric reactions of **3** with other reagents: water, oxygen, and additional equivalents of **2** (Figure 6.2). Both O–H bonds of water are susceptible to reaction with **3** to form **4**. Molecular oxygen is cleaved in the reaction with **3** to form the ketone product **5**. When **3** is introduced to additional equivalents of the diazo compound **2**, the carbene group is transferred to excess **2** to yield the dimeric azine compound **6**. Compounds **4**, **5** and **6** are all by-products identified in Rh_2-mediated catalysis. When no substrate is added, solutions of **3** in halocarbon solvents degrade slowly to form a multitude of unidentified organic products. However, the only Rh-containing product post-decomposition of **3** is **1**, as verified by NMR and EXAFS (the EXAFS data for **3-dec** are not significantly different from those of **1**).

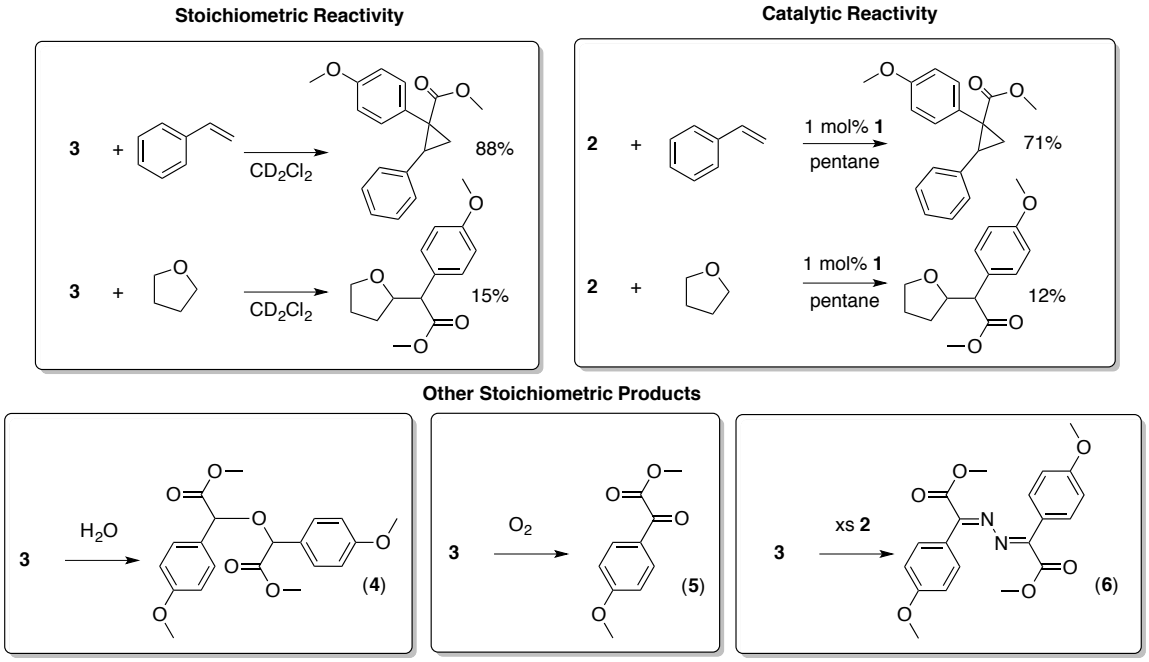

Figure 6.2 Comparison of stoichiometric and catalytic reactivity for donor/acceptor carbenoid **3**.

6.4 Summary

The isolation of **3** has significant implications to the field of catalysis: direct evidence for this type of carbenoid intermediate has remained elusive since work in this arena began in 1952.[3] The characterization of this intermediate provides a firm foundation for future computational and mechanistic investigations of these highly reactive and selective carbenoid species. The carbenoid intermediates proposed in Rh_2-catalyzed C−H functionalization are validated throughout this work, and perhaps more importantly, a broader understanding of bonding and reactivity of transition metal carbene complexes in the stability continuum from isolable Fischer- and Schrock-type carbenes to this newly-observed and less stable donor/acceptor carbenoid, can be developed.

6.5 Acknowledgements

We thank the Chemical Sciences, Geosciences, and Biosciences Division, Office of Basic Energy Sciences, Office of Science, U.S. Department of Energy for support (DE-FG02-10ER16204) as well as the CCI Center for Selective C–H Functionalization supported by NSF (CHE-1205646). KML gratefully acknowledges Cornell University for startup funding. Portions of this research were carried out at the Stanford Synchrotron Radiation Lightsource, a Directorate of SLAC National Accelerator Laboratory and an Office of

Science User Facility operated for the U.S. Department of Energy Office of Science by Stanford University. The SSRL Structural Molecular Biology Program is supported by the DOE Office of Biological and Environmental Research, and by the National Institutes of Health, National Institute of General Medical Sciences (including P41GM103393). The contents of this publication are solely the responsibility of the authors and do not necessarily represent the official views of NIGMS, NCRR, or NIH.

6.6 Supplementary Information

General Considerations and Instrumentation

All reactions were performed using oven-dried glassware under an atmosphere of dry nitrogen, either in a glove box or using Schlenk techniques. Dichloromethane and chloroform were dried over CaH_2 overnight and distilled before use. Styrene was purified over dibutyl magnesium and tetrahydrofuran (THF) was distilled from sodium/benzophenone prior to use in stoichiometric reactions. Methyl 2-diazo-2-(4-methoxylphenyl)acetate (**2**) was prepared according to the published procedure.[34] Prior to use, **2** was purified by passing a diethyl ether solution through two successive silica plugs. After solvent removal, the orange crystalline solid was dried under vacuum in a Schlenk flask for 5h at room temperature. $Rh_2(tpa)_4$ (**1**) was prepared according to the method described by Hashimoto[35], with the exception that the purified product was recrystallized from dichloromethane and 10% methanol. Prior to all reactions, dark green freshly recrystallized $Rh_2(tpa)_4$•2MeOH was dried at 100°C under vacuum to yield **1** free of axial solvent, a yellow powder. Upon dissolution in dry dichloromethane or

chloroform, the color of the solution was green, indicative of axial solvent binding.

UV-Vis Spectroscopy. UV-Vis spectra were collected in real-time using a Miniature BLUE-wave UV-Vis dip-probe with a tugsten/krypton lightsource and a 0.2 cm path length tip under an N_2 atmosphere.

Resonance Raman Spectroscopy. All rR spectra were collected on frozen solution samples in a finger dewar filled with liquid N_2. A Coherent I-305 Ar+ ion laser was used as the excitation source and ~135° backscattered light was dispersed by an Acton Research triple monochromator equipped with 1200 and 2400 grooves/mm gratings. Dispersed light was analyzed by a Princeton Instruments Spec X:100BR deep depletion, back-thinned CCD camera.

NMR Spectroscopy. ^{1}H and ^{13}C NMR spectra were collected on a Bruker Avance-500 spectrometer with DCH Cryoprobe at room temperature. Samples were prepared using Method B (vide infra).

X-ray Absorption Spectroscopy. Rh K-edge XAS including EXAFS to k = 17 $Å^{-1}$ were collected at the Stanford Synchrotron Radiation Lightsource (SSRL) beamline 7-3 under ring conditions of 3 GeV and 500 mA. A Si(220) double-crystal monochromator was used for energy selection and detuned by ~ 50% for harmonic rejection. Internal energy calibration was performed by assigning the first inflection point of a spectrum of Rh foil to 23220 eV. Samples of **3** were prepared according to Method A (vide infra) to avoid the presence of excess **1**. Data were collected in fluorescence mode (using a Canberra Ge 30-

element array detector) with the sample maintained at 10 K in an Oxford liquid He flow cryostat. Elastic scatter was attenuated using a Ru filter. 8-13 scans were averaged and processed using the MAVE and PROCESS modules of the EXAFSPAK software package. Background subtraction was achieved by fitting a polynomial to the pre-edge region and subtracting this polynomial from the entire spectrum. A three-segment fourth-order spline was applied to the EXAFS region. EXAFS fitting was carried out with the OPT module of EXAFSPAK using FEFF7-calculated scattering paths beginning with geometry optimized coordinates. EXAFS data were weighted by k^3. All fits employed k-smoothed data.

X-ray Crystallography. Diffraction data for **1**•$2CH_2Cl_2$ was collected on a Bruker Quazar SMART diffractometer with an APEX-II area detector with a Mo Kα IμS radiation source equipped with an Oxford Cryosystems low temperature device. Diffraction data were indexed by the SMART program,[36] and the structures were solved via direct methods (SHELXTL/OLEX2) and refined by iterative cycles of least-squares refinement on F^2 followed by difference Fourier synthesis.[37,38]

Preparation of ^{13}C labeled 2 (Methyl-2-^{13}C-2-diazo-2-(4-methoxyphenyl)acetate)

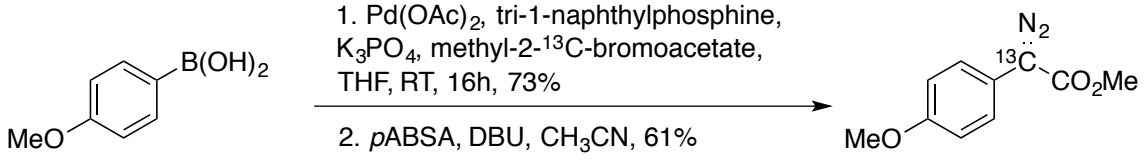

Methyl-2-^{13}C-bromoacetate was synthesized *via* modified literature procedure.[39] To a round bottom flask containing 5.0 g (36.0 mmol) 2-^{13}C-bromoacetic acid was added 3.4 mL (39.6 mmol) of oxalyl chloride dropwise at 0 °C. The solution was slowly warmed to room temperature and stirred overnight after which the reaction was cooled to 0 °C and carefully quenched with anhydrous methanol by slow addition. The reaction was warmed to room temperature and stirred for 4 hrs. Aqueous $NaHCO_3$ was added and then the organic layer was extracted with dichloromethane. The combined organic layers were dried over $MgSO_4$, filtered and then concentrated *in vacuo* to provide the ester as colorless oil. The product was obtained in quantitative yield (5.5 g) and was used for next step without any further purification. ^{1}H NMR (600 MHz) **δ** 3.72 (d, 2H, J = 153.6 Hz), 3.79 (s, 3H). The NMR spectra is consistent with published results.[40]

Methyl-2-^{13}C-2-(4-methoxyphenyl)acetate was synthesized *via* modified literature procedure.[41] To a dry flask was added 40.4 mg (0.18 mmol) $Pd(OAc)_2$, 0.22 mg (0.53 mmol) tri-1-naphthylphosphine, 6.2 g K_3PO_4 (29.1 mmol), 1.0 g (5.9 mmol) 2-^{13}C-methylbromoacetate and 1.8 g (11.6 mmol) 4-methoxyphenylboronic acid. The solids were dissolved in 50 mL anhydrous THF and the resulting reaction mixture was stirred at room temperature under an Argon atmosphere. After 16 hrs, the reaction was quenched with 45 mL of H_2O and the organic layer was extracted with dichloromethane. The combined organic layers were dried over $MgSO_4$, filtered and then concentrated *in vacuo*. The crude material was purified *via* silica gel chromatography using 19:1 hexane/ethyl acetate as the solvent system. The product was obtained in 73% yield (0.78 g) as white solid. ^{1}H NMR (600 MHz) **δ** 7.19 (m, 2H), 6.86 (d, 2H, J = 8.4 Hz), 3.79 (s, 3H), 3.68 (s, 3H), 3.46 (d, 2H, J = 129 Hz).

Methyl-2-^{13}C-2-diazo-2-(4-methoxyphenyl)acetate was synthesized *via* a modified literature procedure.[42] To a solution of 1.2 g (6.7 mmol) ester and 1.9 g (8.0 mmol) *p*-acetamidobenzenesulfonylazide (*p*ABSA) in 20 mL of anhydrous acetonitrile was added 1.4 g (9.4 mmol) of 1,8-Diazabicyclo[5.4.0]undec-7-ene (DBU) at 0 °C. When addition was completed, the reaction was stirred overnight (reaction turned colorless to orange). The resulting orange solution was diluted with diethyl ether then quenched with aqueous NH_4Cl. The organic layer was separated, washed with brine and dried over $MgSO_4$, filtered then concentrated *in vacuo* to afford the crude material. The diazoacetate was purified *via* silica gel chromatography using 19:1 hexane/diethyl ether as solvent system affording the desired product in 61% yield as a dark orange solid. ^{1}H NMR (500 MHz, $CDCl_3$) **δ** 7.39 (m, 2H), 6.95 (d, 2H, J = 9.0 Hz), 3.85 (s, 3H), 3.81 (s, 3H). ^{13}C NMR (125 MHz, $CDCl_3$) **δ** 166.5, 158.1, 126.1, 117.1, 114.6, 62.4 (C=N_2), 55.3, 52.0. IR (neat) 3009, 2961, 2842, 1702, 1511, 1248, 1141, 1029, 830 cm^{-1}. HRMS (ESI) *m/z* calcd for $[C_9{}^{13}CH_{10}N_2O_3]^{\bullet+}$, 207.0720, found $[M]^{\bullet+}$ 207.0723.

Intermediate Generation Procedures

Method A. A 0.5 M solution of **2** (~200 mg, 2 mL) in chloroform (or dichloromethane) was chilled to 0°C. A 0.01 M solution of **1** (3 mg, 0.2 mL) in the same solvent was quickly added without stirring. The dark blue-green color of intermediate **3** appears instantly upon addition but dissipates over the course of 10-30 seconds accompanied by vigorous effervescence.

EXAFS samples prepared by this method were formed directly in a ~0.3 mL capacity Delrin XAS cell with a 9 x 2 mm slit in the cap and were immediately flash

frozen in a liquid N_2 bath. The slits were covered with 38 μm Kapton to make X-ray transparent windows.

Method B. Solutions of **1** (~0.025 mM; 34 mg in 1 mL) and **2** (~0.024 mM; 5 mg in 1 mL) in chloroform were prepared in the glovebox and chilled to ~0°C. Solution **1** (0.4 mL) was quickly added to solution **2** (0.2 mL) without stirring. Vigorous effervescence is observed upon addition and the dark blue-green color of intermediate **3** appears. This solution is stable for up to 20h at 0°C and up to 5h at RT in a *rigorously inert atmosphere*.

*Stoichiometric Reactions of **3**.* A solution of **3** was prepared by Method B in deuterated chloroform. Substrate (5 equivalents) was added neat via microsyringe in a glovebox. The reaction with styrene is fast, immediately yielding a light green solution indicative of precursor **1**. Reaction with THF takes approximately 1h before the color of **1** is observed. Insertion products were identified by their characteristic ^{1}H NMR chemical shift. Stoichiometric percent conversion was determined based on ^{1}H NMR integration versus an added 0.002 M cyclohexane internal standard. Insertion compounds **4** and **5** were observed by ^{1}H NMR in solutions of **3** prepared by Method B and exposed to air. Insertion compound **6** is only observed by ^{1}H NMR when compound **2** is in excess.

*Catalytic Reactions of **1***

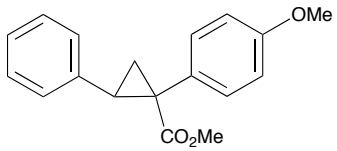

Methyl 1-(4-methoxyphenyl)-2-phenylcyclopropanecarboxylate

A solution of methyl 4-methoxyphenyldiazoacetate (103.10 mg, 0.5 mmol) in 5.0 mL of pentane was added dropwise to a solution of $Rh_2(TPA)_4$ (6.8 mg, 0.005 mmol) and styrene (0.288 mL, 2.5 mmol) in 5.0 mL of pentane over 1h. The reaction was stirred another 15 min after the addition was complete. The solvent was removed under reduced pressure and the residue purified by flash chromatography on silica gel (10% diethyl ether/pentane) to give 100 mg (71% yield) of a white solid. ^{1}H NMR (400 MHz; $CDCl_3$): δ 7.07-7.05 (m, 3H), 6.93 (d, 2H, J = 8.7 Hz), 6.78-6.75 (m, 2H), 6.66 (d, 2H, J = 8.7 Hz), 3.71 (s, 3H), 3.65 (s, 3H,), 3.07 (dd, 1H, J = 9.3, 7.2 Hz), 2.12 (dd, 1H, J = 9.3, 4.8 Hz), 1.82 (dd, 1H, J = 4.8, 7.2 Hz); The spectroscopic data are consistent with previously reported data.[43]

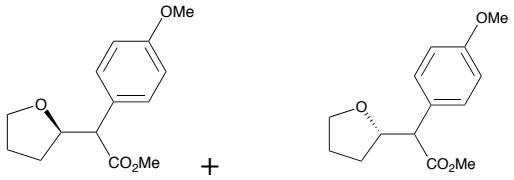

Methyl 2-(4-methoxyphenyl)-2-((R)-tetrahydrofuran-2-yl)acetate

A solution of methyl 4-methoxyphenyldiazoacetate (103.10 mg, 0.5 mmol) in 5.0 mL of rigorously degassed anhydrous chloroform was added dropwise to a solution of $Rh_2(TPA)_4$ (6.8 mg, 0.005 mmol) and anhydrous tetrahydrofuran (0.406 mL, 5.0 mmol)

in 5.0 mL of anhydrous chloroform over 1h. The reaction was stirred another 15 min after the addition was complete. The solvent was removed under reduced pressure and the residue purified by flash chromatography on silica gel (20% diethyl ether/pentane) gave separation of the two diastereomers in a total recovery of 75 mg (60% yield) of a clear oil. ^{1}H NMR (400 MHz, $CDCl_3$): (major diastereomer) δ 7.30 (d, 2 H, *J* = 8.6 Hz), 6.87 (d, 2 H, *J* = 8.6 Hz), 4.52 (dt, 1 H, *J* = 8.3 Hz, 7.0 Hz), 3.83-3.69 (m, 2 H), 3.77 (s, 3 H) , 3.65 (s, 3 H), 3.57 (d, 1 H, *J* = 8.4 Hz), 2.09 (m, 1 H) ,1.86 (m, 2 H), 1.62 (m, 1 H). (minor diastereomer): δ 7.26 (d, 2 H, *J* = 8.4 Hz), 6.85 (d, 2 H, *J* = 8.4 Hz), 4.47 (dt, 1 H, *J* = 9.9 Hz, 7.0 Hz), 3.92-3.81 (m, 2 H), 3.78 (s, 3 H) , 3.69 (s, 3 H), 3.46 (d, 1 H, *J* = 10.2 Hz), 1.88-1.79 (m, 2 H) ,1.69 (m, 1 H), 1.43 (m, 1 H). The spectroscopic data are consistent with previously reported data.[44]

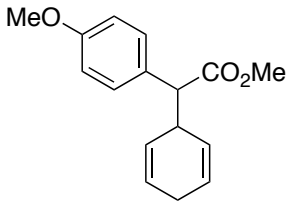

Methyl 2-(cyclohexa-2,5-dien-1-yl)-2-(4-methoxyphenyl)acetate

A solution of methyl 4-methoxyphenyldiazoacetate (103.10 mg, 0.5 mmol) in 5.0 mL of pentane was added drop wise to a solution of $Rh_2(TPA)_4$ (6.8 mg, 0.005 mmol) and 1,4 cyclohexadiene (0.240 mL, 2,54 mmol) in 5.0 mL of pentane over 1h. The reaction was stirred another 15 min after the addition was complete. The solvent was removed under reduced pressure and the residue purified by flash chromatography on

silica gel (10% diethyl ether/pentane) to give 70 mg (54% yield) of a colorless oil. ^{1}H NMR (400 MHz; $CDCl_3$): δ 7.25-7.22 (m, 2H), 6.86-6.82 (m, 2H), 5.80-5.76 (m, 1H), 5.71-5.64 (m, 2H), 5.29-5.24 (m, 1H), 3.76 (s, 3H), 3.65 (s, 3H), 3.47-3.39 (m, 1H), 3.35 (d, 1H, *J* = 10.4), 2.62-2.57 (m, 2H). Spectroscopic data are consistent with previously reported data.[45]

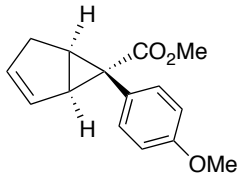

Methyl 6-(4-methoxyphenyl)bicyclo[3.1.0]hex-2-ene-6-carboxylate

A solution of methyl 4-methoxyphenyldiazoacetate (103.10 mg, 0.5 mmol) in 5.0 mL of pentane was added dropwise to a solution of $Rh_2(TPA)_4$ (6.8 mg, 0.005 mmol) and cylcopentadiene (0.210 mL, 2.5 mmol) in 5.0 mL of pentane over 1h. The reaction was stirred another 15 min after the addition was complete. The solvent was removed under reduced pressure and the residue purified by flash chromatography on silica gel (10% diethyl ether/pentane) to give 78 mg (64% yield) of a white solid. ^{1}H NMR (400 MHz, $CDCl_3$): δ 7.03 (d, 2H, *J* = 8.2 Hz), 6.82 (d, 2H, *J* = 8.5 Hz), 5.75-5.74 (m, 1H), 5.24-5.23 (m, 1H), 3.79 (s, 3H), 3.60 (s, 3H), 2.92-2.91 (m, 1H), 2.67-2.60 (m, 2H), 2.07 (dd, 1H, *J* = 18.1, 2.1 Hz). Spectroscopic data are consistent with previously reported data.[12]

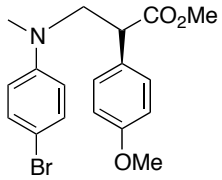

Methyl 3-((4-bromophenyl)(methyl)amino)-2-(4-methoxyphenyl)propanoate

A solution of methyl 4-methoxyphenyldiazoacetate (103.10 mg, 0.5 mmol) in 5.0 mL of pentane was added dropwise to a solution of $Rh_2(TPA)_4$ (6.8 mg, 0.005 mmol) and 4-bromo-N,N,-dimethylaniline (500.2 mg, 2.5 mmol) in 5.0 mL of pentane over 1h. The reaction was stirred another 15 min after the addition was complete. The solvent was removed under reduced pressure and the residue purified by flash chromatography on silica gel (10% diethyl ether/pentane) to give 126 mg (67% yield) of a yellow oil. FTIR (Neat) 2950, 2835, 1731, 1609, 1590, 1496, 1247, 1160, 1032, 805 cm^{-1}; ^1H NMR (400 MHz; $CDCl_3$) δ 7.29 (d, 2H, *J* = 8.8 Hz), 7.21 (d, 2H, *J* = 8.5 Hz), 6.86 (d, 2H, *J* = 8.5 Hz), 6.54 (d, 2H, *J* = 8.8 Hz), 4.05 (dd, 1H, *J* = 14.7, 8.5 Hz), 4.01-3.85 (m, 1H), 3.79 (s, 3H), 3.64 (s, 3H), 3.61-3.45 (m, 1H), 2.77 (s, 3H); ^{13}C NMR (100 MHz, $CDCl_3$) δ 173.52, 159.1, 147.3, 132.6, 131.8, 130.2, 129.0, 128.7, 114.2, 113.7, 108.4, 56.5, 55.2, 52.1, 48.34, 39.29

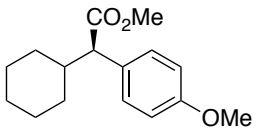

Methyl 2-cyclohexyl-2-(4-methoxyphenyl)acetate

A solution of methyl 4-methoxyphenyldiazoacetate (103.10 mg, 0.5 mmol) in 5.0 mL of anhydrous cyclohexane was added dropwise to a refluxing solution of $Rh_2(TPA)_4$ (6.8 mg, 0.005 mmol) in 5.0 mL of anhydrous cyclohexane over 1h. The reaction was stirred another 15 min after the addition was complete and then cooled to ambient temperature. The solvent was removed under reduced pressure and the residue purified by flash chromatography on silica gel (10% diethyl ether/pentane) to give 100 mg (75%

yield) of a colorless oil. ^{1}H NMR (400 MHz, $CDCl_3$): δ 7.23: (d, 2 H, *J* = 8.4 Hz), 6.84 (d, 2H, *J* = 8.4 Hz), 3.78 (s, 3H), 3.65 (s, 3 H), 3.16 (d, 1H, *J* = 10.6 Hz), 1.93 (m, 1H), 1.78 – 1.55 (m, 4 H), 1.33-0.99 (m, 5H), 0.71 (m, 1H). The spectroscopic data are consistent with previously reported data.[44]

^{1}H NMR data for organic byproducts

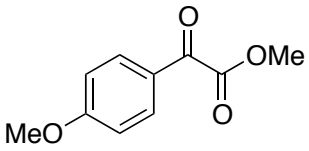

Methyl 2-(4-methoxyphenyl)-2-oxoacetate

^{1}H NMR (400 MHz; $CDCl_3$) δ 8.02 (d, 2H, *J* = 8.8 Hz), 6.98 (d, 2H, *J* = 8.8 Hz), 3.97 (s, 3H), 3.90 (s, 3H); ^{13}C NMR (100 MHz, $CDCl_3$) δ 184.6, 165.3, 164.6, 132.9, 125.7, 114.5, 55.9, 52.9.

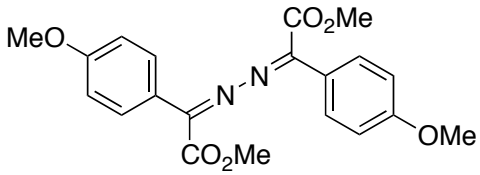

Dimethyl 2,2'-(hydrazine-1,2-diylidene)bis(2-(4-methoxyphenyl)acetate)

^{1}H NMR (400 MHz; $CDCl_3$) δ 7.69 (d, 4H, *J* = 9 Hz), 6.91 (d, 4H, *J* = 9 Hz), 3.98 (s, 6H,), 3.84 (s, 6H); ^{13}C NMR (100 MHz, $CDCl_3$) δ 166.6, 162.9, 161.6, 130, 124.1, 114.6, 55.8, 52.4.

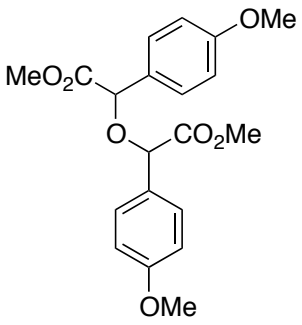

Dimethyl 2,2'-oxybis(2-(4-methoxyphenyl)acetate)

^{1}H NMR (400 MHz; $CDCl_3$) δ 7.31 (d, 4H, J = 8.6 Hz), 6.87 (d, 4H, J = 8.6 Hz), 4.92 (s, 2H), 3.74 (s, 6H), 3.69 (s, 6H).[46] ESI-MS: calc. 374.39; found. 374.28.

Computational Methods. Initial geometry optimization and calculation of vibrational frequencies were performed using the Gaussian 03 software package with B3LYP/Rh-RSC+4f, 6-31G(d) methods.[47] The starting geometry for **3a** was adapted from Hansen et al.[26] Calculation of NMR parameters was performed on this geometry using the Amsterdam Density Functional package[48,49] with the following basis set: Rh, C = TZ2P, O = DZP, H = DZ. Both PBE (GGA) and PBE0 (hybrid, with 25% HF) functionals were employed using either a scalar relativistic correction (ZORA) or spin-orbit ZORA. ^{13}C NMR chemical shifts were calculated relative to the chemical shift of benzene,[50] calculated with B3LYP/6-31G* from CCCBDB. Calculation of the electronic structure of **3a** and its electronic transitions were performed using the ORCA software package (version 2.9.1), utilizing the same optimized geometry as cited above.[51]The Def2-TZV basis sets from the Ahlrichs group were used for all atoms, and several density functionals were used, which all give comparable electronic structures and predicted

electronic transitions: GGA functionals BP86 and PBE0 were used along with hybrid-GGA B3LYP, and meta-GGA TPSS. The latter TPSS functional was used for the results shown in Figure S9.

Geometry optimization of **1** was performed using the crystal structure as a starting point using version 2.9.0 of the ORCA electronic structure package[51] using the BP86 density functional with the segmented all electron relativistically contracted (SARC) def2-TZVP(-f) basis set. Optimizations included the zeroth order relativistic approximation (ZORA) for relativistic effects and solvation as modeled by the conductor-like screening model (COSMO) using a dielectric of 9.08 (CH_2Cl_2).

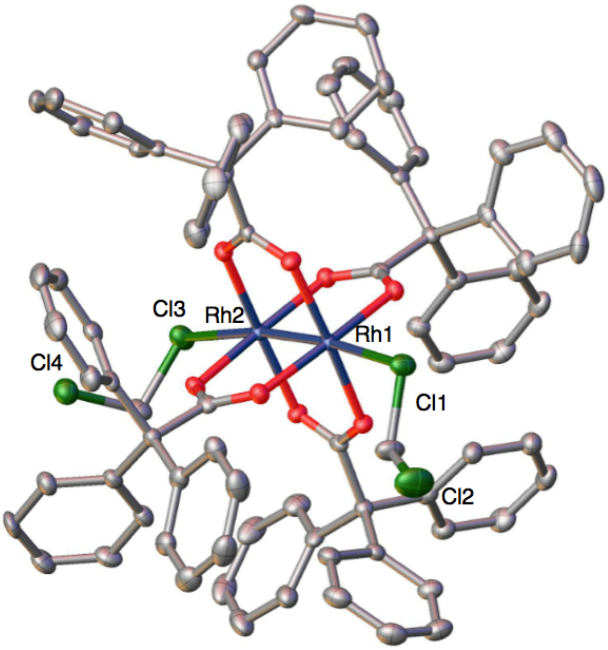

Figure S6.1 X-ray crystal structure of **1**•$2CH_2Cl_2$. Thermal ellipsoids are drawn at 50% probability. Hydrogen atoms are omitted for clarity. This structure crystallizes with four dichloromethane molecules in the lattice. *Formula*: $C_{86}H_{72}Cl_{12}O_8Rh_2$. *Data collection*: Mo Kα radiation, λ = 0.71073 Å; 16445 reflections; T = 100 K, μ = 0.88 mm^{-1}. *Cell*

parameters: $P2_1/c$; a = 22.8533(7) Å, b = 20.0093(5) Å, c = 18.4555(5) Å; α = 90°, β = 109.622(1)°, γ = 90°, V = 7949.2(4) $Å^3$, Z = 4. *Refinement*: R1 [$I \geq 2s(I)$] = 0.0612; wR2 [$I \geq 2s(I)$] = 0.160 ($R1 = 3||F_o| - |F_c||/[3|F_o|]$; $wR2 = (3[w(F_o^2 - F_c^2)^2]/[3[w(F_o^2)^2]])^{½}$, $w = 1/s^2(F_o^2) + (aP)^2 + bP$, where $P = [\max(0 \text{ or } F_o^2) + 2(F_c^2)]/3$). The CIF for this structure is appended.

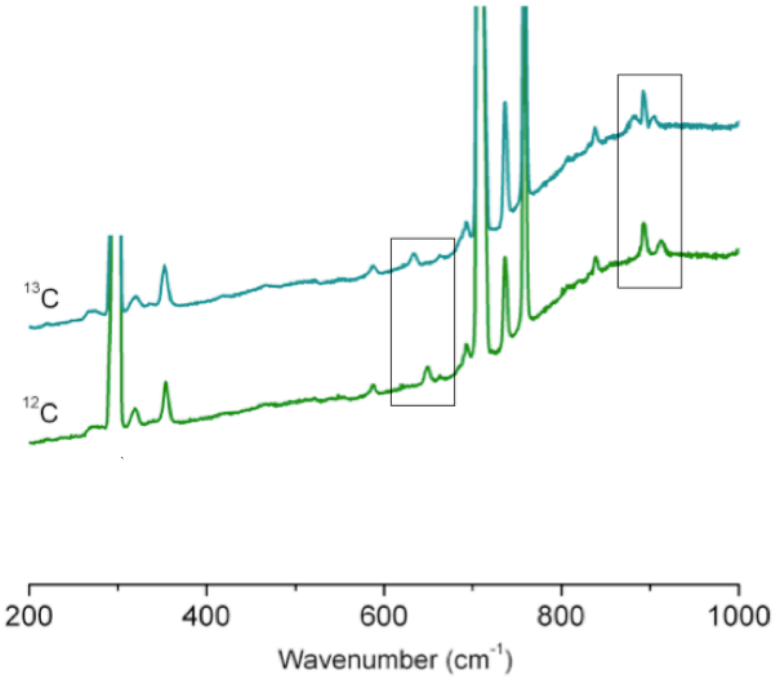

Figure S6.2 Full rRaman spectrum of **3** in the key Rh-C vibrational region. The sample of **3** was prepared using Method A. Boxed areas appear in the main text as blow-ups.

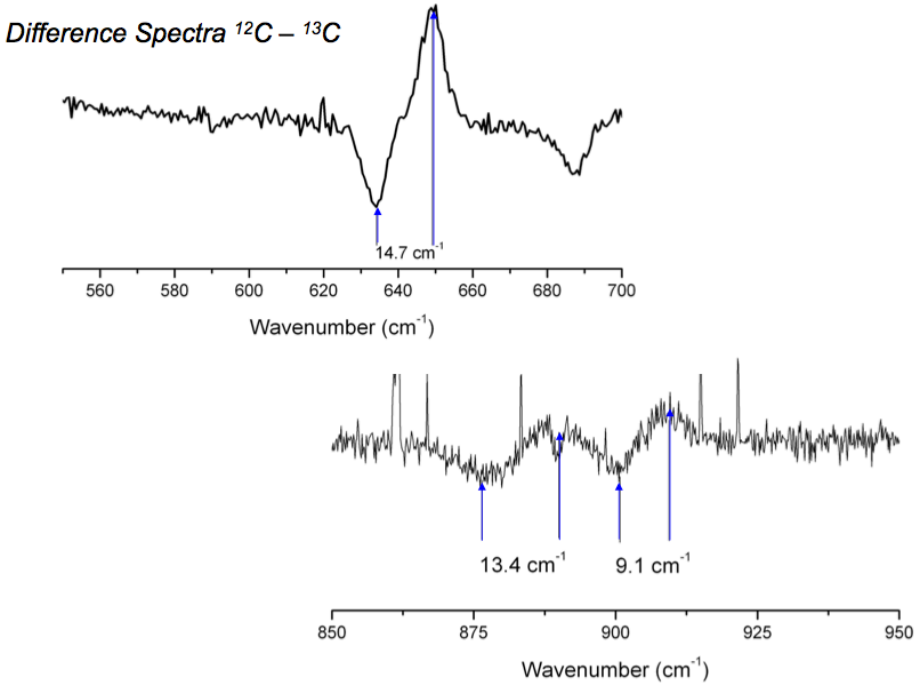

Figure S6.3 Difference rRaman spectra subtracting ^{13}C from ^{12}C.

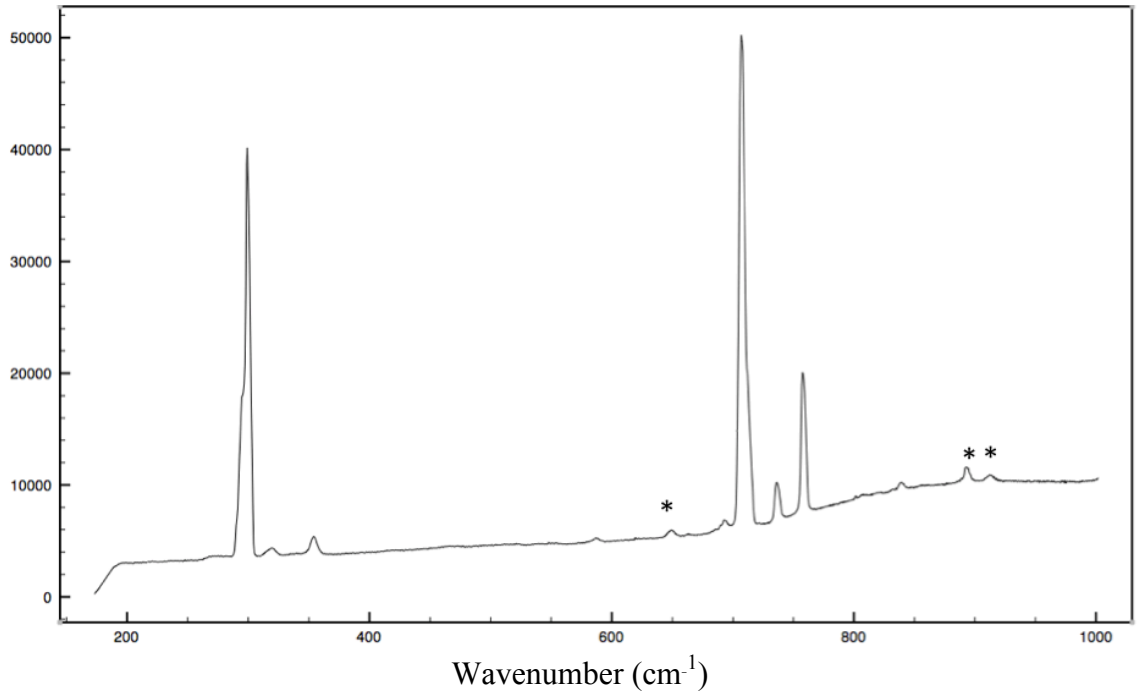

Figure S6.4 rR spectrum of a sample of **3** prepared by Method B. Asterisks indicate vibrational modes identical to those in Figure S1 (**3** prepared by Method A).

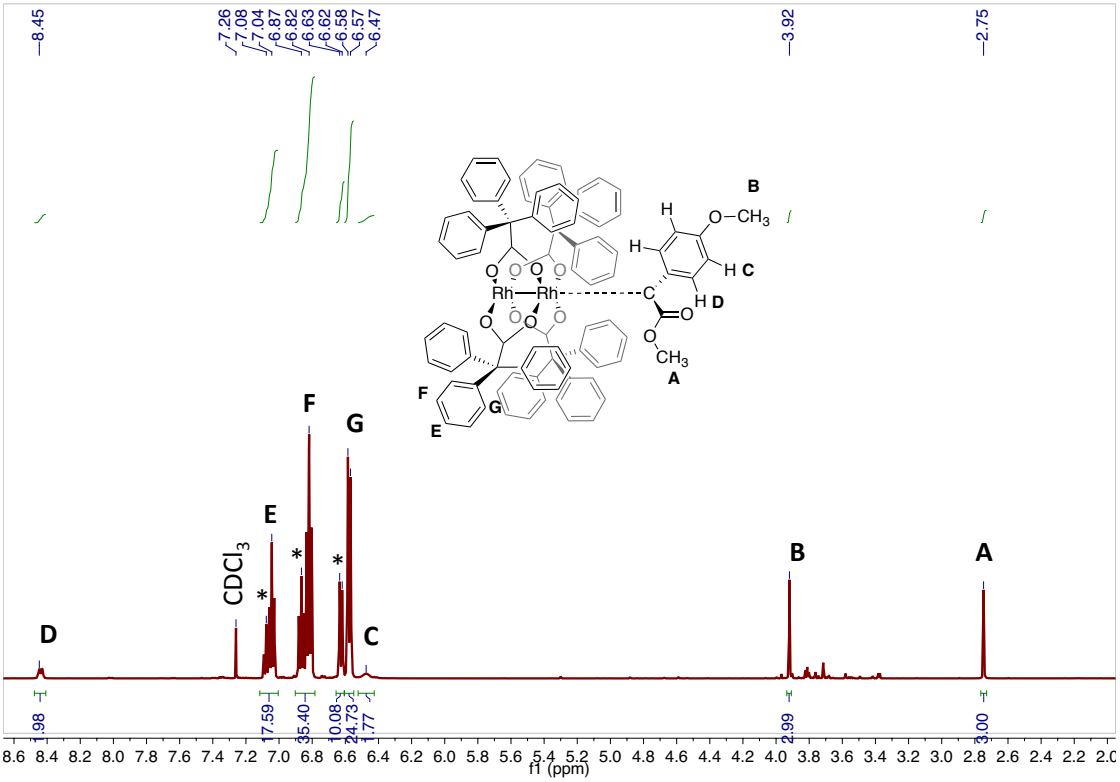

Figure S6.5 ^{1}H NMR spectrum of intermediate **3** prepared by Method B. Asterisks indicate excess **1** (tpa protons). Low intensity peaks in the range from δ = 3.2 – 4.0 ppm are due to unidentified decomposition products.

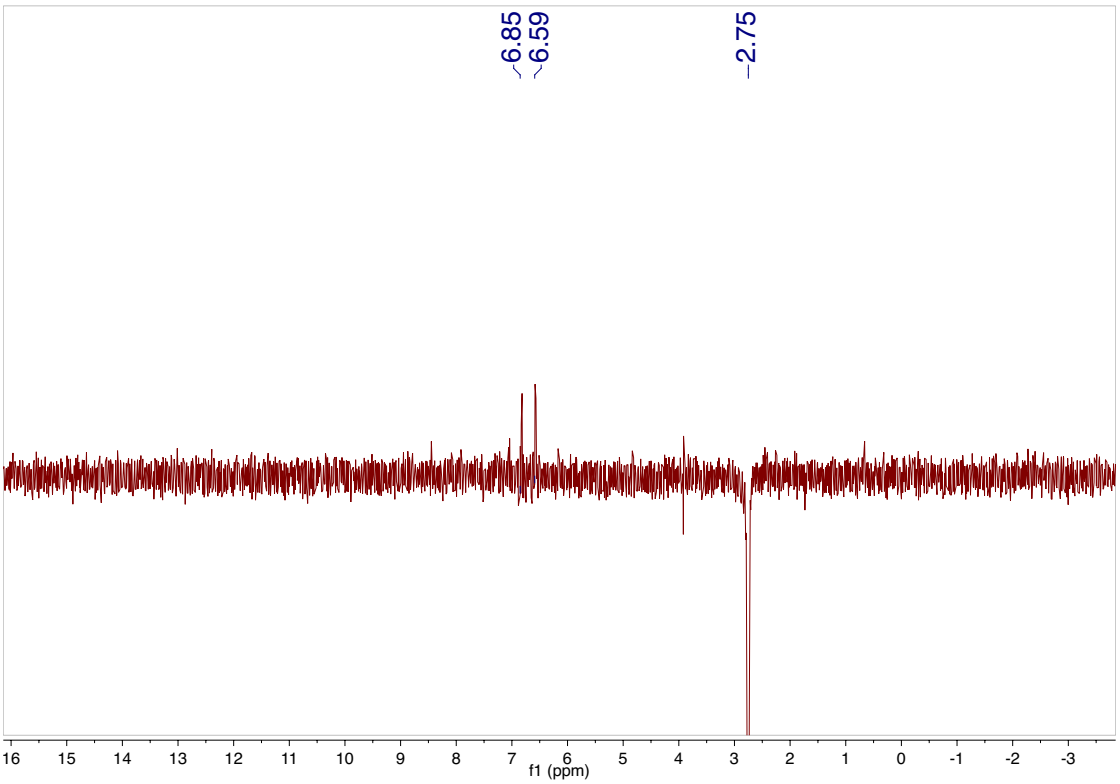

Figure S6.6 1D-gradient NOESY irradiating the methoxy resonance at 2.75 ppm. Resonances belonging to the tpa ligands of **3** are observed.

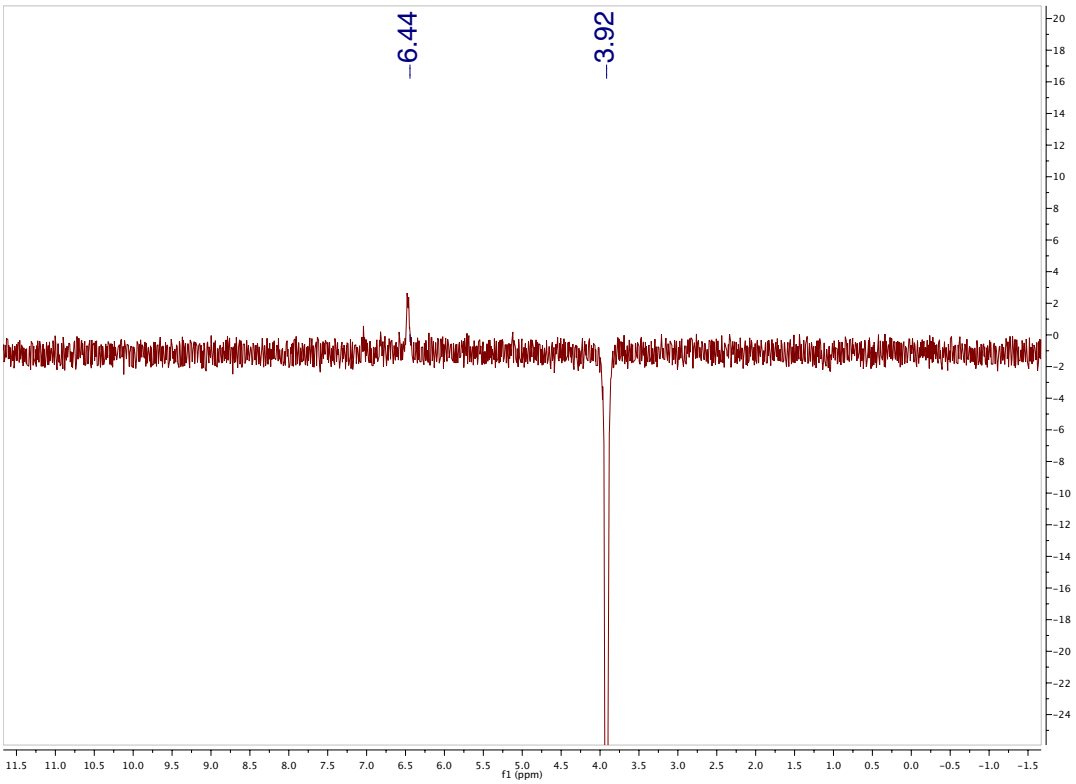

Figure S6.7 1D-gradient NOESY irradiating the methoxy resonance at 3.92 ppm. Resonances belonging to phenyl protons on the carbene fragment at 6.44 ppm are observed. This spectrum positively identifies the 3.92 ppm resonance as belonging to the phenyl methoxy protons of **3**.

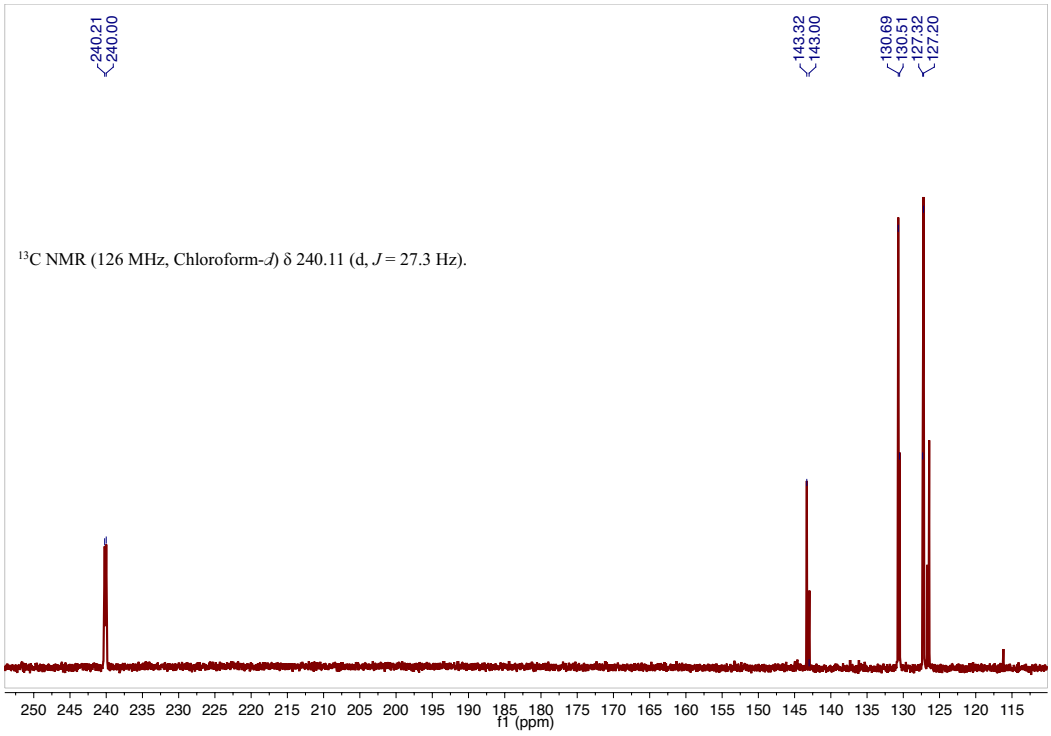

Figure S6.8 ^{13}C NMR spectrum of intermediate **3** generated by Method B. The doublet at 240 ppm is blown up in the main text. The other natural abundance signals in the 127 – 143 ppm region belong to tpa carbons of **3** and excess **1**.

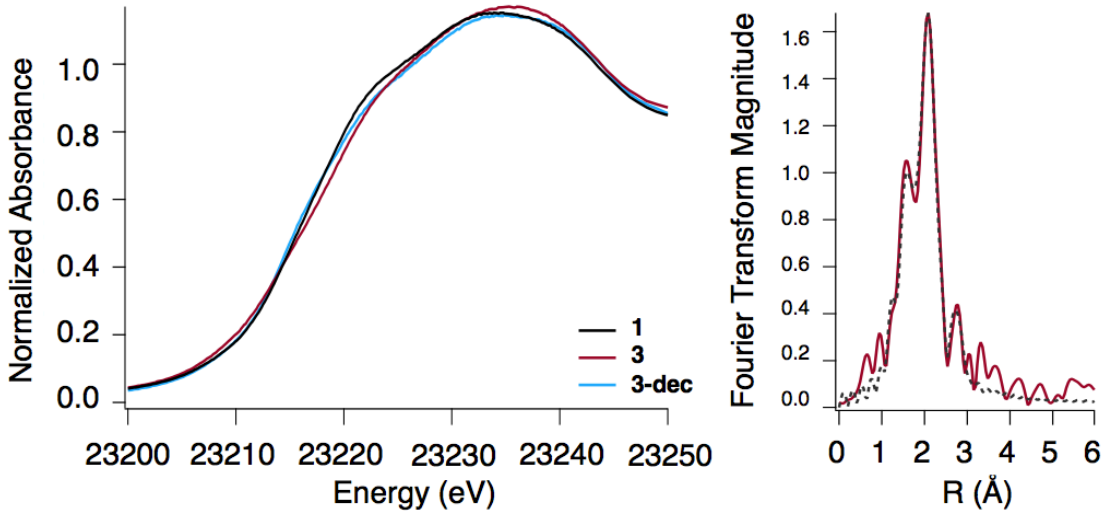

Figure S6.9 XANES for **1**, **3** and **3-dec** (left). EXAFS for complex **3** (right).

Table S6.1 Crystallographic, EXAFS and DFT bond distances for **1**.

	Crystal Structure	**EXAFS**	**DFT**
Rh–Rh (Å)	2.3708(5)	2.378	2.385
Rh–O (Å)	2.033[3]	2.028	2.040
Rh···O_{distal} (Å)	3.074	3.083	3.091
Rh···$C_{carboxyl}$ (Å)	2.867	2.929	2.887
Rh···Cl_{axial} (Å)	2.651[1]	2.625	2.604

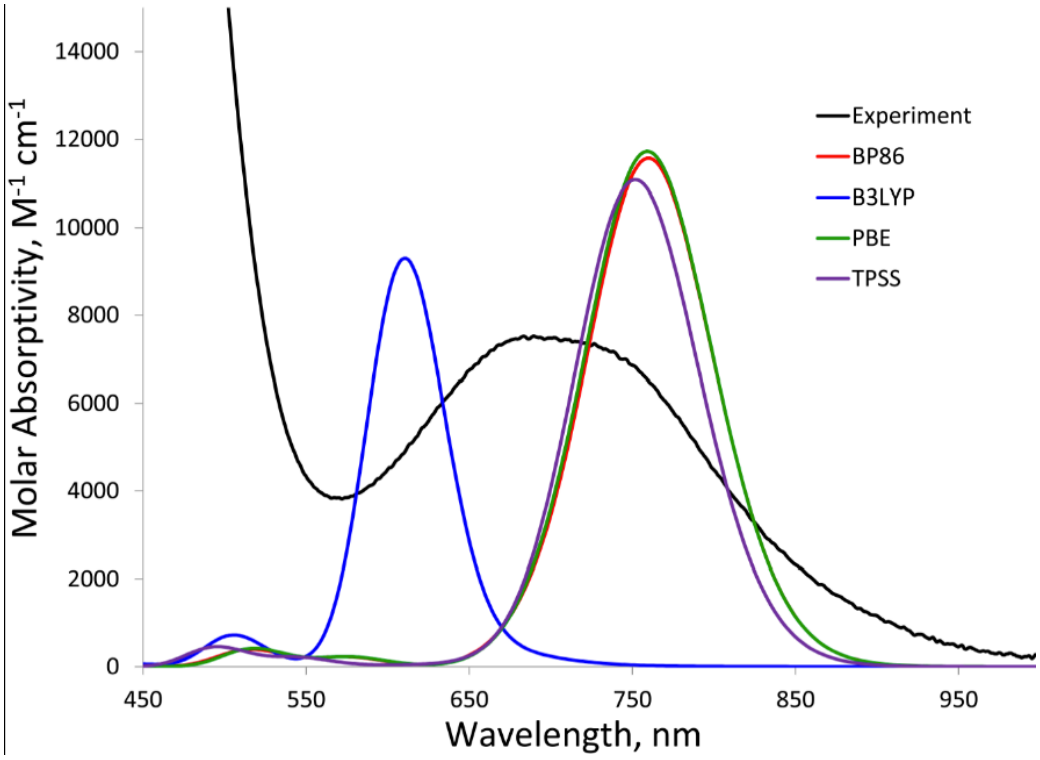

Figure S6.10 TD-DFT for the experimentally observed absorption feature at ~700 nm using various functionals.

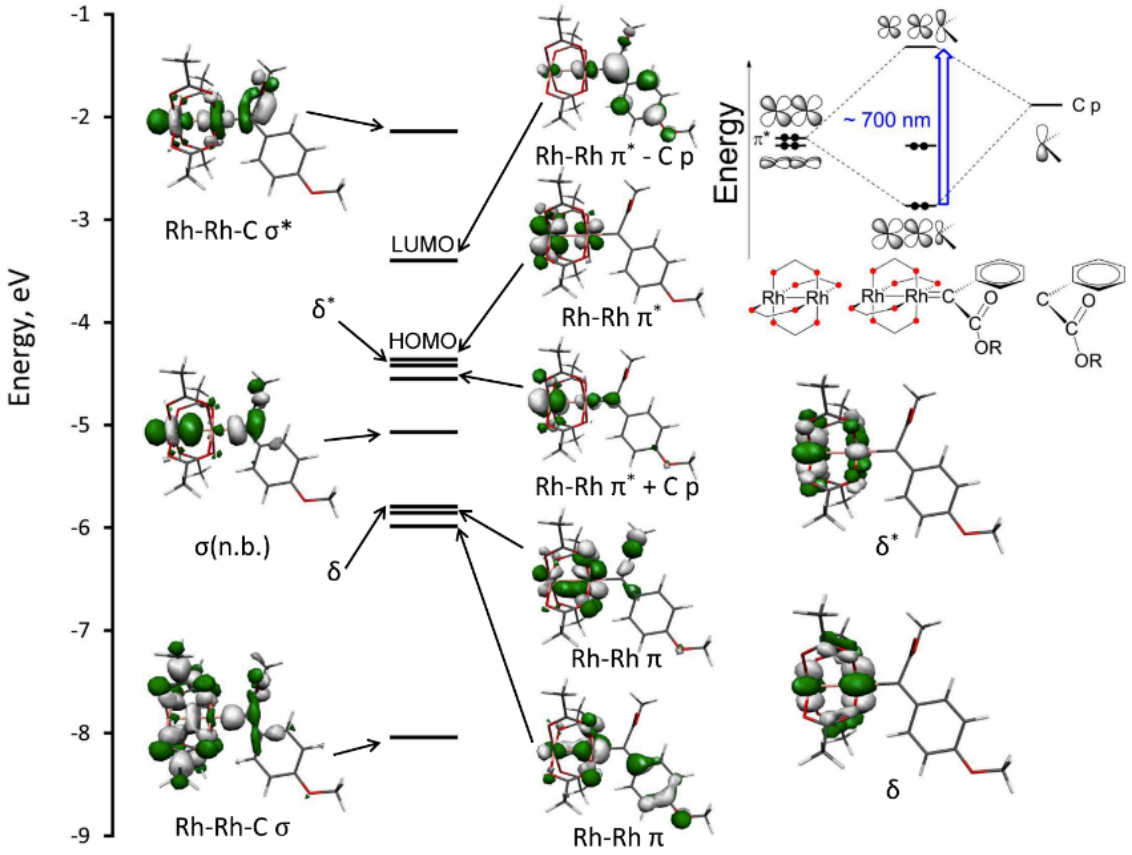

Figure S6.11 Molecular orbital diagram for **3a** with orbital shapes and energies derived from DFT-TPSS calculations. Orbital isosurfaces are drawn with a 0.04 cutoff. Rh_2 σ bonding orbitals are shown at the left, π orbitals are given in the center column, and Rh_2 δ orbitals are shown at the far right. The inset shows the interaction of the Rh_2 π* orbitals with the carbene empty p orbital and the orbitals responsible for the major absorption at ~ 700 nm.

References

(1) *Reactive Intermediate Chemistry*; Moss, R. A.; Platz, M. S.; Jones, M. J., Eds.; John Wiley and Sons, Inc.: Hoboken NJ, 2004.

(2) Sole, S.; Gornitzka, H.; Schoeller, W. W.; Bourissou, D.; Bertrand, G. *Science* **2001**, *292*, 1901.

(3) Yates, P. *J. Am. Chem. Soc.* **1952**, *74*, 5376.

(4) Herrmann, W. A. *Angew. Chem. Int. Ed.* **2002**, *41*, 1290.

(5) Bourissou, D.; Guerret, O.; Gabbaï, F. P.; Bertrand, G. *Chem. Rev.* **1999**, *100*, 39.

(6) Fischer, E. O.; Dötz, K. H. *Chem. Ber.* **1970**, *103*, 1273.

(7) Hoveyda, A. H.; Zhugralin, A. R. *Nature* **2007**, *450*, 243.

(8) Maxwell, J. L.; Brown, K. C.; Bartley, D. W.; Kodadek, T. *Science* **1992**, *256*, 1544.

(9) Shishkov, I. V.; Rominger, F.; Hofmann, P. *Organometallics* **2009**, *28*, 1049.

(10) Deng, Q.-H.; Chen, J.; Huang, J.-S.; Chui, S. S.-Y.; Zhu, N.; Li, G.-Y.; Che, C.-M. *Chem. Eur. J.* **2009**, *15*, 10707.

(11) Che, C.-M.; Huang, J.-S.; Lee, F.-W.; Li, Y.; Lai, T.-S.; Kwong, H.-L.; Teng, P.-F.; Lee, W.-S.; Lo, W.-C.; Peng, S.-M.; Zhou, Z.-Y. *J. Am. Chem. Soc.* **2001**, *123*, 4119.

(12) Pelphrey, P.; Hansen, J.; Davies, H. M. L. *Chem. Sci.* **2010**, *1*, 254.

(13) *Modern Catalytic Methods for Organic Synthesis with Diazo Compounds: From Cyclopropanes to Ylides*; 1 ed.; Doyle, M. P.; McKervey, M. A.; Ye, T., Eds.; John Wiley & Sons, Inc.: New York, 1998.

(14) Davies, H. M. L.; Manning, J. R. *Nature* **2008**, *451*, 417.

(15) Davies, H. M. L.; Beckwith, R. E. J. *Chem. Rev.* **2003**, *103*, 2861.

(16) Davies, H. M. L.; Loe, O. *Synthesis* **2004**, 2595.

(17) Doyle, M. P.; Duffy, R.; Ratnikov, M.; Zhou, L. *Chem. Rev.* **2009**, *110*, 704.

(18) Davies, H. M. L.; Lian, Y. *Acc. Chem. Res.* **2012**, *45*, 923.

(19) Lebel, H.; Marcoux, J.-F.; Molinaro, C.; Charette, A. B. *Chem. Rev.* **2003**, *103*, 977.

(20) Davies, H. M. L.; Hedley, S. J. *Chem. Soc. Rev.* **2007**, *36*, 1109.

(21) Padwa, A. *Chem. Soc. Rev.* **2009**, *38*, 3072.

(22) Zhang, Y.; Wang, J. *Coord. Chem. Rev.* **2010**, *254*, 941.

(23) Nakamura, E.; Yoshikai, N.; Yamanaka, M. *J. Am. Chem. Soc.* **2002**, *124*, 7181.

(24) Snyder, J. P.; Padwa, A.; Stengel, T. *J. Am. Chem. Soc.* **2001**, *123*, 11318.

(25) Davies, H. M. L.; Morton, D. *Chem. Soc. Rev.* **2011**, *40*, 1857.

(26) Hansen, J.; Autschbach, J.; Davies, H. M. L. *J. Org. Chem.* **2009**, *74*, 6555.

(27) Bezuidenhout, D. I.; Barnard, W.; van der Westhuizen, B.; van der Watt, E.; Liles, D. C. *Dalton Trans.* **2011**, *40*, 6711.

(28) Nugent, W. A.; Mayer, J. M. *Metal-Ligand Multiple Bonds*; Wiley-Interscience, 1988.

(29) Cohen, R.; Rybtchinski, B.; Gandelman, M.; Rozenberg, H.; Martin, J. M. L.; Milstein, D. *J. Am. Chem. Soc.* **2003**, *125*, 6532.

(30) Doyle, M. P.; Winchester, W. R.; Hoorn, J. A. A.; Lynch, V.; Simonsen, S. H.; Ghosh, R. *J. Am. Chem. Soc.* **1993**, *115*, 9968.

(31) Pirrung, M. C.; Morehead, A. T. *J. Am. Chem. Soc.* **1994**, *116*, 8991.

(32) Sheehan, S. M.; Padwa, A.; Snyder, J. P. *Tetrahedron Lett.* **1998**, *39*, 949.

(33) Berry, J. F. *Dalton Trans.* **2012**, *41*, 700.

(34) Davies, H. M. L.; Hansen, T.; Churchill, M. R. *J. Am. Chem. Soc.* **2000**, *122*, 3063.

(35) Hashimoto, S.-i.; Watanabe, N.; Ikegami, S. *Tetrahedron Lett.* **1992**, *33*, 2709.

(36) *SMART; Bruker-AXS: Madison, WI* **2009**.

(37) Sheldrick, G. M. *Acta Cryst.* **2008**, *A64*, 112.

(38) Dolomanov, O. V.; Bourhis, L. J.; Gildea, R. J.; Howard, J. A. K.; Puschman, H. J. *Appl. Cryst.* **2009**, *42*, 339.

(39) Wijdeven, M. A.; Wijtmans, R.; Berg, R. J. F.; Noorduin, W.; Schoemaker, H. E.; Sonke, T.; Delft, F. L.; Blaauw, R. H.; Fitch, R. W.; Spande, T. F.; Daly, J. W.; Rutjes, F. P. J. T. *Org. Lett.* **2008**, *10*, 4001.

(40) Naser, U.; Pierik, A. J.; Scott, R.; Cinkaya, I.; Buckel, W.; Golding, B. T. *Bioorg. Chem.* **2005**, *33*, 53.

(41) Ntai, I.; Phelan, V. V.; Bachman, B. O. *Chem. Commun.* **2006**, 4518.

(42) Zhou, J.; Xu, X.; Hu, W. *Org. Synth.* **2011**, *88*, 418.

(43) Rappe, A. K.; Casewit, C. J.; Colwell, K. S.; Goddard III, W. A.; Skiff, W. M. *J. Am. Chem. Soc.* **1992**, *114*.

(44) Davies, H. M. L.; Hansen, T. *J. Am. Chem. Soc.* **1997**, *119*.

(45) Suematsu, H.; Katsuki, T. *J. Am. Chem. Soc.* **2009**, *131*.

(46) *This compound cannot be prepared cleanly. The shifts reported are consistent between crude stoichiometric and catalytic 1H NMR spectra.*

(47) Frisch, M. J.; Trucks, G. W.; al., e. *Gaussian 09, Revision A.1, Gaussian, Inc., Wallingford CT* **2009**.

(48) te Velda, G.; Bickelhaupt, F. M.; van Gisbergen, S. J. A.; Fonseca Guerra, C.; Baerends, E. J.; Snijders, J. G.; Ziegler, T. *J. Comp. Chem.* **2001**, *22*, 931.

(49) *ADF2012, SCM, Theoretical Chemistry, Vrije Universiteit, Amsterdam, The Netherlands,* http://www.scm.com.

(50) http://www.chem.wisc.edu/areas/reich/handouts=/nmr-c13/cdata.htm.

(51) Neese, F. *ORCA - An ab Initio DFT Semi-Empirical Electronic Structure Package, Version 2.9.1; University of Bonn: Bonn, Germany* **2010**.

Appendix 1

CCHF Collaboration:
Synthesis of a Mixed-Valent Rh_2-carboxamidate Catalyst with Chiral Ligands

A1.1 Background

More efficient ways to construct complex structures are constantly sought-after, particularly for the synthesis of pharmaceuticals and other industrially relevant targets. A catalyst that is powerful enough to cleave C–H bonds but is also amenable to fine-tuning of selectivity is necessary to achieve this goal.[1] Excellent enantioselectivities have been reported by Davies and coworkers using Rh_2 catalysts that have chiral prolinate ligands:[1-6] Rh_2(*S*-DOSP)$_4$ (**1**) (Figure A1.1) is one such prolinate-derived catalyst. Enantiomeric excesses greater than 90% have been reported using **1** as a catalyst for intermolecular C–H functionalization and cyclopropanation[7]. These high enantioselectivities are rationalized by a D_2 conformation of the ligands about the Rh_2 core, since the symmetry at both axial faces of the catalyst would give the same asymmetric induction.[3] Unfortunately, structural information for **1** is lacking. Precedent exists for high levels of enantiocontrol using C_2 symmetric catalysts as well.[8,9]

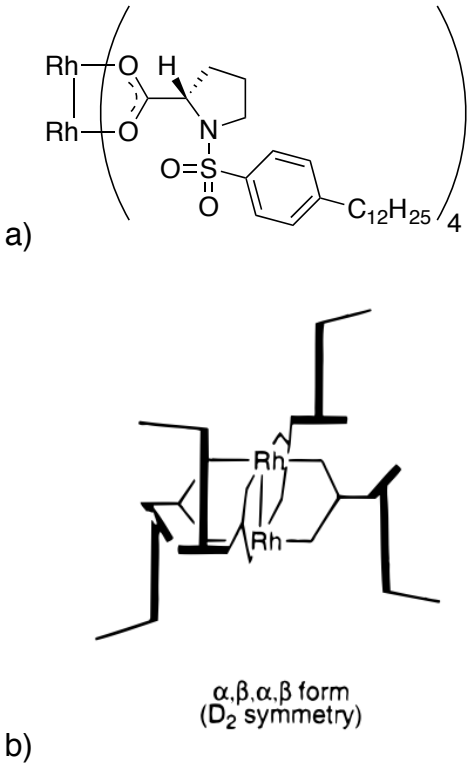

Scheme A1.1 a) Structure of Rh_2(*S*-DOSP)$_4$ (**1**); b) Predicted ligand conformation around catalyst **1**.

The findings summarized in Chapter 5 indicate that Rh_2 mixed-valency may lead to high-turnover catalysis, particularly in C–H amination. The goals of this project are to modify existing chiral carboxylate ligands to amides so as to readily access chiral mixed-valent Rh_2 species. This new class of catalysts is envisioned to perform reactions with both high turnover numbers and enantiocontrol. Furthermore, the ionic nature of mixed-valent Rh_2 complexes may make these complexes more amenable to crystallographic characterization than their Rh_2-carboxylate congeners. Below we report the preparation of Rh_2(*S*-DOSP$_{amide}$)$_4$Cl (**2**).

A1.2 Experimental

S-*DOSP*$_{amide}$. This ligand was synthesized by Davies and coworkers (Scheme A1.2)

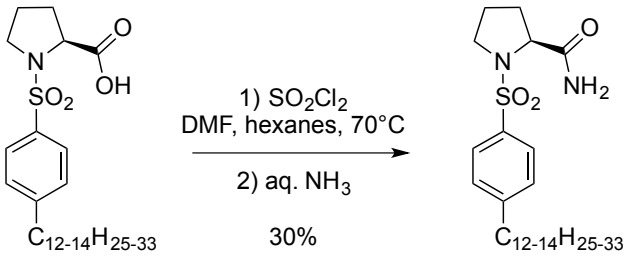

Scheme A1.2 Synthesis of *S*-DOSP$_{amide}$.

Ligand exchange

Freshly recrystallized $Rh_2(OAc)_4$•2MeOH (150 mg, 0.357 mmol) and *S*-DOSP$_{amide}$ (755 mg, 1.78 mmol) were added to a Schlenk flask and dried under vacuum for 5 hours at room temperature. Degassed, anhydrous chlorobenzene was added to the reaction flask and the reaction was equipped with a Soxhlet extractor filled with K_2CO_3. The reaction was stirred at 160°C for two days under N_2 to yield a forest green solution. After cooling, the residue was concentrated by rotary evaporation. The $Rh_2^{II,II}$ compound was purified by chromatography on silica gel, gradient elution 2% - 15% acetone in dichloromethane to yield a blue microcrystalline solid, 52% yield. ^{1}H NMR ($CDCl_3$, 500 MHz) ppm: 7.655 (d, 8H), 7.599 (d, 8H), 6.521 (br s, 4H), 4.031 (dd, 4H), 3.41 (m, 4H), 3.011 (m, 4H), 2.5 – 0.4 (multiplets, 100H). UV-Vis(dichloromethane) λ_{max} = 450 nm,

595 nm. CV (0.001 M in dichloromethane, 0.1 M tetrabutylammonium hexafluorophosphate) $E_{1/2}$ = –84 mV (versus Fc/Fc^{+}).

The blue solid was dissolved in dichloromethane and 1.1 equivalents of *N*-chlorosuccinimide was added at room temperature in air with stirring. The solution changes color from blue to red within 60 seconds. After 10 minutes stirring, the reaction was concentrated by rotary evaporation. The resulting species was purified through a silica plug in neat dichloromethane, resulting in a burgundy microcrystalline solid in 87% yield. MALDI-MS (Anthracene matrix) m/z exp. 1929.88, calc. 1929.82; UV-Vis (dichloromethane) λ_{max} = 456 nm, 1013 nm. CV (0.001 M in dichloromethane, 0.1 M tetrabutylammonium hexafluorophosphate) $E_{1/2}$ = –84 mV (versus Fc/Fc^{+}).

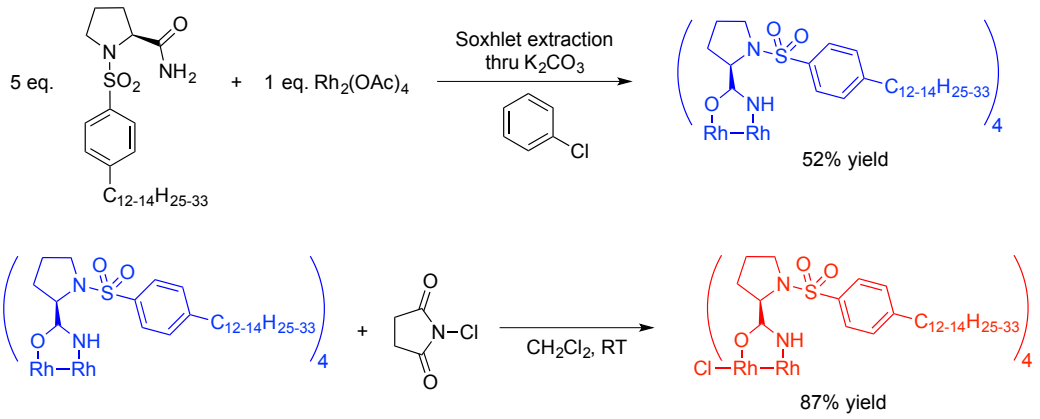

Scheme A1.3 Synthesis of Rh_2(*S*-$DOSP_{amide}$)$_4$ and Rh_2(*S*-$DOSP_{amide}$)$_4$Cl (**2**).

A1.3 Outlook

Since the synthesis of mixed-valent Rh_2-carboxamidate complexes is shown to be facile, we envision the synthesis of more complexes of this type to assess the possibility

of enantioinduction from mixed-valent catalysts. High levels of enantioinduction using Rh_2(*S*-tcptad)$_4$ in C–H amination reactions were recently reported (Scheme A1.4).[10]

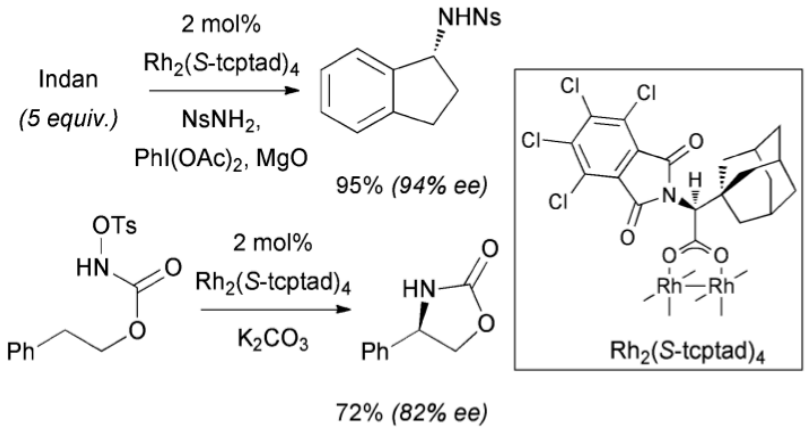

Scheme A1.4 Amination activity of Rh_2(*S*-tcptad)$_4$.

This result is particularly exciting, since mixed-valency has been shown to be most relevant to amination chemistry (vide supra). Similar methods will be used to access Rh_2(*S*-tcptad$_{amide}$)$_4$Cl as described above for Rh_2(*S*-DOSP$_{amide}$)$_4$Cl, and catalytic experiments will follow.

References

(1) Davies, H. M. L.; Beckwith, R. E. J. *Chem. Rev.* **2003**, *103*, 2861.

(2) Pelphrey, P.; Hansen, J.; Davies, H. M. L. *Chem. Sci.* **2010**, *1*, 254.

(3) Davies, H. M. L.; Bruzinski, P. R.; Lake, D. H.; Kong, N.; Fall, M. J. *J. Am. Chem. Soc.* **1996**, *118*, 6897.

(4) Davies, H. M. L.; Kong, N. *Tetrahedron Lett.* **1997**, *38*, 4203.

(5) Davies, H. M. L.; Dick, A. R. In *Top. Curr. Chem.*; Yu, J.-Q., Shi, Z., Eds.; Springer-Verlag Berlin: Berlin, 2010; Vol. 292, p 303.

(6) Davies, H. M. L.; Morton, D. *Chem. Soc. Rev.* **2011**, *40*, 1857.

(7) Briones, J. F.; Hansen, J.; Hardcastle, K. I.; Autschbach, J.; Davies, H. M. L. *J. Am. Chem. Soc.* **2010**, *132*, 17211.

(8) Doyle, M. P.; Eismont, M. Y.; Bergbreiter, D. E.; Gray, H. N. *J. Org. Chem.* **1992**, *57*, 6103.

(9) Doyle, M. P.; Westrum, L. J.; Wolthuis, W. N. E.; See, M. M.; Boone, W. P.; Bagheri, V.; Pearson, M. M. *J. Am. Chem. Soc.* **1993**, *115*, 958.

(10) Collet, F.; Lescot, C.; Dauban, P. *Chem. Soc. Rev.* **2011**, *40*, 1926.